POLITECNICO DI TORINO

Corso di Laurea Specialistica

in Ingegneria Aerospaziale

Tesi di Laurea Specialistica

Application of thermo-electrical generator modules to solar powered aircrafts

Relatore:

Prof. Enrico Cestino

Candidato:

Marco Zucca

Anno Accademico 2020/2021

To my family and my wife

Abstract

This work focuses on the combination of solar panels installed on wing profiles and thermo electrical generator modules. The concept of these two systems working together has the scope to increase the electrical output of the solar cells.

A model of the panel-module system is proposed, based on the energy balance of each component of the system, including radiation, conduction and convection phenomena. Data of solar panels and thermal electric generators are taken from existing products available in the market and their values are averaged and derived by trendlines to adapt the available data to the temperature range that are relevant for aeronautical applications. All the results are then shown as functions of the altitude, in a range between zero and $30{,}000\ m$.

The model solves the energy balance around the solar panel-thermo electrical generator module system. Temperatures of the external environment (atmosphere) and inside the profile are defined based on Standard Atmosphere, and therefore they depend on the altitude.

The model also considers a 2-D profile, therefore tridimensional effects around the wing are not considered. In addition to this, the air flow around the profile is considered non-viscous.

The proposed model can then be used on any airfoil profile, however, due to the limitations mentioned above, it is more relevant for low speed airplanes. An example using the airfoil profile of HeliPlat solar aircraft is shown.

The results are shown under different environment conditions, such as day of the year, time, positions and under different angle of incidence of the profiles.

A final mention on a possible application of this system in different fields is proposed, since this approach could be relevant for solar panels in installations on the ground.

Table of Contents

List of figures

List of tables

List of symbols

Symbol	Description	Unit of measure[1]
∞	Subscript, unperturbed conditions	-
0	Subscript, sea level conditions	-
α_{air}	Diffusivity of air	$\frac{W}{m^2 \cdot K}$
β	Albedo	-
γ	Constant of air	-
δ	Declination angle	°
ε	Power density	$\frac{W}{m^2}$
η	Efficiency	-
θ	Longitude	°
λ	Thermal conductivity	$\frac{W}{m \cdot K}$
μ	Viscosity	$Pa \cdot s$
ν	Kinematic viscosity	$\frac{m}{s^2}$
ξ	Elevation angle	°
ξ_{dep}	Depression angle	°
ξ_{ref}	Refraction angle	°
π	Pi	-
ρ	Density	$\frac{kg}{m^3}$
σ_B	Boltzmann's constant	$\frac{W}{m^2 \cdot K^4}$

[1] Unit of measure considered for all the variables used in formulas and calculations, unless otherwise specified

τ	TEG module coefficients	-
φ	Latitude	$\circ$
ψ	Incidence angle	$\circ$
ψ_Z	Solar zenith angle	$\circ$
ω	Hourly angle	$\circ$
Λ	Avogadro number	mol^{-1}
a	Speed of sound	$\frac{m}{s}$
c_p	Specific heat at constant pressure	$\frac{J}{kg \cdot K}$
c_v	Specific heat at constant volume	$\frac{J}{kg \cdot K}$
d	Thickness	m
e	Body emissivity	-
g	Acceleration of gravity	$\frac{m}{s^2}$
h	Altitude	m
i	Tilting angle	$\circ$
l	Characteristic length	m
p	Pressure	Pa
r	Azimuth angle	$\circ$
r_E	Earth's radius	m
t	Time of day	h
I	Solar irradiation	$\frac{W}{m^2}$
M	Mach number	-
M	Molar mass	$\frac{kg}{mol}$
N	Day of year	-
T	Temperature	K

R	Constant of gas	$\frac{J}{kg \cdot K}$
V	Speed	$\frac{m}{s}$
Nu	Nusselt number	-
Pr	Prandtl number	-
Re	Reynolds number	-

1. Introduction

Solar powered applications are widely available in current days, with solar cells technology improving every year. The same technology has also been tested and proved in these past years in flying concepts of aircrafts powered by solar cells, with the goal of long endurance missions or flight profiles. The efficiency of the solar cells is certainly increasing but it still is within the range of 20%-30% (for aerospace applications), while it is around 18%-22% for residential and commercial applications (such as installations on the ground).

This work evaluates the possibility, from a theoretical perspective, of the use of a thermo-electric generator module (also called TEG module) to operate in conjunction with the solar cell, to generate additional power during sunlight conditions and therefore increase the efficiency output of the power generation system.

Many variables influence the power generated by a solar cell, just to mention a few: atmosphere, time, date, orientation of the panel, airspeed, altitudes. These variables are also linked to each other and several other ones are considered in this work and are necessary for the model to process and provides the desired output.

The scope is then to calculate the balance of the energy generated around a solar panel when it works in conjunction with a thermo-electric generator module (or modules). Since the main focus is the application of this system in the aerospace industry, the variables and the generated power are generally shown as functions of the altitude.

The code for the model is written using Scilab® software and it is based on 2-D calculations along an airfoil profile or along a solar panel. Since the characteristics are defined for a 2-D environment, the energy values are generally presented as power densities, such as Watts over a surface: this also helps in the comparison between the power generated by the solar panel and the power generated by the TEG module, since the surface areas of these two components can be different. Also, the use of XFoil® software is necessary for the variables related to the profile geometry and air flow over the profile itself.

This work can be divided in three parts. The first part refers to the descriptions and definitions of all the variables considered in the model, either for atmospheric characteristics and for navigational data. The second part describes the model and provides information on the calculations to solve the equations of the energy balance. The last part shows an application of this model to HeliPlat airfoil profile, using profile data from HeliPlat research.

This model has some limitations: there are no considerations of winds and gusts as well as no atmospheric effects due to seasons. The data used for the TEG module are based on datasheets taken from existing products in the markets, which have not been tested. Therefore, the values used in some of the calculations can be updated in the future to increase the accuracy of the calculations.

Another limitation in the TEG module is that the model only considers the temperature difference between the hot and cold surfaces, without taking in account the specific values of the hot and cold temperatures: the implications of having a TEG module working at very low temperatures (common case in flight profiles of an aircraft) are not covered in this work. This means that the performances of the module at low temperatures can differ from the values listed in the datasheets used in this document and therefore the references data may vary. Further tests of TEG modules in cold environments could provide more accurate data that can be implemented in this model.

2. Atmospheric and Navigational Data

2.1 Standard Atmosphere

In this model, the ISO Standard Atmosphere is considered. The calculations are valid in the interval of altitude between 0 and 30,000 m. The effect of winds is not considered in the following paragraphs and calculations.

Using the ISO model means that reference temperatures and their variations are statistically calculated, and they do not depend on season changes.

In Table 1, the list of variables used in the model is shown. For reference, the table also indicates whether the variable depends directly or indirectly (through other variables) on the altitude h.

Variable	Direct dependance on h	Indirect dependance on h
Temperature	Yes	No
Pressure	Yes	Yes
Density	Yes	Yes
Speed of sound	No	Yes
Mach number	No	Yes
Viscosity	No	Yes
Kinematic viscosity	No	Yes
Specific heat, constant pressure	No	Yes
Specific heat, constant volume	No	Yes
Thermal conductivity	No	Yes
Reynolds number	No	Yes
Prandtl number	No	Yes
Nusselt number	No	Yes

Table 1: Dependency of variables on altitude

2.1.1 Temperature

Based on the definition of the Standard Atmosphere, the relationship between temperature and altitude can be written in compact form as:

$$T_\infty = \begin{Bmatrix} T_0 \\ T_{11,000} \\ T_{20,000} \end{Bmatrix} + \begin{bmatrix} -0.0065 \\ 0 \\ 0.001 \end{bmatrix} \cdot \left(h - \begin{Bmatrix} 0 \\ 11,000 \\ 20,000 \end{Bmatrix} \right) \qquad \begin{matrix} 0 \le h \le 11,000 \\ 11,000 < h \le 20,000 \\ 20,000 < h \le 32,000 \end{matrix}$$

2.1.2 Pressure

Based on the definition of standard atmosphere, the relationship between pressure, temperature and altitude can be written in compact form as:

$$p_\infty = \begin{Bmatrix} p_o \\ p_{11,000} \\ p_{20,000} \end{Bmatrix} \cdot \begin{Bmatrix} \left(\frac{T_\infty}{T_0}\right)^{-\frac{g}{-0.0065 \cdot R}} \\ e^{-\frac{g}{R \cdot T_\infty} \cdot (h-11,000)} \\ \left(\frac{T_\infty}{T_{20,000}}\right)^{-\frac{g}{0.001 \cdot R}} \end{Bmatrix} \qquad \begin{matrix} 0 \le h \le 11,000 \\ 11,000 < h \le 20,000 \\ 20,000 < h \le 32,000 \end{matrix}$$

2.1.3 Density

Based on the definition of standard atmosphere, the relationship between density, temperature and altitude can be written in compact form as:

$$\rho_\infty = \begin{Bmatrix} \rho_o \\ \rho_{11,000} \\ \rho_{20,000} \end{Bmatrix} \cdot \begin{Bmatrix} \left(\frac{T_\infty}{T_0}\right)^{-\frac{g}{-0.0065 \cdot R + 1}} \\ e^{-\frac{g}{R \cdot T_\infty} \cdot (h-11,000)} \\ \left(\frac{T_\infty}{T_{20,000}}\right)^{-\frac{g}{0.001 \cdot R + 1}} \end{Bmatrix} \qquad \begin{matrix} 0 \le h \le 11,000 \\ 11,000 < h \le 20,000 \\ 20,000 < h \le 32,000 \end{matrix}$$

2.1.4 Speed of sound

The model considers a constant air speed as input, therefore the speed of sound (and ultimately the Mach number) is calculated merely to check that the airflow around the panel is maintained as incompressible. The formula below shows that this variable is indirectly influenced by the altitude:

$$a_\infty = \sqrt{\gamma \cdot R \cdot T_\infty}$$

2.1.5 Mach number

Following the definition of paragraph 2.1.4, the Mach number represents the ratio between the air speed and the speed of sound:

$$M_\infty = \frac{V_\infty}{a_\infty}$$

For the purpose of this model, Mach number is solely included to verify that the fluid (air) is incompressible, therefore $M_\infty < 0.3$.

The model does not consider behaviours and characteristics of a compressible fluid, therefore the calculations are applicable to low speed aircrafts only.

2.1.6 Viscosity

Sutherland's law provides the relationship between air viscosity and temperature:

$$\mu_\infty = 1.458 \cdot 10^{-6} \cdot \frac{T_\infty^{\frac{3}{2}}}{T_\infty + 110.4}$$

2.1.7 Kinematic viscosity

It is defined as the ratio between viscosity and density:

$$\nu_\infty = \frac{\mu_\infty}{\rho_\infty}$$

2.1.8 Specific heats

Based on [1, Eq. 3.31], the specific heat (at constant pressure) can be expressed as a function of the temperature (and consequently the altitude) as:

$$c_p = 1{,}000 \cdot (1.0037 + 1.75 \cdot 10^{-5} \cdot T_\infty + 9.524 \cdot 10^{-8} \cdot T_\infty^2)$$

In this formula, the value of T_∞ is expressed in $[°C]$. This formula is accurate in the interval between $-60° \leq T_\infty \leq +60°$, which is within the range of interest of the atmospheric considered in this work.

The specific heat (at constant volume) can be expressed as:

$$c_v = \frac{c_p}{\gamma} \tag{1}$$

2.1.9 Thermal conductivity of air

Based on [2, Eq. 2.11], the thermal conductivity of air can be expressed as a function of the temperature:

$$\lambda_{air} = \frac{9\gamma - 5}{4} \cdot \frac{c_v}{\pi d_{fp}^2} \cdot \sqrt{\frac{M \sigma_B T_\infty}{\Lambda \pi}} \tag{2}$$

Where the term c_v is the specific heat at constant volume, calculated using Equation (1).

The terms M and Λ indicate the molecular weight of air and the Avogadro number:

$$\mathrm{M} = 28.97 \cdot 10^{-3} \; {}^{mol}/_{kg} \quad ; \quad \Lambda = 6.022 \cdot 10^{23} \; mol^{-1}$$

The term d_{fp} represents the mean free path for the air molecules. In the model, it is approximated and considered constant, with reference to the typical value at normal pressure:

$$d_{fp} = 0.372 \cdot 10^{-9}\, m$$

2.2 Reference values at sea level

Some variables need to be set up at a reference altitude. In the model, following the standard atmosphere, these particular references are seat at sea level. Their related altitude is conventionally set as $h = 0\ m$. In Table 2 below the values at sea level of the atmospheric variables are listed.

Variable	Value at Seal Level	Unit of Measure
ρ_0	1.225	$\left[\frac{kg}{m^3}\right]$
p_0	101,325	$[Pa]$
T_0	15	$[°C]$

Table 2: Atmospheric values reference to sea level

Figure 1 below summarizes the profiles of the variables as defined in paragraphs 2.1 and 2.2. The x-axis shows the values scaled as ratio of the variables to sea level (defined as ratio to sea level). The kinematic viscosity is scaled down by a factor of 100 to match the limits imposed by the plot area.

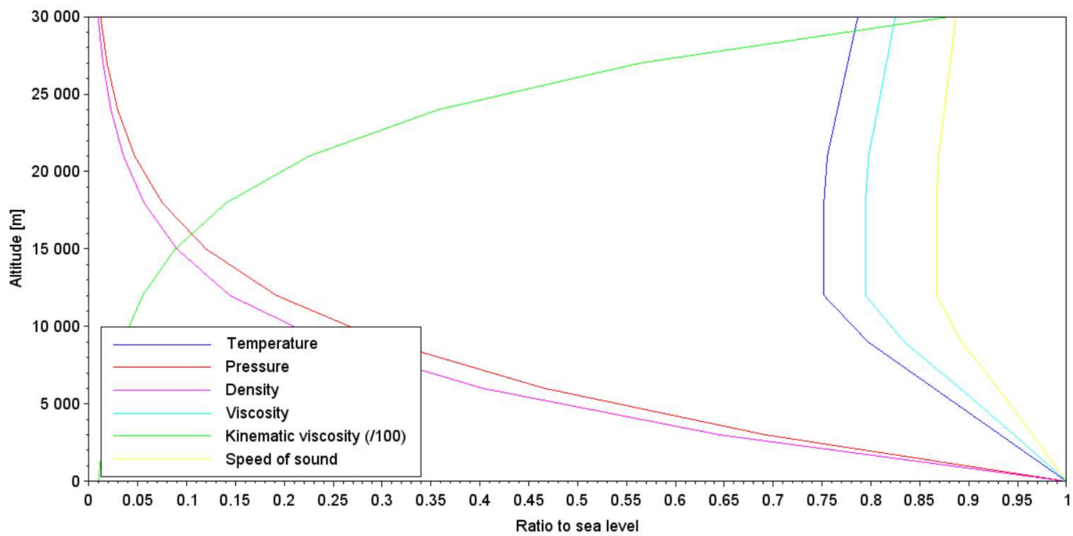

Figure 1: Standard atmosphere

The acceleration of gravity varies with the altitude. In the model, the following formula is used to relate g to h:

$$g = g_0 \cdot \left(\frac{r_E}{r_E + h}\right)^2$$

The value of the acceleration of gravity at sea level is defined as $g_0 = 9.806\ {}^{m}/_{s^2}$.

Therefore, the model considers the gravity to decrease with the altitude (Figure 2).

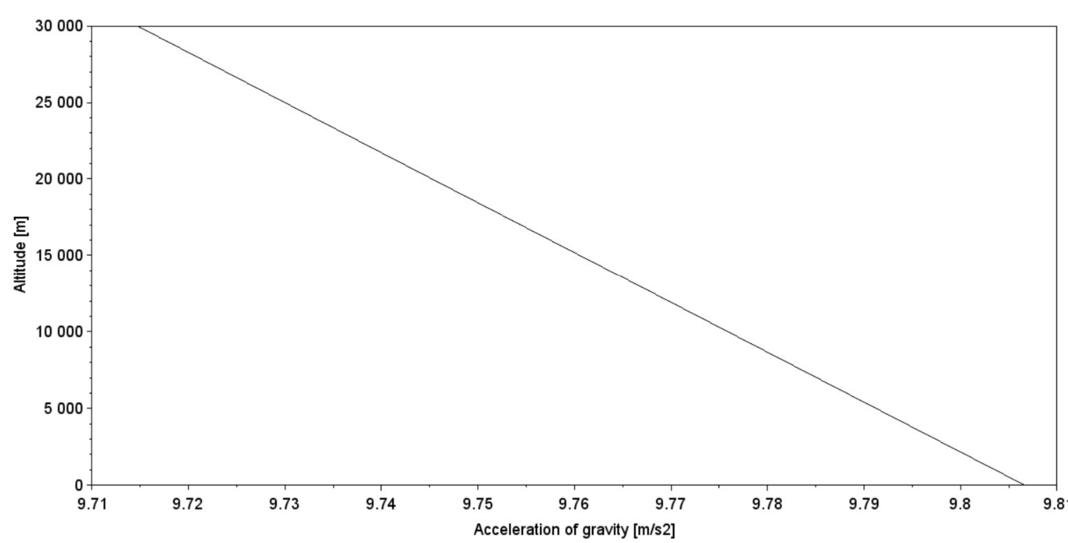

Figure 2: Acceleration of gravity as function of altitude

2.3 Geographical and navigational data

Several information must be known relatively to the position and the orientation of the panel (whether it is installed on an aircraft or it is placed in a system on the ground). In normal conditions, references such as altitude, position on Earth and direction are known. Information on time of day and day of the year are also known. Starting from these data, an additional series of information can be calculated.

Here below in Table 3, the necessary information related to position and direction are listed. This set of data constitutes the navigational and positional input to the model to calculate the powers and the temperatures.

Set	Data	Symbol
Position	Altitude	h
	Latitude	φ
	Azimuth	θ
	Tilting	i
Time	Day of the year	N
	Time of day	t

Table 3: Set of geographical and time related inputs

As a replacement of the azimuth angle, the longitude angle can be used. The direction provided by the initial and final latitude and longitude coordinates would define the azimuth. However, it must be noted that the azimuth defines the direction of the panel with respect to the South direction. This means that, when the azimuth angle is at 0°, the panel is oriented, or the aircraft is flying to, the South direction.

The tilting angle represents the angular orientation of the panel with respect to the horizontal plane or the ground surface's plane.

From these six data, it is possible to calculate other important angles. These are detailed and defined in the paragraphs below.

2.3.1 Declination angle

The declination angle of the sun is the angle between the Equator and the line drawn from the centre of Earth to the centre of Sun:

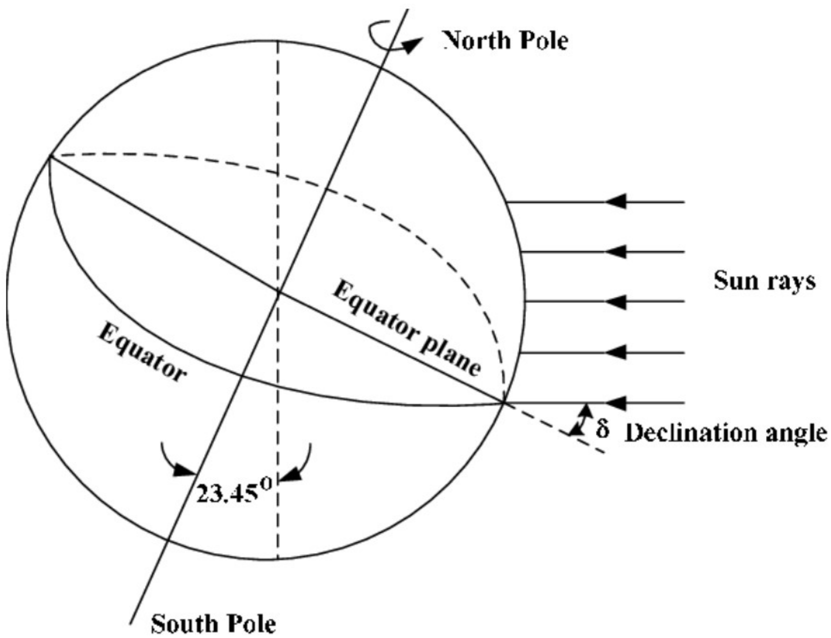

Figure 3: Declination angle of Sun

The declination angle varies seasonally, either because Earth is tilted on its axis of rotation and because Earth rotates around the sun. For any day of the year, it is possible to calculate the declination angle as:

$$\delta \cong -23.45 \cdot cos\left[\frac{2\pi}{365}(N+10)\right] \tag{3}$$

The value number 10 is introduced to consider the shifting in the starting point of the days from Winter's solstice to January 1st of every year. The measurement of the declination angle starts on 21st December, while the traditional calendar year starts on 1st January (10 days difference between the two dates). The exception is a leap year, where the total days are 366.

Figure 4 shows the declination angle as function of the day of the year.

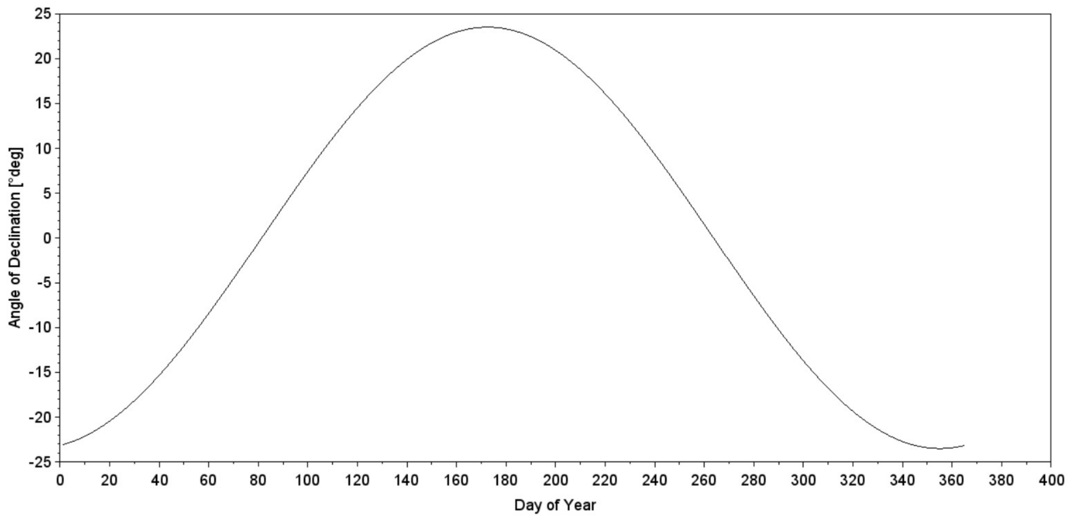

Figure 4: Declination angle as function of the day of the year

The declination angle has a minimum value of $\delta_{min} = -23.45°$, which occurs on Winter's solstice day (for northern hemisphere) and a maximum value of $\delta_{max} = 23.45°$, which occurs on Summer's solstice day (northern hemisphere). The declination angle is equal to 0° on Spring and Autumn's equinoxes.

2.3.2 Hour angle

The time of day can be also defined as an angle: this conversion becomes useful in the next paragraphs to calculate other angles such as zenith and incidence.

For a given time of day t, the hour angle is defined as:

$$\omega = \pi \left(\frac{t}{12} - 1 \right) \tag{4}$$

The angle range is $-180° \leq \omega \leq 180°$ and the starting value of $\omega = 0°$ is set at midday when $t = 12\ h$.

2.3.3 Solar zenith angle

This is the angle between the normal direction to the horizontal plane and the direction of the solar rays and can be represented as in Figure 5.

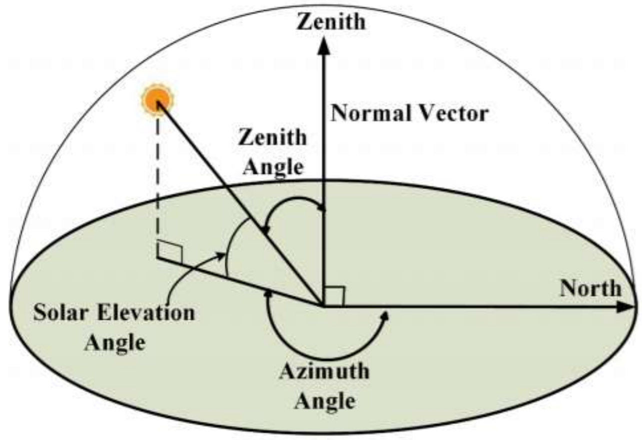

Figure 5: Representation of solar zenith angle and solar elevation angle

For any specific location on Earth, the solar zenith angle depends on the latitude, declination, and time of day according to the following formula:

$$\cos\psi_Z = \sin\varphi \cdot \sin\delta + \cos\varphi \cdot \cos\delta \cdot \cos\omega \tag{5}$$

2.3.4 Incidence angle

The incidence angle has a similar definition as the zenith angle. However, the incidence angle and the zenith angle do not generally coincide. This is because the incidence angle is defined as the angle between the normal line to the reference surface of the photovoltaic panel or a panel installed on a wing profile and the direction of sunlight. The difference is the in the surface used as a reference: surface of Earth for the solar zenith angle and the surface of the photovoltaic panel for the observer. Therefore, it can be defined by the following relation:

$$\cos\psi = (\cos i \cdot \sin\varphi - \cos\varphi \cdot \cos r \cdot \sin i)\sin\delta + (\sin\varphi \cdot \cos r \cdot \sin i + \cos i \cdot \cos\varphi)\cos\delta \cdot \cos\omega + \sin r \cdot \sin i \cdot \cos\delta \cdot \sin\omega \tag{6}$$

Equation (6) is an expansion of Equation (5), with the additional terms of tilting (inclination) angle i and panel azimuth angle r. Figure 5 can also be used to represent the incidence angle, if the reference surface which the normal vector applies to is replaced by the panel or airfoil profile surface: in this case the panel surface can also be oriented with respect to Earth's surface, therefore the tilting angle and the azimuth angle are generally not set at zero degrees.

2.3.5 Elevation angle

With reference to Figure 5, it is possible to see that the incidence angle and the elevation angle are complementary: the sum of these two angles is equal to 90°.

Therefore, the relationship between the angle ψ and the angle ξ is the following:

$$\psi + \xi = 90°$$

Given Equations (3), (4) and (6), it is possible to calculate the elevation angle as a function of the time of day. Figure 6 below represents the curve of the elevation angle for a specific latitude ($\varphi = 45°$). The three curves are based on three specific days of the year (December 21st, $N = 355$, March 21st, $N = 80$, and June 21st, $N = 172$) and on a reference altitude of $h = 10{,}000\ m$.

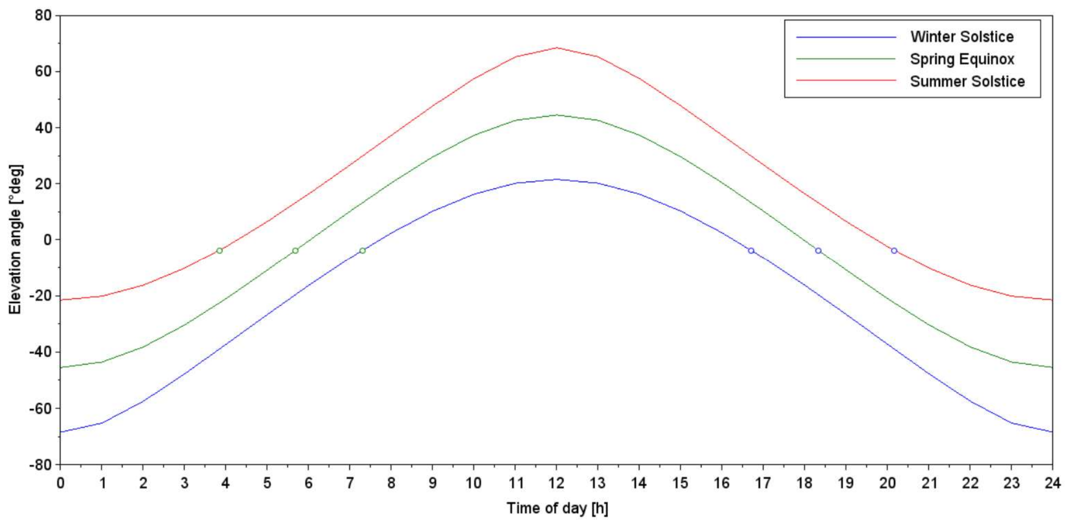

Figure 6: Typical curve of elevation angle as function of time of day for three different days of the year

The three dots on the left represents the sunrise times for each day, while the three dots on the right represents the sunset times respectively. These limit points are important in case of operations close to sunset or sunrise, since the power received by the panels depends on these limits. Having longer daily hours allow to store more energy and therefore enables longer flights durations.

2.3.6 Solar depression angle

In order to calculate the time of sunset and sunrise, it is necessary to define when sunset or sunrise occur: for the calculations it is considered the sunset or sunrise occurs when the centre of the Sun hits the horizon and becomes visible (or become invisible in the case of sunset). However, due to the diffraction phenomena in the atmosphere, the sunlight is visible when it is still below the line of the horizon. The diffraction phenomena are due to sunrays refractions and scatter phenomena in the atmosphere.

The depression angle due to refraction phenomena at sea level $h = 0\ m$, has the value of $\xi_{ref} = 0.57°$.

The angle of depression increases with the increase of the altitude, therefore at a higher altitude, the angle at which the sun is still visible at the horizon increases. This is a benefit for solar powered high-altitude flights, since they can receive light for a longer time. The relationship between the solar depression angle and the altitude is given by:

$$\xi_{dep} = \xi_{ref} + \cos^{-1}\left(\frac{r_E}{r_E + h}\right) = 0.57 + \cos^{-1}\left(\frac{r_E}{r_E + h}\right)$$

In the calculations, an average value of the radius of Earth is considered as $r_E = 6{,}356{,}766\ m$.

The relation between the solar depression angle and the altitude is shown in Figure 7 below.

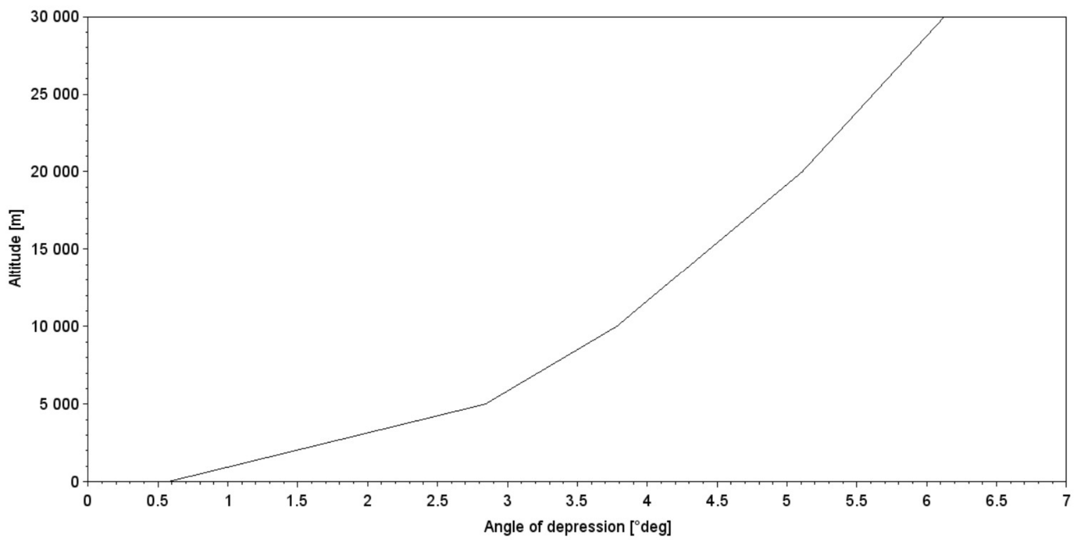

Figure 7: Solar depression angle as function of altitude

2.3.7 Sunset and Sunrise

Based on the equations above, it is possible to calculate the time of sunset and sunrise. These two specific times are dependent of the latitude and the declination (and therefore the day of the year).

In particular, the time of sunset can be derived directly from Equation (5) of the zenith angle. At sunset, it is possible to consider the zenith angle equal to $\psi_Z = 90°$. In addition, the diffraction phenomena of the atmosphere must be considered, hence the solar depression angle must be added.

Therefore, the hour angle at sunset (subscript S) is calculated as:

$$\omega_S = \cos^{-1}\left[\frac{\cos(90 + \xi_{dep}) - \sin\varphi \cdot \sin\delta}{\cos\varphi \cdot \cos\delta}\right] \quad [rad]$$

The hour angle at sunrise (subscript D) is the opposite of the hour angle at sunset, therefore:

$$\omega_D = -\omega_S \quad [rad]$$

These two hour angles can be converted into time of day (hours) by using Equation (4):

$$t_S = 12\left(1 + \frac{\omega_S}{\pi}\right) \quad [h]$$

$$t_D = 12\left(1 + \frac{\omega_D}{\pi}\right) \quad [h]$$

3. Solar Radiation

3.1 Solar flux density

The average solar flux density that reaches Earth outside of the atmosphere is considered constant with a defined value of $\bar{I} = 1{,}367\ {}^{W}/_{m^2}$.

Due to the elliptic orbit of Earth, the distance between our planet and our sun varies along the year. The ellipticity of the orbit differs in about 3.3% from a perfect circle. Therefore, it is possible to correct the value of $\bar{\varepsilon_0}$ to obtain a more accurate value of the solar flux along the year. For a given day N, it is possible to find the corrected value as follows:

$$I = \bar{I} \cdot \left\{1 + 0.033 \cdot \cos\left[\frac{2\pi}{365}(N + 10)\right]\right\}$$

This value is independent to the position of the object on Earth or its altitude: it simply represents the amount of radiation that the Sun emits and reaches Earth. It solely depends on the day of the year (and therefore on the distance from the Sun and on the inclination of sunlight with respect to Earth).

To include the position of the object, it is necessary to consider the incidence angle ψ: this angle will refer the solar flux to the vertical axis based on the position of the observer. Therefore, it is possible to consider the following formula:

$$\varepsilon_{sun} = I \cdot \cos\psi$$

Figure 8 below shows the power density as function of the day of the year as well as at different latitudes. Other variables such as the tilt angle i and the azimuth angle r are set to 0°.

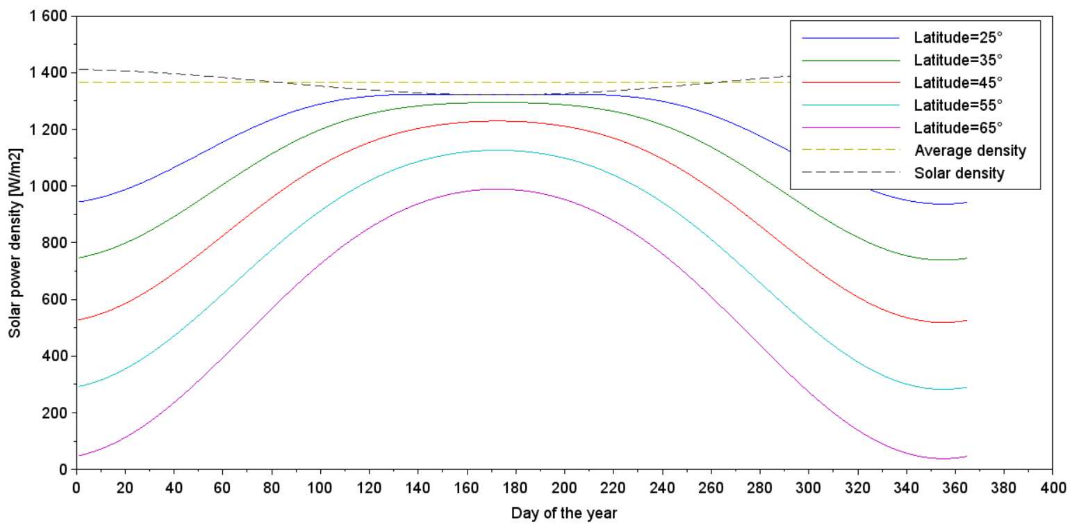

Figure 8: Variation of the solar power density with day of the year and latitude

At lower latitudes the power density is higher, and the values tend to match the solar flux. This is because at lower latitudes the sunrays (and therefore the flux) hit the horizontal plane more perpendicularly.

3.2 Atmospheric effects on Solar flux density

So far, the altitude has not been considered. This is because the presence of the atmosphere has effects on the solar flux. In the atmosphere, three effects contribute to the solar flux: direct radiation, diffusive radiation and reflective radiation.

Figure 9 below shows a representation of these three contributes. As it can be seen, the diffused flux depends directly on the atmosphere and on the altitude, while the reflected flux depends on the albedo, and therefore on the type of ground and surface.

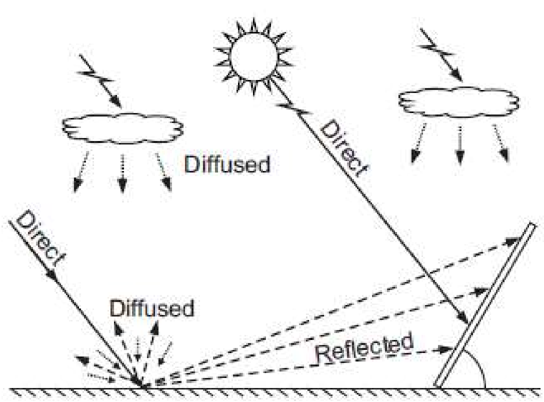

Figure 9: Contributions to the solar radiation

3.2.1 Direct flux

The model considers altitudes up to $30{,}000\ m$, for this reason an accurate formula that is valid for relatively high altitudes must be used. An empirical formula was derived [1, Eq. 3.12], based on measured atmospheric values and it is used in this model. It also considers the incidence angle and the angle of depression, to include the position of the sun as well as the beneficial extended sunlight which increases with the altitude.

$$\varepsilon_{dir} = I \cdot e^{\left\{-\frac{c \cdot e^{\left(-\frac{h}{h_s}\right)}}{\left[sin\left(\frac{0.5\cdot\pi\cdot(\xi+\xi_{dep})}{0.5\cdot\pi+\xi_{dep}}\right)\right]^{s+\frac{h}{b}}}\right\}} \tag{7}$$

The empirical constants shown in Equation (7) are defined as:

$$c = 0.357 \quad ; \quad s = 0.678 \quad ; \quad b = 40{,}000\ m \quad ; \quad h_s = 7{,}000\ m$$

Figure 10 shows the relation between the elevation angle and the direct flux ε_{dir} for different altitudes:

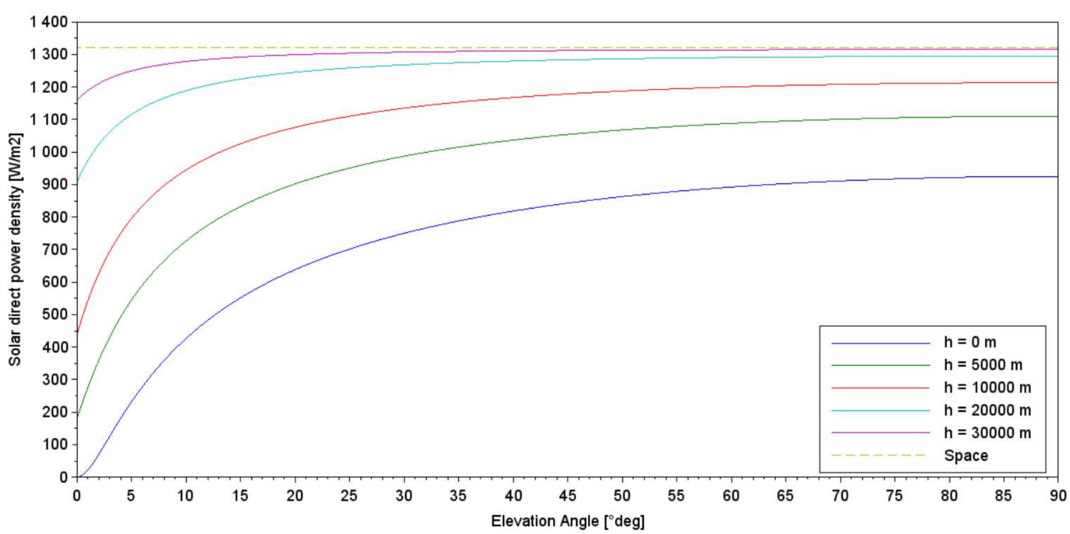

Figure 10: Elevation angle as function of solar direct power density and altitude

It is possible to note that the higher the altitude, the higher the power density available from the sun. Ultimately, the curve will match the flux from the sun, since at very high altitude (in space) the dependence from the latitude and the other angles will lower down and become negligible.

As additional reference and graphical explanation, the plot as in Figure 11 can be derived: it links the latitudes with the solar direct panel available, for different altitudes. In this plot is also possible to see the effect of the declination angle to the position of the maximum available power density.

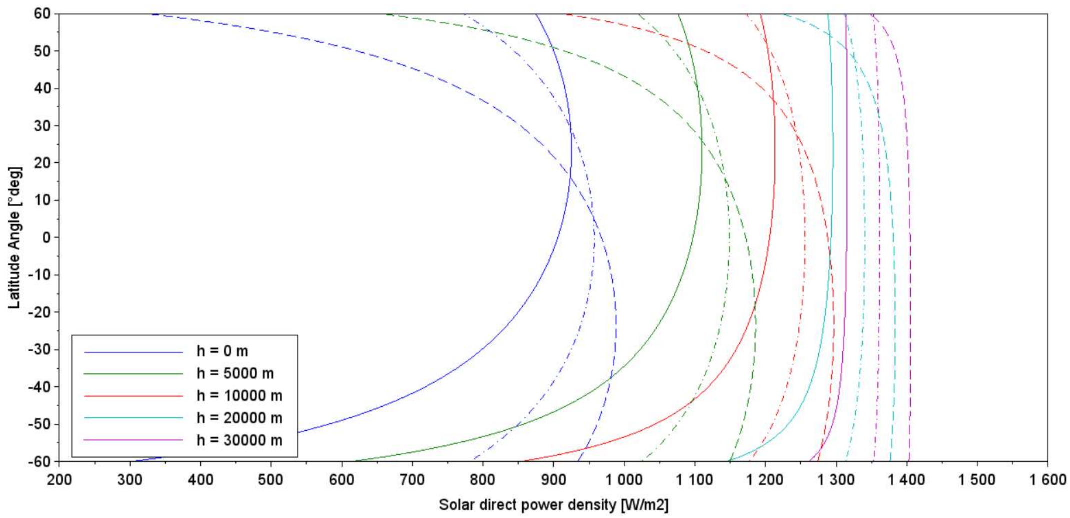

Figure 11: Typical curve of solar direct power density as function of latitude and altitude

The graph above considers a specific time of day ($t = 12\ h$, noon). The solid lines represent the solar direct power on June 21st, the dotted lines represent the solar direct power on December 21st and the mixed dotted lines represent the intermediate values on March 21st.

The solar power density increases with the altitude as well as with the latitude itself. Each curve at every day of the year presents a maximum value that moves as function of the day of the year. For example, the maximum value for the solid lines is located at $23.45°$ of latitude and is due to the declination angle. This is because in the graph for the solid lines is defined at June 21st when the declination angle is at its maximum (23.45°). The same logic can be seen for the dotted lines representing December 21st: in this case the maximum is located at $-23.45°$. In the case of the curves at Spring's solstice, the maximum value of solar density is at a latitude of 0° (since the declination angle is be 0° on this day).

These considerations have an impact in the calculations that follow in the next chapters.

3.2.2 Diffusion

An approximated formula from [1, Eq. 3.13] is considered in this model for the diffusion. The diffusion is considered as a small contribution (8%) of the direct radiation, and the approximation of having the diffusion radiated from all direction is also present. From Figure 9, it is possible to see that this is not correct, since diffusion does depend on the direction. However, since the contribution of diffusion is very limited compared to the direct radiation, this approximation is considered acceptable. Moreover, the diffusion is also considered as dependent of the altitude, which is included as ratio of pressures, with reference to sea level:

$$\varepsilon_{dif} = 0.08 \cdot \varepsilon_{dir} \cdot \frac{\rho}{\rho_0}$$

Therefore, it can be seen that the diffusive radiation reduces when the altitude increase, having ultimately a value of zero when outside the atmosphere.

A similar graph to Figure 10 can be created for the diffusive flux as well:

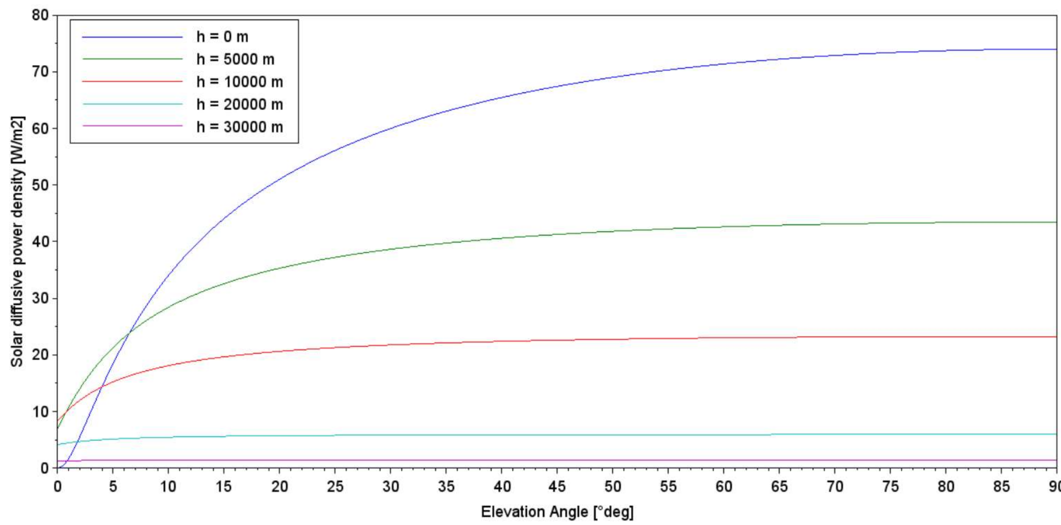

Figure 12: Solar diffusive power density as function of elevation angle

It is clear from Figure 12 that the higher the altitude, the lesser the value of the diffusion, since the pressure ratio lowers with the increasing of altitude.

Therefore, for each specific day of the year and for a specific position and orientation on Earth (given by latitude, azimuth and tilt angles), the contribution of diffusive power to the total power density received by an object varies. The table below shown values calculated at specific altitudes. The day of the year is fixed and considered as June 21st, where the maximum direct and diffusive flux occur:

Altitude [m]	Solar direct power [W/m2]	Solar diffusive power [W/m2]	% Power ratio (diffusive / direct)
0	845.23	67.62	8.00%
5,000	1022.26	40.03	3.91%
10,000	1122.53	21.52	1.92%
20,000	1202.58	5.52	0.46%
30,000	1222.89	1.35	0.11%

Table 4: Comparison between direct and diffusive solar flux

Since the direct power flux increases with the altitude, where the diffusive flux decreases, it is possible to see that the contribution of the diffusive flux compared to the direct one becomes negligible. Even at very low altitudes, the diffusive flux is one order of magnitude smaller than the direct flux. Although the diffusive power is included in all the calculations, it is possible not to consider it without incurring in a big error: this simplification is even more valid at high altitudes.

3.2.3 Reflection

This parameter can be expressed as function of the direct flux as well as the albedo, among other variables. The relation is as follow:

$$\varepsilon_{ref} = \frac{1}{2}[(\varepsilon_{dir})_{h=0} \cdot \sin\xi + (\varepsilon_{dir})_{h=0} \cdot 0.08] \cdot \beta \cdot (1 - \cos i)\left[1 + \sin^2\left(\frac{\psi_Z}{2}\right)\right] \cdot |\cos(r - \omega)|$$

The albedo β depends on the type of terrain and which materials are present. Therefore, it is very difficult to specify it, particularly when the type of terrain or terrain characteristics vary, such as during a flight. For this reason, a constant value of 0.2 is considered as an indicative average value. However, a shown in the formula above, the albedo can still vary with the day of the year, therefore it still depends on the distance between Earth and Sun.

The albedo can be approximated by the following formula:

$$\beta = 0.2 \cdot \left\{1 + \cos\left[\frac{2\pi}{365} \cdot (n + 10)\right]\right\}$$

Since the reflection component to the solar flux is very low compared to either the direct flux and the diffusive flux, the reflection is not included in the model and therefore its contribution is conservatively set to a value of zero.

3.2.4 Total radiation from the sun

Summing the three types of flux we obtain:

$$\varepsilon_{in} = \varepsilon_{dir} + \varepsilon_{dif} + \varepsilon_{ref}$$

As already mentioned, in the following Chapters and calculations, the contribution of the power density derived from reflection ε_{reef} will be considered negligible, thus:

$$\varepsilon_{in} \approx \varepsilon_{dir} + \varepsilon_{dif}$$

As it can be seen in Figures 10, 11 and 12, the higher the altitude, the higher the solar density. Moreover, the curve tends to become flat and less dependent on the time of day. It also asymptotically tends to the value of the solar flux in outer space. For usual flight altitudes, the curve is relatively flat with a constant value of solar flux around $1200 - 1250\ {}^{W}/_{m^2}$.

4. Solar cells and TEG modules

4.1 Solar cells

Solar cells are devices that produce electric current by conversion of solar energy. Solar cells are widely used in space applications because of the availability of solar power for extended periods of time.

A solar cell is made of wafers of semiconductors, typically built in layers to achieve better performances when compared a single layer cell. These multi-layer cells are more expensive but can offer higher values of efficiency, since each layer can capture specific wavelength regium of the solar spectrum.

Different types of solar cells exist, depending on the material used for their construction, the production process, etc. Silicon is widely used, thanks to his abundance on the planet. Depending on the type of crystal used, solar cells can be divided in three different groups [11]:

- Monocrystalline: pure semiconducting material is used, giving high efficiencies at the expense of high costs
- Polycrystalline: are made of different crystal structures in different sizes, giving more affordable production cost at the expense of their efficiency
- Amorphous: a thin layer of silicon film is deposited on a supporting material (glass or other substrate). The advantage is that the solar panel made from these cells can be shaped in various form or it can be adapted to a structure. Production costs are low and efficiencies are not high as well.

This paragraph has not the scope to provide an exhaustive and detailed information on solar cells, but merely the purpose to provide the background information on the parameters and variables of a solar cell used in this work.

4.1.1 The Air Mass

As the solar light passes through the atmosphere, it is attenuated by scattering and absorption phenomena. The more atmosphere the light passes through (therefore the closer the light comes to the ground) the more attenuated it is. This is because the atmosphere absorbs certain wavelengths of the sunlight and consequently varies the amount of wavelength that reaches the surface of Earth. By the time the light reaches the ground, it is confined between the infrared and the ultraviolet band of the spectrum. The reference of the solar irradiance at the top of the atmosphere is defined as $AM0$ (Air Mass 0), while is defined as $AM1.5$ when it is referenced at sea level.

Figure 3 [1] shows the different wavelengths and radiations for $AM0$ and $AM1.5$. An ideal solar cell would be able to absorb the light from the entire spectrum, and therefore having an efficiency of 100%. In reality, only a part of the spectrum is absorbed, hence the use of different layers of semiconductors, to increase the wavelengths that can be absorbed.

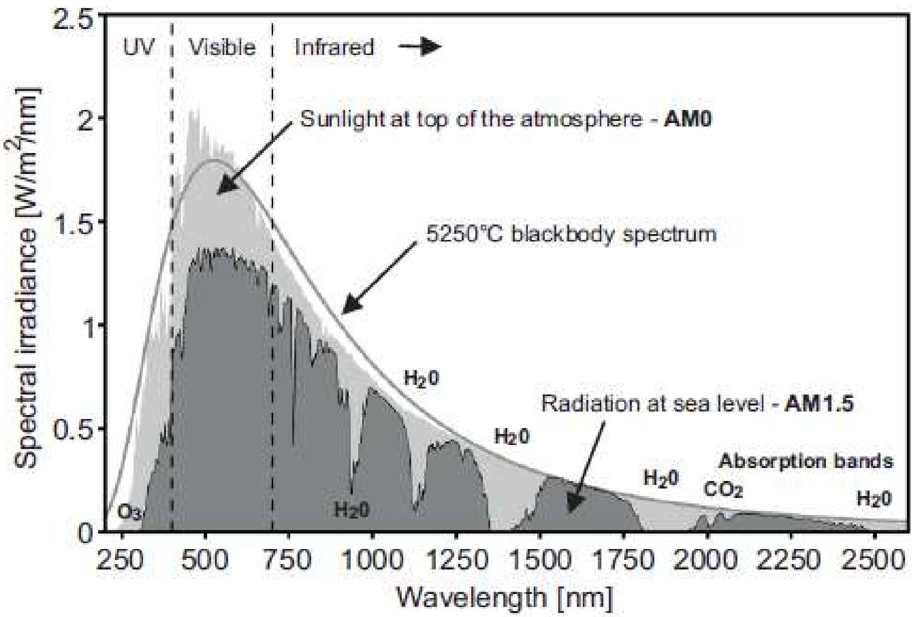

Figure 13: Spectral irradiance through the atmosphere

In general terms, the Air Mass (AM) can be defined as the ratio between a path length L through the atmosphere and the solar path length at zenith angle at sea level L_0:

$$AM = \frac{L}{L_0}$$

Since the term L_0 can be expressed as $L_0 = L \cdot \cos \psi_Z$, the Air Mass can be calculated, as a first approximation as:

$$AM \approx \frac{1}{\cos \psi_Z}$$

The term ψ_Z indicates the solar zenith angle and it is introduced in more details in paragraph 2.3.3.

More accurate formulas for AM have been proposed, in particular to include the curvature of Earth's surface. In addition to this, altitude has also an effect on the Air Mass, as the atmosphere gets less dense by increasing the altitude. Therefore, in the model, a formula proposed in [1] is considered:

$$AM = \frac{p}{p_0} \cdot \{[\cos \psi_Z + 0.15 \cdot (93.885 - \psi_Z)]^{-1.253}\}^{-1}$$

The pressure ratio is then introduced as a measure of the altitude.

The formula below is valid for solar zenith angles in the range $0 \leq \psi_Z \leq 90°$, which is of use in the model since it does not limit other factors such as latitude, for example.

The panel efficiency is generally defined, according to standards, for an Air Mass value of $AM = 1.5$ and under a radiation flux of $1{,}000\ {}^{W}/_{m^2}$ [14-15].

4.2 Thermo-electrical generator

The thermo-electrical module (also called TEG module) is a two-way solid-state energy converter that can be used as a generator when it converts thermal energy into electric energy. One side of the module is exposed to high temperature (hot side) while the other one is at a lower temperature (cold side). The voltage generated in the module is directly proportional to the difference of temperature between the hot and the cold parts [3]. The model uses formulas based on work [3] to derive the performances of a TEG module. Data for some of the variables are taken from datasheets of commercial products in the market [16-20].

Figure 14 shows the internal part of a TEG module.

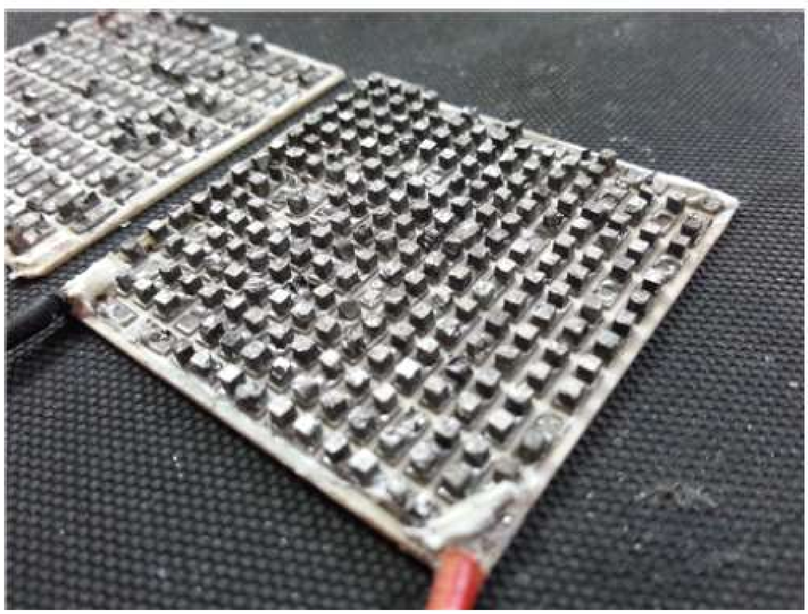

Figure 14: Internal view of a TEG module

The module is made of type $n-p$ semi-conductor pellets; the semiconductors are electrically connected in series to increase the generated voltage while they are in thermically connected in parallel to reduce the thermal resistance. Material for the top and bottom surfaces are made from ceramic materials, particularly to withstand high temperatures. The same surfaces can then be plated in order to increase the adhesion and connection performances between the structure a TEG module is installed on and the module itself.

Following [3], It is possible to represent the module like the thermo-electrical scheme in Figure 15 below.

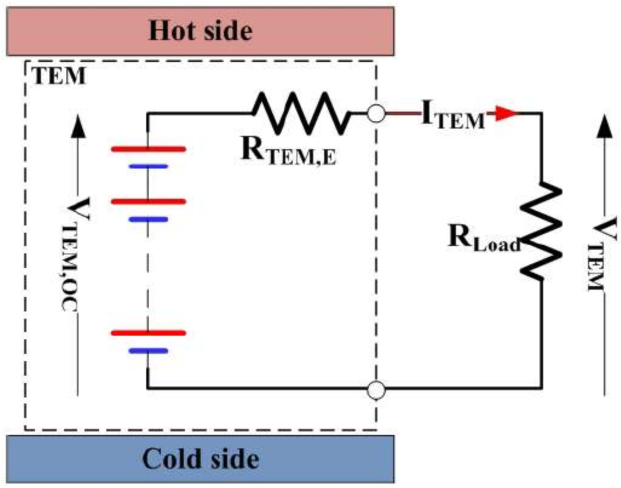

Figure 15: Schematic representation of a TEG module

In a TEM pellet pair, the following phenomena take place:

- Seebeck effect: generation of a difference of potential between two materials when there is a gradient of temperature
- Peltier effect: heat absorption or dissipation due to the flow of current through a junction of two materials
- Joule effect: heat generated by the current flow through a resistive element
- Thermal conduction effect: described the thermal conductivity (or resistivity) through a material

4.2.1 Seebeck effect

The Seebeck effect is responsible for the generation of the open-circuit voltage V_{OC}:

$$V_{OC} = \alpha_{TOT}(T_{hot} - T_{cold}) \tag{8}$$

Where the term α_{TOT} $[{}^{V}/_{K}]$ is the Seebeck coefficient.

Since the generation of the voltage happens in every couple of semi-conductors, the value of α_{TOT} can be defined as:

$$\alpha_{TOT} = N_{TEG}(\alpha_p - \alpha_n)$$

Multiplying the coefficient α by the total number of semiconductor couples N, leads to:

$$\alpha_{TOT} = N \cdot \alpha$$

4.2.2 Peltier effect

It is responsible for the generation of heat due to the current flow through different materials, can be written as:

$$Q = \alpha \cdot I \cdot T \tag{9}$$

4.2.3 Joule effect

The Joule's effect is described as:

$$Q = I^2 \cdot R_E$$

Where R_E indicates the electrical resistance of the module.

4.2.4 Internal heat transfer

The thermal conduction in a semiconductor can be expressed as a Fourier process:

$$Q_{p,n}(x) = -\frac{A_{p,n}}{\rho_{p,n}^{(t)}} \cdot \frac{dT_{p,n}(x)}{dx} \tag{10}$$

Where the terms $A_{p,n}$ and $\rho_{p,n}^{(t)}$ indicates the surface areas and the thermal resistivity of the semiconductors p and n respectively.

The incremental dx can be considered starting at 0 up to the length $L_{p,n}$ of the semiconductor p or n, therefore it is possible to rewrite Equation (10) as:

$$Q_{p,n}(x) \cong -\left(\frac{A_p}{\rho_p^{(t)} L_p} + \frac{A_n}{\rho_n^{(t)} L_n}\right) \cdot \Delta T = -\frac{\Delta T}{R_T}$$

The term R_T represents the thermal resistivity of the module.

In a pellet pair, the variation of heat is due to conduction and can be expressed by the differential equation:

$$dQ_{p,n}(x) = Q_{p,n}(x + dx) - Q_{p,n}(x) = I_{TEM}^2 \cdot dR_{p,n}^{(e)}(x)$$

Considering the Fourier's process and defining the temperature boundary conditions as:

$$T_{p,n}(0) = T_{hot} \quad ; \quad T_{p,n}(L) = T_{cold}$$

The conduction heat flow can be then expressed as:

$$\begin{cases} Q_p(0) = \dfrac{T_{ho} \ - T_{cold}}{R_p^{(t)}} - \dfrac{I_{TEM}^2 \cdot R_p^{(e)}}{2} \\ Q_p(L) = \dfrac{T_{hot} - T_{cold}}{R_p^{(t)}} + \dfrac{I_{TEM}^2 \cdot R_p^{(e)}}{2} \end{cases}$$

$$\begin{cases} Q_n(0) = \dfrac{T_{ho} \ - T_{cold}}{R_n^{(t)}} - \dfrac{I_{TEM}^2 \cdot R_n^{(e)}}{2} \\ Q_n(L) = \dfrac{T_{hot} - T_{cold}}{R_n^{(t)}} + \dfrac{I_{TEM}^2 \cdot R_n^{(e)}}{2} \end{cases}$$

Adding the Peltier effect from Equation (9) and referring to the total number of semiconductor pairs, the heat flow can be written as:

$$\begin{cases} Q_{hot} = \frac{T_{hot} - T_{cold}}{R^{(t)}} - \frac{I_{TEM}^2 \cdot R_{TEM}^{(e)}}{2} + \alpha \cdot I_{TEM} \cdot T_{hot} \\ Q_{cold} = \frac{T_{hot} - T_{cold}}{R^{(t)}} + \frac{I_{TEM}^2 \cdot R_{TEM}^{(e)}}{2} + \alpha \cdot I_{TEM} \cdot T_{cold} \end{cases} \tag{11}$$

4.2.5 Output values of a TEG module

The difference in heat flow between the hot and the cold side is equal to the electrical power generated by the TEG module:

$$P_{TEM} = Q_{ho} \ - Q_{cold}$$

The electrical power can also be expressed as:

$$P_{TEM} = V \cdot I = V_{OC} \cdot I - I^2 \cdot R_E \tag{12}$$

Dividing the expression by the current I_{TEM}, it is possible to find the value of the output voltage V:

$$V = V_{OC} - I \cdot R_E$$

Equation (12) is in a parabolic form, second-grade polynomial equation; therefore, the power has a parabolic curve dependance to the current and the voltage. The vertex of the parabolic curve gives the optimal (maximum) value of power for the specific associated voltage and current. Figure 16 shows a typical curve or power and voltage for a TEG module ([16], from product datasheet).

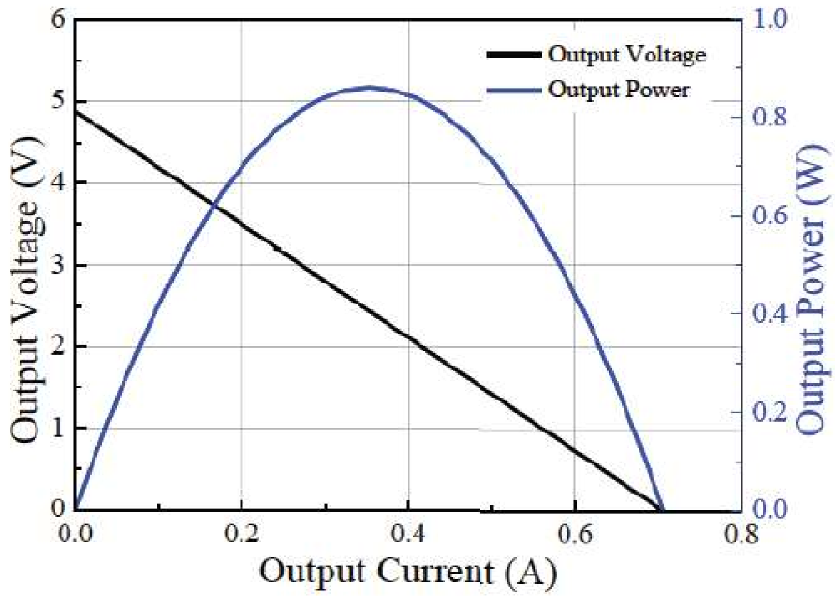

Figure 16: Typical voltage and power curves in TEG modules

When around the optimal points, the TEG module works at its optimal condition and theoretically according to the relations below:

$$I^* = \frac{V_{OC}}{2R_E}$$

$$V^* = \frac{V_{OC}}{2}$$

$$P^* = V^* \cdot I^*$$

$$\eta^* = \frac{P^*}{Q_{hot}}$$

The superscript * indicates that the associated variable is at optimal conditions.

The optimal conditions are achieved when the external resistance load matches the value of the internal resistance R_E.

4.2.6 TEG modules data

Datasheets of products available in the market consider values around the maximum power point of the TEG module. This is because the optimal conditions are the recommended working range of these products. Values such as I^* and R_E^* can be found in datasheets of TEG modules manufacturers.

Table 5 presents a list of some the TEG modules available in the market. These modules are commercially available solutions, not bespoke nor dedicated to aerospace applications.

They also have different ratings and different internal characteristics: for the scope of this work average values based on trendlines are considered. The values of the different variables vary with the temperature difference between hot side and cold side in the module.

Manufacturer	**Name**	ΔT $[°C]$	V_{OC} $[V]$	V^* $[V]$	I^* $[A]$	R_E^* $[\Omega]$
Custom Thermoelectric	1261G-7L31-04CQ	25	0.90	0.50	0.20	2.00
		50	1.95	1.10	0.40	2.14
		75	3.00	1.62	0.60	2.26
		100	3.95	2.15	0.77	2.37
		125	4.90	2.62	0.98	2.45
		150	5.80	3.10	1.08	2.57
		175	6.65	3.55	1.22	2.63
		200	7.50	3.97	1.32	2.70
		225	8.30	4.35	1.44	2.73
		250	9.00	4.72	1.52	2.78
	1261G-7L31-04CL	25	-	0.55	0.16	-
		50	-	1.10	0.23	-
		75	-	1.70	0.40	-
		100	-	2.25	0.56	-
		125	-	2.80	0.62	-
		150	-	3.35	0.70	-
TEG Pro	TE-MOD-1W2V-21S	50	1.40	0.70	0.12	5.50
		100	2.75	1.40	0.22	6.20
		150	4.20	2.10	0.31	6.60
		175	4.80	2.40	0.35	6.90
TCS	TCS-TEG	50	2.58	1.43	0.70	1.65
		100	5.17	2.73	1.10	2.22
		150	7.75	3.75	1.60	2.50
		200	10.34	5.00	2.00	2.67

Table 5: List of commercial TEG modules (continue)

Manufacturer	**Name**	ΔT $[°C]$	V_{OC} $[V]$	V^* $[V]$	I^* $[A]$	R_E^* $[\Omega]$
TEC	TEG2-07025HT-SS	50		0.60	1.10	-
		80		1.00	2.00	-
		100	2.60	1.30	2.20	0.50
		120		1.40	2.40	-
		150		1.80	3.00	-
		170		1.90	3.20	-
		180		2.00	3.40	-
Makerlab Electronics	126G-7L31-04CL	25		0.55	0.16	-
		50		1.10	0.23	-
		75		1.70	0.40	-
		100		2.25	0.56	-
		125		2.80	0.62	-
		150		3.35	0.70	-

Table 6: List of commercial TEG modules (end)

Values of V_{OC}, V^*, I^* and R_E^* (when available) from the TEG modules listed in Table 5 are plotted in Figures 17 to 20. This gives an indication of the trends of these variables with respect to temperature differences ΔT. Similar plots with curves divided by each TEG modules are listed in Appendix II for reference.

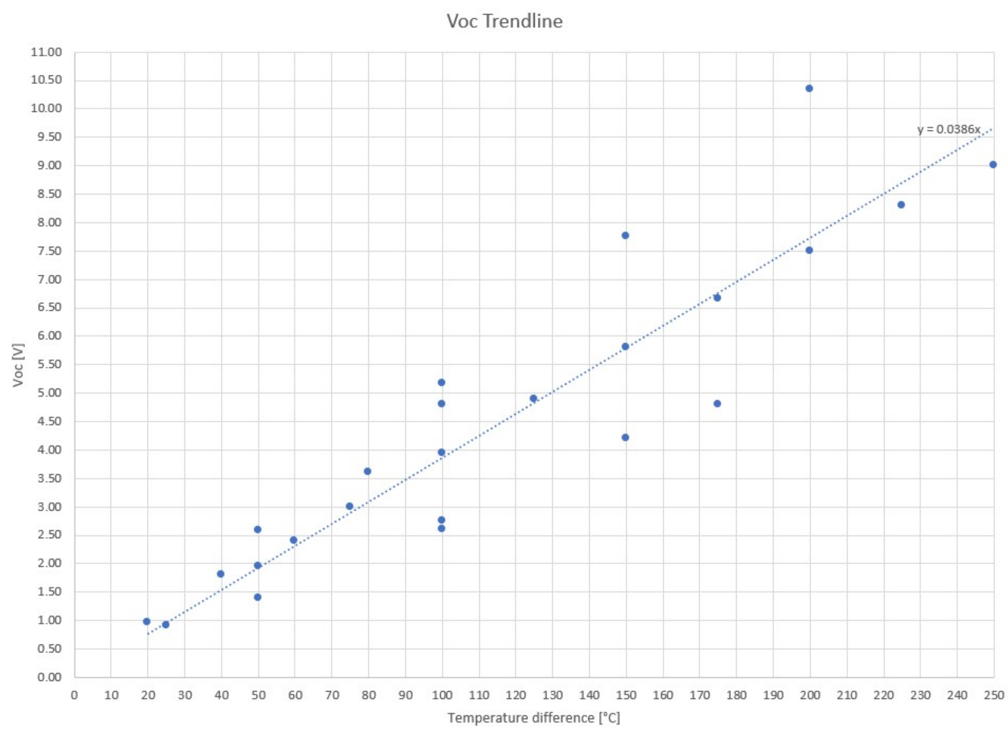

Figure 17: Open circuit voltage trendline

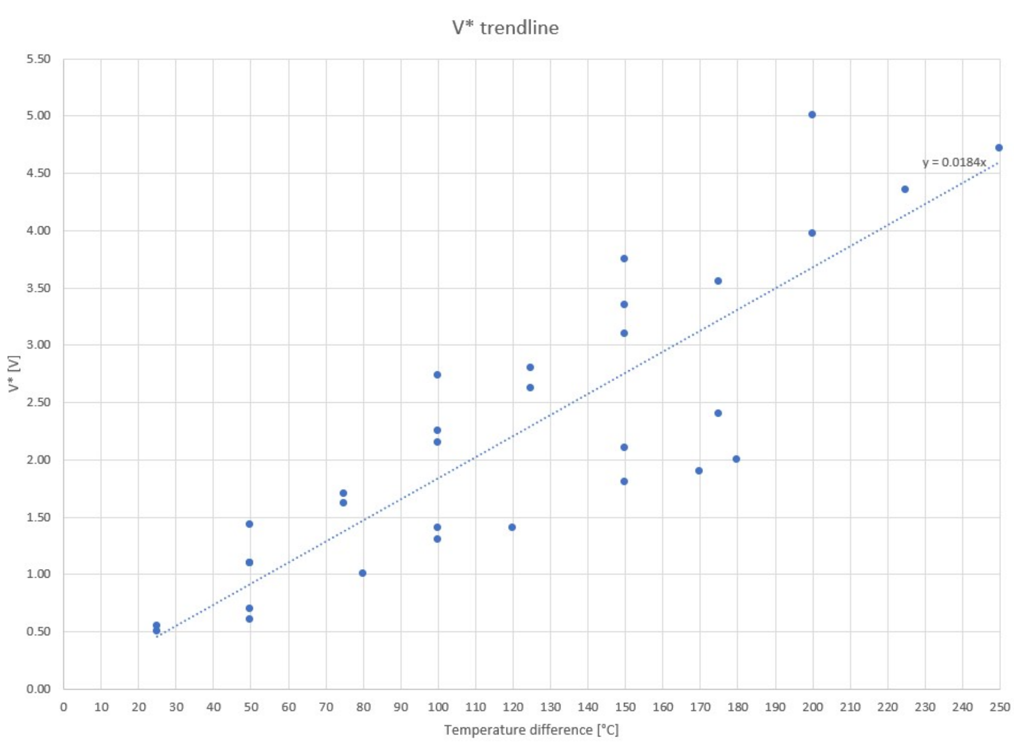

Figure 18: Voltage trendline

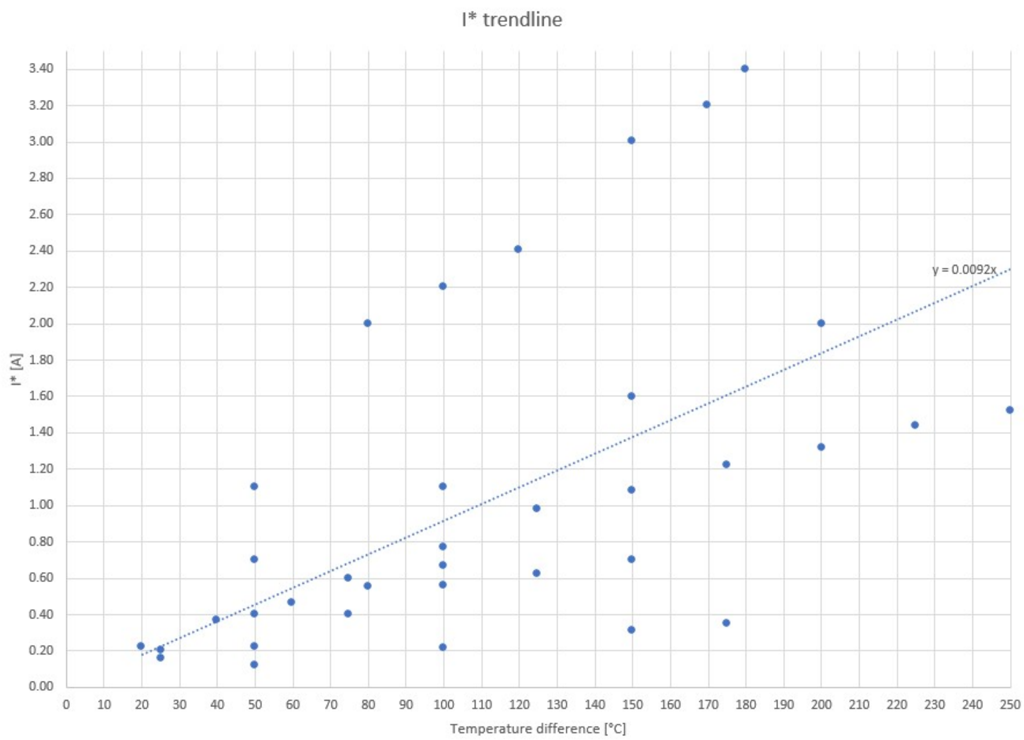

Figure 19: Current trendline

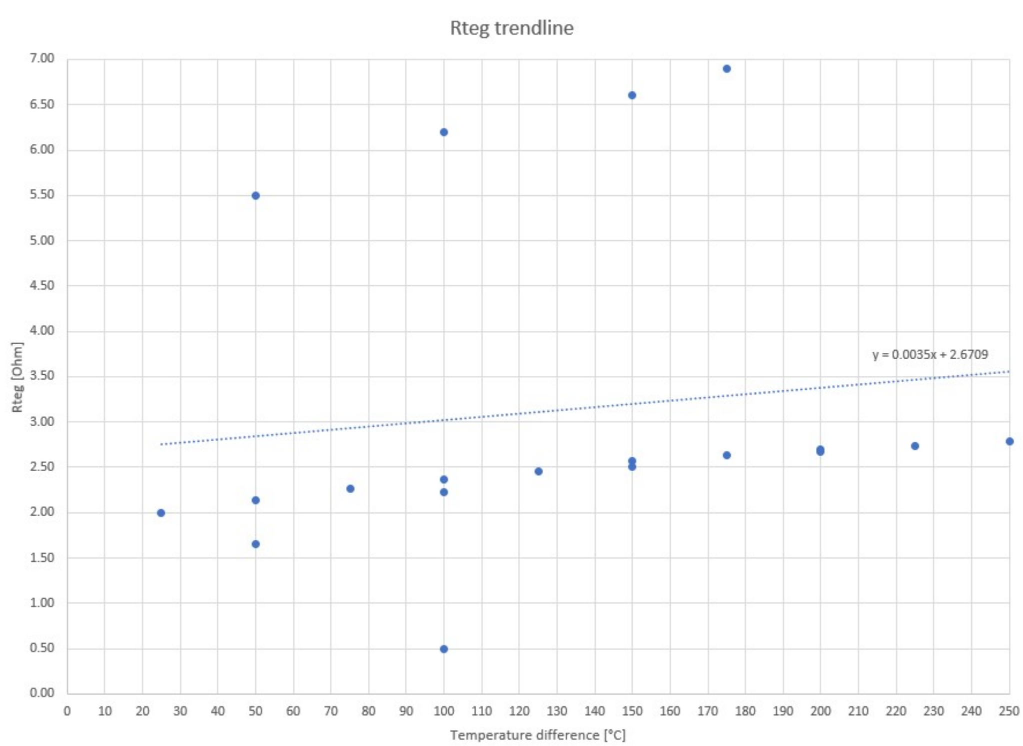

Figure 20: Resistance trendline

These trendlines are used in the model to consider the variations of current and resistance with respect to the temperature difference between the hot and cold sides. This temperature difference also depends on the altitude.

Based on the trend lines shown in Figures 19 and 20, it is possible to express the values of I^* and R_E^* as functions of $\Delta T = T_{hot} - T_{cold}$:

$$I^* = \tau_I \cdot (T_{hot} - T_{cold}) \tag{13}$$

$$R_E^* = \tau_{Ra} \cdot (T_{hot} - T_{cold}) + \tau_{Rb} \tag{14}$$

Based on the trendlines shown in Figures 19 and 20, the values of the constants τ_I, τ_{Ra} and τ_{Rb} are as shown:

$$\tau_I = 0.0092\ \frac{A}{K}$$

$$\tau_{Ra} = 0.0035\ \frac{\Omega}{K}$$

$$\tau_{Rb} = 2.6709\ \Omega$$

In addition, considering Equation (8) and trendline Figure 17, it is possible to statistically evaluate the Seebeck coefficient as:

$$\alpha_{tot} = 0.0386\ \frac{V}{K}$$

5. Description of the model

The model used for the calculations is based on the linearization of a 2-D wing profile (airfoil), starting from a known set of coordinates (x, y) that defines the profile curve itself. Each adjacent set of coordinates represents a discretization of the curved solar panel that lies directly on the profile. The panel curve is then represented by a spline of points that starts at defined coordinates (x_i, y_i) and ends at another defined set of coordinates (x_f, y_f). In the model, these arbitrary limits are specified at 10% of the chord length from the leading edge up to 80% of the chord length from the leading edge (20% of the chord length from the trailing edge). This to consider the panel limited in the central and more flatter area pf the top profile, and in an area where there is sufficient profile thickness to allow the installation of TEG modules. However, these values can be redefined, if necessary, allowing a wider surface for the panel.

Therefore, at each coordinates of the profile, the elements included in this model are:

- Solar panel: it is considered applied directly on the wing profile and it follows the geometry of the airfoil. The geometry of the solar panel is defined by the coordinates of the points on the profile
- TEG module: it is installed directly underneath the solar panel and it is considered a spot point defined at specific coordinates points of the profile. Multiple modules can be installed at different points along the airfoil profile
- Underneath the TEG module and the supporting structure, the space is supposed to be in calm air with a temperature of T_∞.

An adhesive epoxy can ensure the contact between the solar panel and the TEG module. A thermal paste can increase the thermal heat transfer as well. Both the epoxy and the paste are not considered in this model; thus, the heat is assumed to be transferred entirely from the panel to the module.

The solar cells are protected at the top and bottom faces by layers of insulating material.

The frame of the wing profile would support the panel and is supposed to ensure that structural reinforcements are applied around the panel and the module, in order to have the bottom face of the panel and the top face of the TEG module in contact with an adequate and constant pressure.

Figure 21 below shows a schematic representation of components considered in the model: it is a schematic representation of a portion of the profile, which is supposed to be linearized between two adjacent coordinate points.

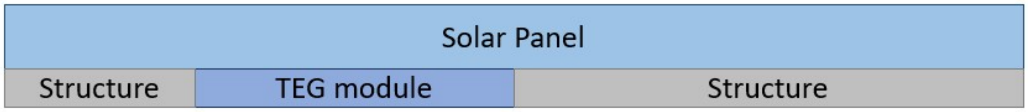

Figure 21: Schematic representation of the model

The input values for the model that depends on the airfoil geometry are as listed in Table 7.

Input	Notes	Values
Profile geometry	Using XFoil	Depending on profile
C_p data	Using XFoil	Depending on profile
N_{TEG}	Number of TEG semiconductors	199
Position of TEG modules	-	Depending on profile
λ_p	Coefficient of conductivity, panel	$0.25\ \left[\frac{W}{mK}\right]$
λ_s	Coefficient of conductivity, structure	$0.03\ \left[\frac{W}{mK}\right]$
d_p	Thickness of panel	Depending on profile
d_s	Thickness of the structure	Depending on profile

Table 7: Airfoil geometry inputs

For each altitude and for each point of the profile, the model evaluates the power balance in the system and provides the temperature values of the solar panel T_p, of the TEG module $T_h$and of the structure T_s. From these variables, it is possible to derive the exact values of power densities and the power generated by the TEG module.

A vector in the model defines the positions of the TEG module along the coordinates of the profile, allowing to add or reduce the number of TEG modules installed on the profile, as well as to change positions of the same along the profile.

5.1 Airfoil profile

As already mentioned, the model is designed for low airspeed; consequently, the calculation on the airfoil profile is done considering incompressible fluid. In this way we can consider Bernoulli's equation for the pressure around the profile:

$$p^0 = p + \frac{1}{2}\rho V^2 = p_\infty + \frac{1}{2}\rho_\infty V_\infty^2 \qquad (15)$$

Where p^0 indicates the total pressure. Considering the fluid as incompressible has the consequence of having the total pressure constant around the airfoil: this means that the value of the total pressure calculated in the unperturbed state (defined by p_∞, ρ_∞ and V_∞) will be the same around the profile.

Based on this principle, it is possible to define a coefficient of pression C_p:

$$C_p = \frac{p - p_\infty}{\frac{1}{2}\rho_\infty V^2} \qquad (16)$$

Substituting the values of p and p_∞ from Equation (15) into Equation (16), in case of incompressible flow, the expression of C_p can be written as:

$$C_p = 1 - \left(\frac{V}{V_\infty}\right)^2 \qquad (17)$$

In this way, knowing the value of C_p around the profile, it is possible to calculate the value of the local speed of the flow around the profile as well.

The angle of incidence of the profile α_i, defined as the angle between the direction of the air flow V_∞ and the cord of the profile, has an influence on the C_p, therefore:

$$C_p = C_p(\alpha_i)$$

Given the airfoil data, it is possible to use the coordinate of the curve modelling the top profile as the coordinate where the solar panel is installed. Since the profile is curved, it is more accurate not to simplify the panel as a flat surface. This as a direct influence on the tilt angle i: while on a flat solar panel the tile angle is constant, on an airfoil profile it varies along the curve of the top surface.

Based on the (x, y) coordinates of the points of the profile (defined along the cord direction and the thickness direction respectively) it is possible to calculate the curved length of the panel as shown in Figure 17:

$$l_p = c \cdot \sum_k \sqrt{(x_{k+1} - x_k)^2 + (y_{k+1} - y_k)^2}$$

For this specific case, the index k represents the counter for each relevant data point of the curve profile x_k.

5.2 Tilting angle

In a similar way it is possible to calculate the local tilting angle for each data point of the profile:

$$i_k = tan^{-1}\left(\frac{y_{k+1} - y_k}{x_{k+1} - x_k}\right) \qquad (18)$$

Since the geometry of the profile can rotate depending on the angle of incidence, the tilting angle can be generally expressed as a function of α_i.

Using commercially available software like XFoil, is possible to calculate the values of $(C_p)_x$ for each point of the profile: this allows to know the values of the airflow speed for each point of the profile $V(x)$, based on Equation (17).

Since an incompressible fluid is assumed, the model calculates the Mach number for each relevant point of profile:

$$M_x = \frac{V_x}{a_\infty}$$

And it verifies that is does not increase above $M_x = 0.3$.

In this model, the speed of the airflow is considered constant at every altitude, therefore the Mach number is a function of the altitude as well.

5.3 Reynolds, Prandtl and Nusselt numbers

Other important variables used in the model are Nusselt, Prandtl and Reynolds' numbers. Since the model calculates the numbers and the atmospheric variables for each altitude and position on the profile, the Reynolds and Prandtl numbers (and consequently the Nusselt number) are ultimately dependent on the altitude h an on the air speed around the profile:

$$Re_x = \frac{V \cdot x}{\nu_\infty}$$

$$Pr = \frac{\nu_\infty \cdot \rho_\infty \cdot c_p}{\lambda_{air}}$$

Nusselt number depends on the type of flow as well, whether it is a laminar flow or a turbulent flow. In this model, the equations used to calculate the Nusselt number are the ones for the flat plate. Therefore, the model approximates locally at each coordinate point the profile of the airfoil as a plate. From [2] the following local, averaged relations for Nu as function of Pr and Re can be used, depending on the type of flow.

- Laminar flow:

$$Nu_x = 0.664 \cdot \sqrt{Re_x} \cdot Pr^{\frac{1}{3}}$$

- Turbulent flow:

$$Nu_x = \left(0.037 \cdot Re_x^{\frac{4}{5}} - A\right) \cdot Pr^{\frac{1}{3}}$$

The term A is a coefficient that depends on the critical number of Reynolds $(Re_x)_{cr}$:

$$A = 0.037 \cdot (Re_x)_{cr}^{\frac{4}{5}} - 0.664 \cdot \sqrt{(Re_x)_{cr}}$$

These equations are valid in the range $0.6 \leq Pr \leq 60$.

This term is introduced to consider the transition between laminar to turbulent flow. The transition is defined by $(Re_x)_{cr} = 500{,}000$: if $Re_x \leq (Re_x)_{cr}$ the flow is laminar, if $Re_x > (Re_x)_{cr}$ then the flow is turbulent.

Knowing $V(x)$ is important for the calculation of Reynolds and Nusselt numbers:

$$Re_x = f[V(x)] \quad ; \quad Nu_x = g[V(x)]$$

As mentioned above, any airfoil profile can be used in the model, providing the data points of the geometry and the values of the coefficient of pressures on these data points. An important reminder is that the state of the fluid must be incompressible.

It is possible to consider the solar cells as continuously distributed along the profile or placed at specific coordinates along the profile itself.

6. Energy balance

The power each solar cell generates directly depends on the power that reaches the top surface of the panel. A certain amount of energy is then absorbed by the panel, while the rest is dissipated by irradiation, convection and conduction. With the installation of a TEG module, part of the conduction can then be converted in useful electric power.

The energy balance for the model can then be represented as in Figure 22 below:

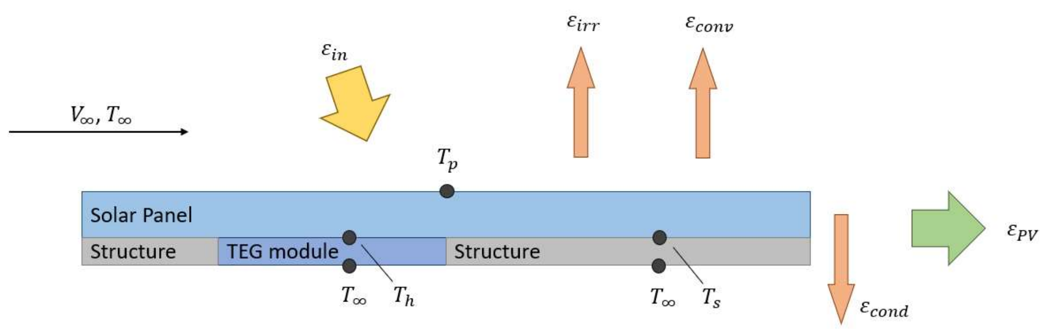

Figure 22: Energy flow around the panel

Therefore, the balance equation is given by:

$$\varepsilon_{in} = \varepsilon_{PV} + \varepsilon_{irr} + \varepsilon_{cond} + \varepsilon_{conv} \tag{19}$$

Where the term ε_{PV} defines the power density taken by the photovoltaic (panel) system, the terms ε_{irr}, ε_{cond} and ε_{conv} indicates respectively the power densities due to irradiation, conduction and convection. The unit of measure for the balance is $W/_{m^2}$.

A more detailed consideration on the conduction interface between the PV panel, the TEG module and the free air is mentioned in Paragraph 6.5 below.

6.1 Photovoltaic system

The power density of the solar panel can be calculated as directly proportional to the power density from solar radiation ε_{in} using the formula below [1]:

$$\varepsilon_{PV} = \eta_{PV} \cdot \eta_u \cdot \varepsilon_{in} \cdot \cos\psi$$

Where η_u indicates the percentage of the panel that is utilized, therefore exposed to sunlight. The term η_{PV} indicates the efficiency of the panel, which can be expanded as:

$$\eta_{PV} = \eta_{PV(AM)} \cdot \left[1 + \frac{d\eta}{dT}\left(T_p - T_{ref}\right)\right]$$

Where T_{ref} indicates the standard reference temperature at which the panel efficiency was measured, typically in laboratory test conditions at $25\ °C$.

This equation shows that the efficiency of the panel directly depends on the temperature.

The term ${}^{d\eta}/_{dT}$ indicates the variation in the panel efficiency, due to the variation in temperature and it decreases with the increasing of temperature. The panel efficiency is defined at laboratories standard conditions and is related to a standard air mass value of $AM = 1.5$.

To relate the efficiency to each value of Air Mass (and therefore to the altitude), it is possible to use the following the correlation formula as in [1]:

$$\eta_{PV(AM)} = \eta_{PV(1.5)} \cdot \left[1 + 0.007 \cdot (AM - 1.5) + 0.021 \cdot \ln\left(\frac{AM + 0.01}{1.51}\right)\right]$$

As it can be seen, for the reference value of $AM = 1.5$, the correlation gives back the measured efficiency value $\eta_{PV(1.5)}$.

6.2 Irradiation

The irradiation from the panel can be defined by the following formula:

$$\varepsilon_{irr} = e \cdot \sigma_B\left(T_p^4 - T_\infty^4\right)$$

Where e indicates the emissivity of the body (black body or grey body) and σ_B is the Boltzmann's constant, $\sigma_B = 5.67 \cdot 10^{-8}\ \frac{W}{m^2K^4}$.
The emissivity of the body is considered constant for the entire panel, while the values of T_∞ depends on the altitude and on the geometry of the profile, therefore:

$$(\varepsilon_{irr})_{x,h} = e\sigma_B\left[\left(T_p\right)_{x,h}^4 - (T_\infty)_{x,h}^4\right]$$

6.3 Conduction

Conduction is generated by the difference of temperature between the two sides of the panel. The heat flow by conduction is directed from the hotter surface to the colder surface. It also depends on the distance between the two surfaces.

Based on Figure 22, some parts of the bottom area of the panel can be considered covered by TEG modules. The area of the panel without TEG modules are considered attached to the supporting structure of the wing profile.

Each coordinate points of the profile can be used in the model as points where the TEG modules are attached to the panel: their position is defined by a vector with the same length as the vector of the coordinates of the profile.

The thickness of the bottom part of the profile may differs for each coordinate points, and it depends on the presence or not of the TEG module. Therefore, a vector defining the thickness at each coordinate points is defined. It has the same length as the vector defining the coordinate of the profile. Each value of temperature is also a function of the altitude.

For these reasons, the expression of heat by conduction for at a point x along the profile and at an altitude h can be expressed as:

$$(\varepsilon_{cond})_{x,h} = \lambda_p \frac{\left(T_p\right)_{x,h} - (T_{air})_{x,h}}{d_x}$$

The term λ_p is the thermal conductivity of the photovoltaic panel material. In this model, a fixed value of $\lambda_p = 0.25 \frac{W}{m \cdot K}$ is used, based on Teflon material. This value reflects an insulating material that supports the solar cells.

6.4 Convection

The convection is caused by the air flowing around the panel. In this model, free air convection is considered, and it is as well dependent on the coordinate of the profile and on the altitude. It can be calculated as [2]:

$$(\varepsilon_{conv})_{x,h} = (\alpha_{air})_{x,h} \left[\left(T_p\right)_{x,h} - (T_{air})_{x,h}\right]$$

The conductivity of air is defined as:

$$(\alpha_{air})_{x,h} = \frac{Nu_{x,h} \cdot (\lambda_{air})_{x,h}}{x}$$

The value of the thermal conductivity of air is defined in Equation (2).

6.5 Power density balance on the panel

Since the conduction depends on the geometry of the profile (and if the TEG module is present or not), the model calculates the power balance for each point of the profile. The two paragraphs below show the balance calculated in these two conditions.

In the equations in paragraphs 6.2, 6.3 and 6.4, the notation x, h indicating each step of coordinates and altitude is omitted for clarity. However, in the model, the equations shown in paragraphs 6.5.1 and 6.5.2 are calculated for each point of the profile and for each altitude level.

6.5.1 Coordinates where the TEG module is installed

On the coordinate where the TEG module is installed, the expanded balance Equation (10) is given as:

$$\varepsilon_{in} = \eta_{PV(AM)}\eta_u \left[1 + \frac{d\eta}{dT}\left(T_p - T_{ref}\right)\right] \varepsilon_{in} \cos\psi + e\sigma_B\left(T_p^4 - T_{air}^4\right) + \frac{\lambda_p}{d_p}\left(T_p - T_h\right) + \alpha_{air}\left(T_p - T_{air}\right) \tag{20}$$

This equation has two unknown variables, T_p and T_h. Therefore, to solve this equation, a second one in the same variables is necessary.

Considering the interface between the bottom surface of the panel and the TEG module, it is possible to assume that the heat generated by conduction in the panel is equal to the heat generated on the hot surface of the TEG module (which is assumed in direct contact with the panel):

$$S_{TEG} \cdot \varepsilon_{cond,TEG} = Q_h \tag{21}$$

From Equation (11) it is possible to expand the heat Q_h, thus Equation (20) above equals to:

$$S_{TEG} \cdot \frac{\lambda_p}{d_p} \cdot \left(T_p - T_h\right) = \frac{1}{R_T}\left(T_h - T_{air}\right) - \frac{1}{2} \cdot (I^*)^2 \cdot R_E^* + \alpha \cdot I^* \cdot T_h \tag{22}$$

Equations (20) and (22) represent a system with unknown variables T_p and T_h, which can be re-written in the form:

$$\begin{cases} AT_p^4 + BT_p + CT_h + D = 0 \\ ET_h^3 + FT_h^2 + GT_h + HT_p + L = 0 \end{cases} \tag{23}$$

All the coefficients and the unknown temperatures generally depend on the coordinate x and on the altitude h.

Based on Equations (20) and (22), the coefficients can be expanded as:

$$A = e\sigma_B$$

$$B = \eta_{PV(AM)}\eta_u \frac{d\eta}{dT} \varepsilon_{in} \cos\psi + \alpha_{air} + \frac{\lambda_p}{d_p}$$

$$C = -\frac{\lambda_p}{d_p}$$

$$D = -e\sigma_B T_\infty^4 - \eta_{PV(AM)}\eta_u \frac{d\eta}{dT} \varepsilon_{in} \cos\psi \, T_{ref} - \alpha_{air} T_\infty + \left[\eta_{PV(AM)}\eta_u \cos\psi - 1\right]\varepsilon_{in}$$

$$E = -\frac{1}{2}\tau_I^2 \tau_{Ra}$$

$$F = \frac{3}{2}\tau_I^2 \tau_{Ra} T_\infty - \frac{1}{2}\tau_I^2 \tau_{Rb} + \alpha_{tot}\tau_I$$

$$G = \frac{1}{R_T} - \frac{3}{2}\tau_I^2 \tau_{Ra} T_\infty^2 + (\tau_I^2 \tau_{Rb} - \alpha_{tot}\tau_I) T_\infty + S_{TEG} \frac{\lambda_p}{d_p}$$

$$H = -\frac{\lambda_p}{d_p}$$

$$L = \frac{1}{2}\tau_I^2\tau_{Ra}T_\infty^3 - \frac{1}{2}\tau_I^2\tau_{Rb}T_\infty^2 - \frac{T_\infty}{R_T}$$

System Equation (23) is non-linear and consists of two polynomial equations with two unknown variables, T_p and T_h. It is possible to numerically solve it by using Newton's method, defined for a multi-variable system. In a general form, this method calculates the values of the general variable s at each iteration k:

$$s^{(k+1)} = s^{(k)} - J_f^{-1}\left[s^{(k)}\right] \cdot f\left[s^{(k)}\right] \quad k \geq 0$$

Where $\{s\}$ represents the vector of the variables, $\left[J_f\right]$ the Jacobian matrix and $\{f\}$ is the vector of the functions evaluated in s.

Therefore, the model solves the system for each value of altitude h and coordinate point x and gives the values of $T_p(x,h)$, $T_h(x,h)$ and $T_s(x,h)$. The following steps describe the part of the code that solves system Equation (23) and are valid for each coordinate point x along the solar panel.

Step 1

- The iteration counter is set to 0: $k = 0$
- A maximum number of iterations k_{max} is defined
- A tolerance level is defined: $tol = 1 \cdot 10^{-6}$
- The guessed values of T_p and T_h for $k = 0$ are initialized: $T_p^{(0)} = T_\infty$, $T_h^{(0)} = T_\infty$

Step 2

- A `while` operation cycle is defined to iteratively solve system Equation 14 until $k > k_{max}$ and $err > tol$. The variable that calculates the error err is defined in step 4
- For each iteration k, the code evaluates the functions:

$$f_p^{(k)} = A\left[T_p^{(k)}\right]^4 + BT_p^{(k)} + CT_h^{(k)} + D$$

$$f_h^{(k)} = E\left[T_h^{(k)}\right]^3 + F\left[T_h^{(k)}\right]^2 + GT_h^{(k)} + HT_p^{(k)} + L$$

And memorises these three functions into a vector b:

$$b = -\begin{Bmatrix} f_p^{(k)} \\ f_h^{(k)} \end{Bmatrix} \tag{24}$$

- For each iteration k, the code evaluates the Jacobian matrix:

$$J_f^{(k)} = \begin{bmatrix} \frac{df_p^{(k)}}{dT_p} & \frac{df_p^{(k)}}{dT_h} \\ \frac{df_h^{(k)}}{dT_p} & \frac{df_h^{(k)}}{dT_h} \end{bmatrix}$$

And for each step it memorizes the values in a matrix A:

$$A = J_f^{(k)} \tag{25}$$

Step 3

- For each iteration k, the code solves the linearized system with input from Equations (24) and (25):

$$A \cdot z = b \tag{26}$$

Where z is the solution vector containing the variables calculated by solving the linearized system Equation (26).

- The solution is then updated for the next iteration as:

$$\begin{Bmatrix} T_p^{(k+1)} \\ T_h^{(k+1)} \end{Bmatrix} = \begin{Bmatrix} T_p^{(k)} \\ T_h^{(k)} \end{Bmatrix} + \begin{Bmatrix} z_1 \\ z_2 \end{Bmatrix}$$

Step 4

- The error between the solution at iteration k and iteration $k+1$ is given by:

$$err = \left\| \begin{Bmatrix} T_p^{(k+1)} \\ T_h^{(k+1)} \end{Bmatrix} - \begin{Bmatrix} T_p^{(k)} \\ T_h^{(k)} \end{Bmatrix} \right\| = \|z\|$$

- The iteration number is then updated to the next one: $k = k + 1$

After completing step 4, the code checks the conditions defined in the `while` operation: when those are not met, the cycle ends and provides the values of $\left(T_p\right)_{x,h}$ and $(T_h)_{x,h}$.

6.5.2 Coordinates where the TEG module is not installed

In this case, the expanded Equation 10 has a different form since the power density from conduction is different due to the geometry of the profile and the lack of a TEG module installed underneath the solar panel:

$$\varepsilon_{in} = \eta_{PV(AM)}\eta_u \left[1 + \frac{d\eta}{dT}\left(T_p - T_{ref}\right)\right] \varepsilon_{in} \cos\psi + e\sigma_B\left(T_p^4 - T_\infty^4\right) + \frac{\lambda_s}{d_s}(T_s - T_\infty) + \alpha_{air}\left(T_p - T_\infty\right) \tag{27}$$

Equation (27) has two unknown variables, T_p and T_s. Therefore, also for this case, a second equation is necessary to solve it. The new equation is given by the equivalence between the conductive heat generated in the panel and the conductive heat generated in the Aluminum structure:

$$\frac{\lambda_p}{d_p} \cdot \left(T_p - T_s\right) = \frac{\lambda_s}{d_s} \cdot (T_s - T_\infty) \tag{28}$$

Equations (27) and (28) represent a non-linear system, which can be written in the form:

$$\begin{cases} AT_p^4 + BT_p + CT_s + D = 0 \\ ET_s + FT_p + G = 0 \end{cases} \tag{29}$$

In this case, the expressions of the terms C, D, E, F and G are different from the ones of paragraph 7.5.1:

$$C = \frac{\lambda_s}{d_s}$$

$$D = -e\sigma_B T_\infty^4 - \eta_{PV(AM)}\eta_u \frac{d\eta}{dT}\varepsilon_{in}\cos\psi\, T_{ref} - \left(\alpha_{air} + \frac{\lambda_s}{d_s}\right)T_\infty + \left[\eta_{PV(AM)}\eta_u \cos\psi - 1\right]\varepsilon_{in}$$

$$E = \frac{\lambda_s}{d_s} + \frac{\lambda_p}{d_p}$$

$$F = -\frac{\lambda_p}{d_p}$$

$$G = -\frac{\lambda_s}{d_s}T_\infty$$

Coefficients A and B are the same as the ones defined in paragraph 6.5.1, while coefficients H and L are not present since Equation (29) is linear in T_p and T_s.

The solving process is the same as described in paragraph 7.5.1, but now the guess values to initialize the solution are $T_p^{(0)} = T_\infty$ and $T_s^{(0)} = T_\infty$. In addition, the evaluation functions $f_p^{(k)}$ and $f_s^{(k)}$ are:

$$f_p^{(k)} = A\left[T_p^{(k)}\right]^4 + BT_p^{(k)} + CT_s^{(k)} + D$$

$$f_s^{(k)} = ET_s^{(k)} + FT_p^{(k)} + G$$

And consequently, the vector b is defined as:

$$b = -\begin{Bmatrix} f_p^{(k)} \\ f_s^{(k)} \end{Bmatrix}$$

In this case, the Jacobian matrix is defined as:

$$J_f^{(k)} = \begin{bmatrix} \dfrac{df_p^{(k)}}{dT_p} & \dfrac{df_p^{(k)}}{dT_s} \\ \dfrac{df_s^{(k)}}{dT_p} & \dfrac{df_s^{(k)}}{dT_s} \end{bmatrix}$$

Again in this case, the linearized system to solve is in the form $A \cdot z = b$ and the vector of the solutions is now defined as:

$$\begin{Bmatrix} T_p^{(k+1)} \\ T_s^{(k+1)} \end{Bmatrix} = \begin{Bmatrix} T_p^{(k)} \\ T_s^{(k)} \end{Bmatrix} + \begin{Bmatrix} z_1 \\ z_2 \end{Bmatrix}$$

In this case the error is defined as:

$$err = \left\| \begin{Bmatrix} T_p^{(k+1)} \\ T_s^{(k+1)} \end{Bmatrix} - \begin{Bmatrix} T_p^{(k)} \\ T_s^{(k)} \end{Bmatrix} \right\| = \|z\|$$

After completing the iterative cycle, the code provides the values of $\left(T_p\right)_{x,h}$ and $(T_s)_{x,h}$.

7. Reference case study: HeliPlat®

The acronym HeliPlat® stands for HELIos PLATform and was a project lead by Politecnico di Torino to concept for the first European very long-endurance stratospheric unmanned air vehicle. The design is a monoplane with eight brushless motors and twin-boom tail type. The wings and wing profile was optimized to have the best possible aerodynamic efficiency.

In this Chapter, the airfoil profile of HeliPlat is considered and its coefficient of pressure (for given values of incidence) is calculated using external software programs such as XFoil. The airfoil profile designed for HeliPlat was the HPF-118 (11.8% thickness).

The inputs related to HeliPlat that are relevant to the calculations for the model are shown in Table 8 and Table 9.

Input Variable	Symbol	Value	Unit of Measure
Altitude	h	$17{,}000 - 20{,}000$	m
Day of the year	N	1st February to 30th November	-
Time of day	t	12 pm	h
Latitude	φ	36°-40°	°
Azimuth	θ	0° (South)	°
Panel absorption	ε	0.90	-
Efficiency variation of panel	$\frac{d\eta}{dT}$	-0.29%	$\frac{1}{K}$
Panel efficiency	$\eta_{PV(1.5)}$	22%	-
Panel utilisation	η_u	0.90	-
No. TEG modules	N_{TEG}	3	-
No. TEG pairs	N_{p-n}	199	-
TEG module area	S_{TEG}	$40 \cdot 40$	mm^2
TEG thermal resistance	R_T	49	$\frac{K}{W}$
Air speed	V_∞	20	$m/_s$

Table 8: Input data for the reference case (continue)

Input Variable	Symbol	Value	Unit of Measure
Thermal conductivity, panel	λ_p	0.25	$\frac{W}{m \cdot K}$
Thermal conductivity, structure	λ_s	0.04	$\frac{W}{m \cdot K}$
Angle of incidence	α_i	0°	°
$\frac{C_L^{\frac{3}{2}}}{C_D}$	-	36	-
Efficiency propulsion	η_{prop}	0.81	-

Table 9: Input data for the reference case (end)

The TEG modules are placed in three positions with respect to the airfoil profile, one in the front part of the profile, one at the centre and one at the end of the profile. This to verify whether there is a dependance of the position of the module with respect to the maximum power the module can generate. These positions do not represent any specific working configuration but are only for indication of single performances.

Based on the HeliPlat design, the material of the wing support structure is Rohacell®, therefore an average value of thermal conductivity for this material is considered, as listed in Table 9.

7.1 Geometry

The geometry for this reference case, based on HPF-118 profile is shown in Figure 23 below. The solar panel is supposed to be applied from 10% of x direction in the front to 20% of x direction from the trailing edge. This to have a sufficient variation in curvature of the profile to evaluate the impact of the profile itself on the performances of the TEG modules while ensuring sufficient room inside the profile structure to make the installation of e TEG module possible.

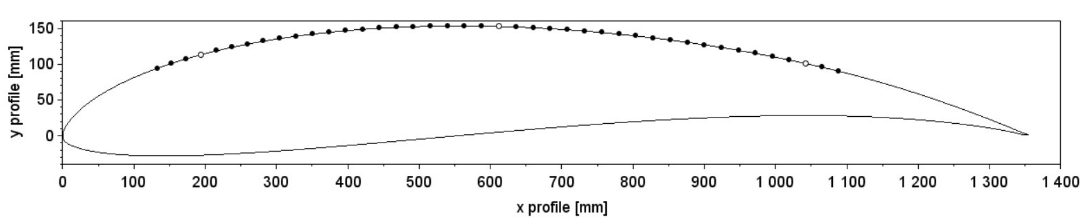

Figure 23: Reference geometry of the profile, HeliPlat®

A thickness of 1 mm for the panel (skin) is considered, isolating material on the solar panel is Teflon. The support structure underneath the panel is made in Rohacell®, its thickness is 5 mm. The TEG modules underneath the solar cells have a thickness of 3.5 mm, as listed in TEG module datasheets [17].

The black dots on the top part of the profile define the position and spline curve of the solar panel, while the three white dots indicate the positions of the TEG modules with respect to the solar panel.

Since the panel changes its curvature along the x direction, the tilting angle does also change accordingly. Using Equation (18) and applying it to this reference profile, the values in Figure 24 are found:

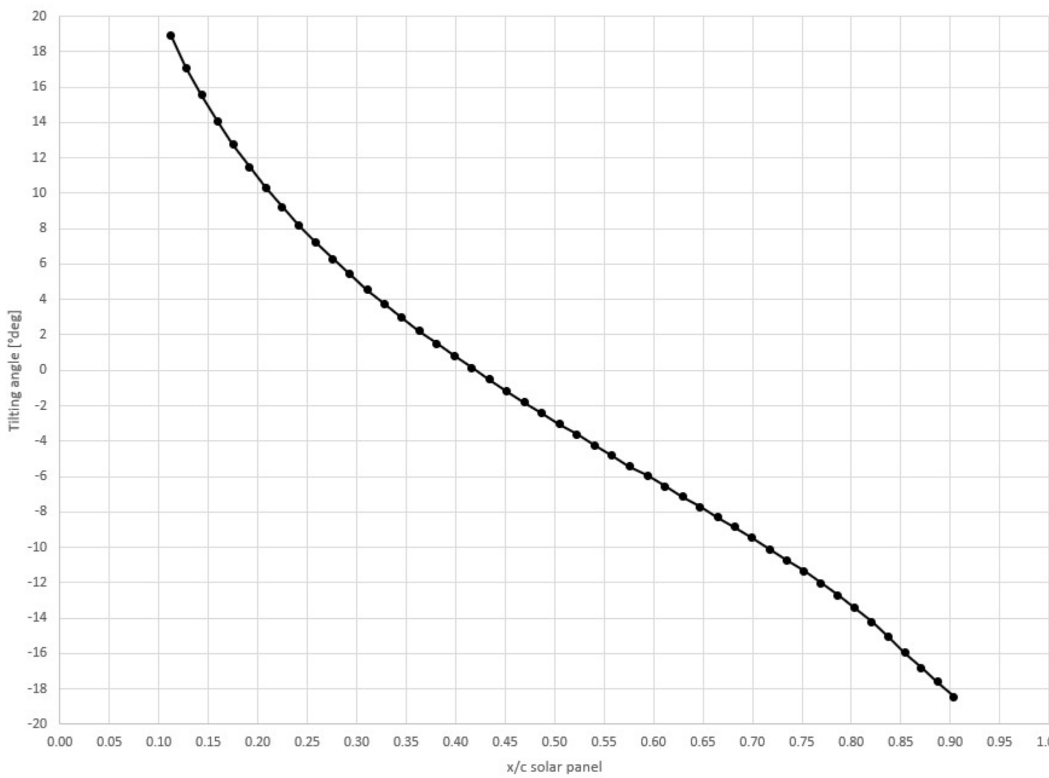

Figure 24: Tilting angle for solar panel on HPF-118 profile at 0° incidence

The azimuth angle has the effect of indicating the sunlight direction. The tilting shown in Figure 24 refers to a condition of flight towards the South direction. If a different direction is considered, the tilting angle referred to the direction of the sunlight will be different, up to a East or West direction where the coordinates on the wing profile will not see any appreciable difference in generated power along the profile.

.

7.2 Convergence of the model

The convergence of Newton's method described in Chapter 6 to solve Equations (23) and (29) is shown in Figure 25.

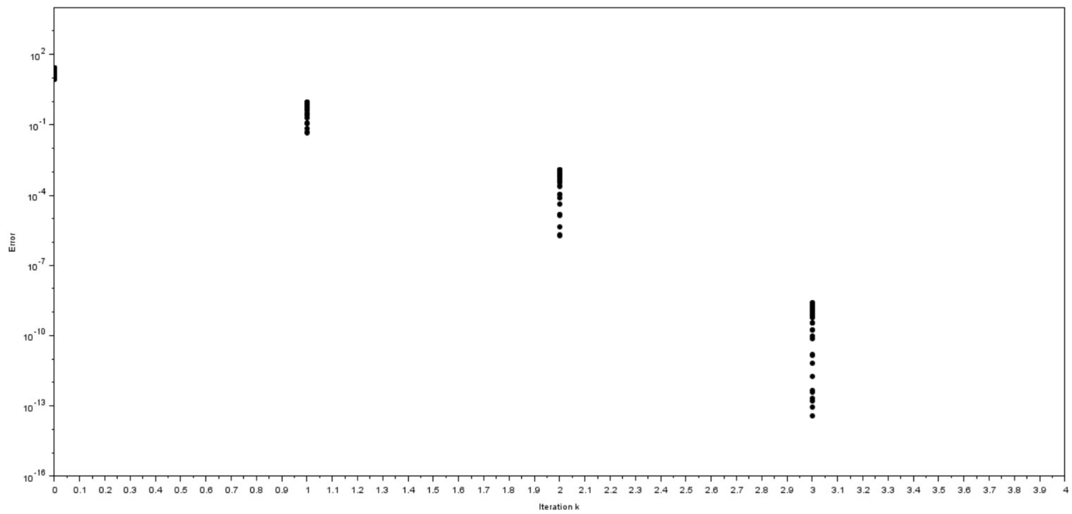

Figure 25: Convergence of the method

Each dot represents a value of the error at each coordinate of the profile and at each altitude level. The higher the iteration, the lower the error. The system converges after a maximum of four iterations.

In the model, the value of the error is set as:

$$err \leq 1 \cdot 10^{-6}$$

7.3 Error of the solution

Similarly to Figure 25 above, it is possible to represent the numerical error ϵ generated in solving Equations (20) or (27). The error is calculated as:

$$\epsilon = \varepsilon_{in} - (\varepsilon_{PV} + \varepsilon_{irr} + \varepsilon_{cond} + \varepsilon_{conv})$$

And it is shown for each coordinate points and altitude in Figure 26.

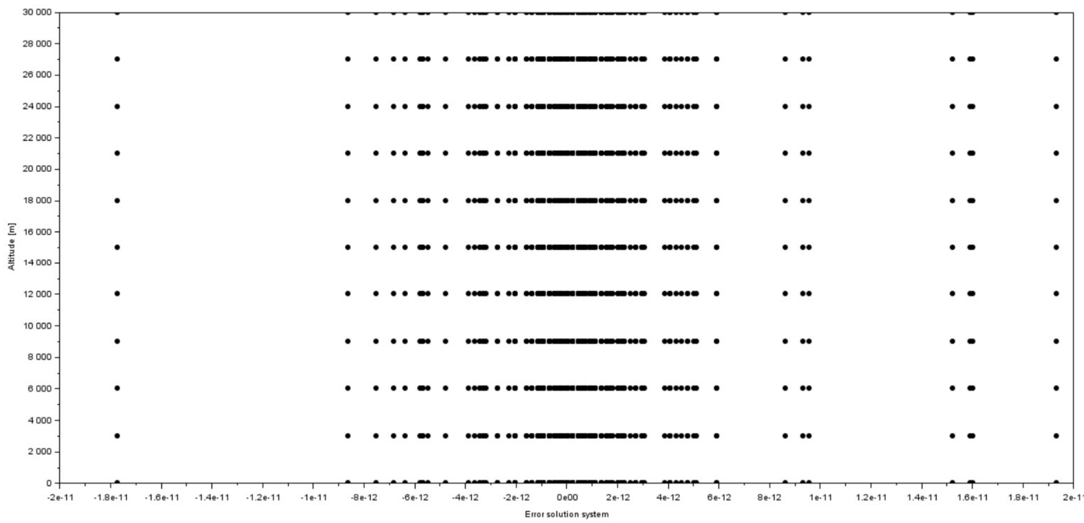

Figure 26: Numerical error for Equations (20) and (27)

Values are consistently low, with orders of magnitude in the range $-2 \cdot 10^{-1}$ to $+2 \cdot 10^{-11}$. The reason for measuring this error is to have a visual reference that the calculations are correct and that the values of the unknown temperatures do solve correctly the energy balance Equation (20) or (27).

7.4 Air speed on the profile

Given the profile and the air speed of the unperturbed state V_∞, using software such as XFoil allow to calculate the coefficient of pressure and therefore the air speed on each point of the profile.

The range of C_p values considered in the model are the ones located on the top profile, with starting and ending coordinates that match the one defined in the geometry of the panel (paragraph 7.1). A complete representation of the coefficient of pressure over the HeliPlat profile is given in Figure 27.

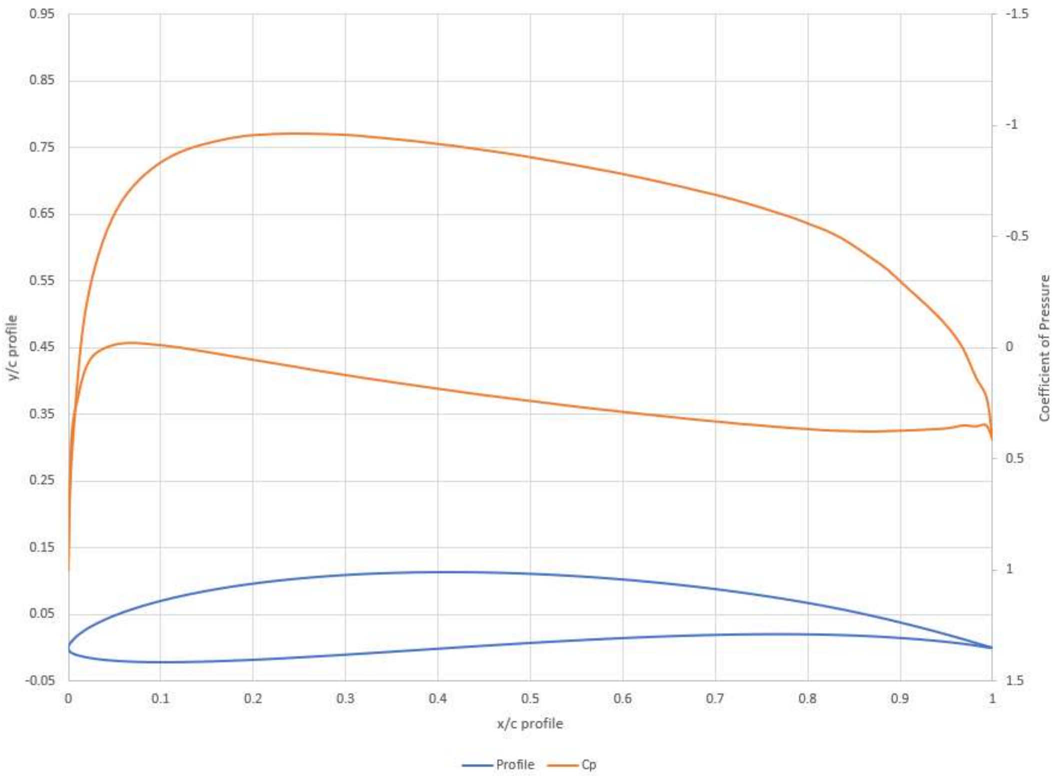

Figure 27: Coefficient of pressure on the HPF118 profile, α_i=0°

Using Equation (17) it is possible to derive the value of the air speed for each coordinate of the panel. The coordinates on the x directions are set from the first point closest to the leading edge to the last final points of the solar panel towards the trailing edge on the airfoil profile.

Since V_∞ is an input of the program and it is independent from the altitude, the air speed along the airfoil is also considered independent from the altitude, hence the model considers $V = V(x)$. However, the Mach number is influenced by the altitude since the speed of sound varies with h.

The speed profile for the portion of airfoil on which the solar panel is applied to is shown in Figure 28.

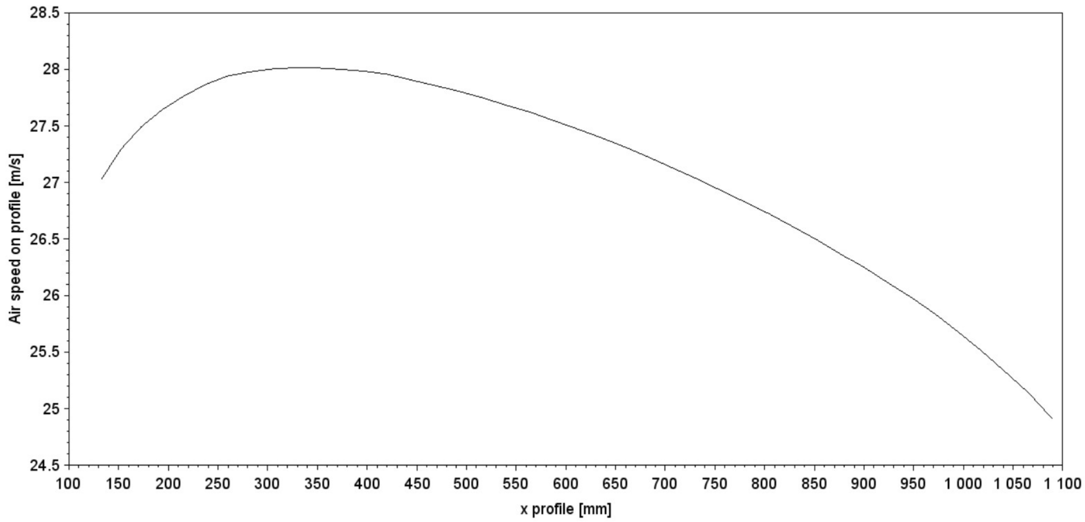

Figure 28: Air speed over the solar panel

7.5 Reynolds, Prandtl and Nusselt numbers

Based on the definitions in Paragraph 5.3, Reynolds and Nusselt numbers vary with both coordinates and altitude, while Prandtl number is only dependent to the altitude. Figures 29 to 31 below show the variations of the three numbers with respect to the coordinate points and altitude.

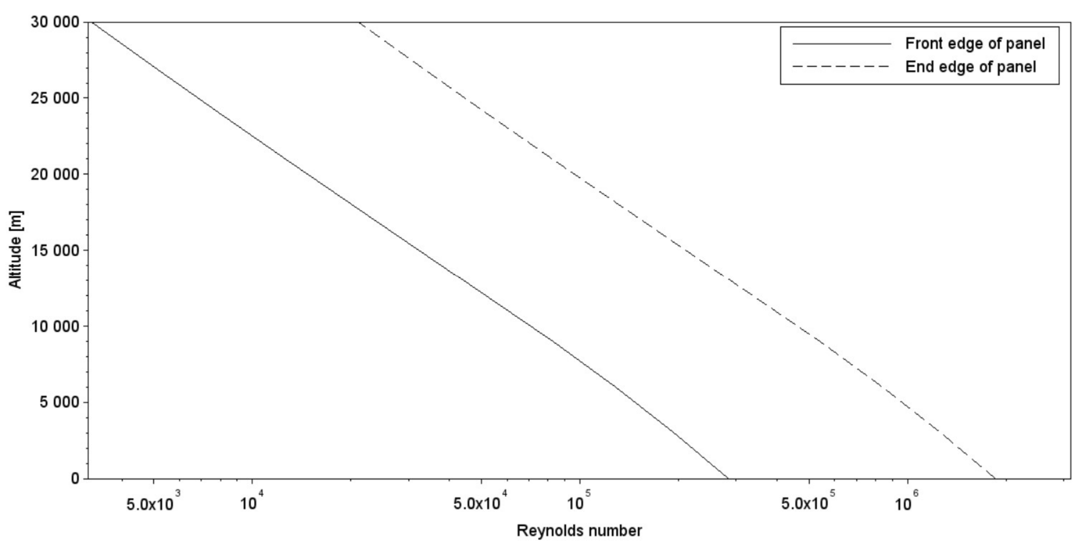

Figure 29: Reynolds number over the solar panel

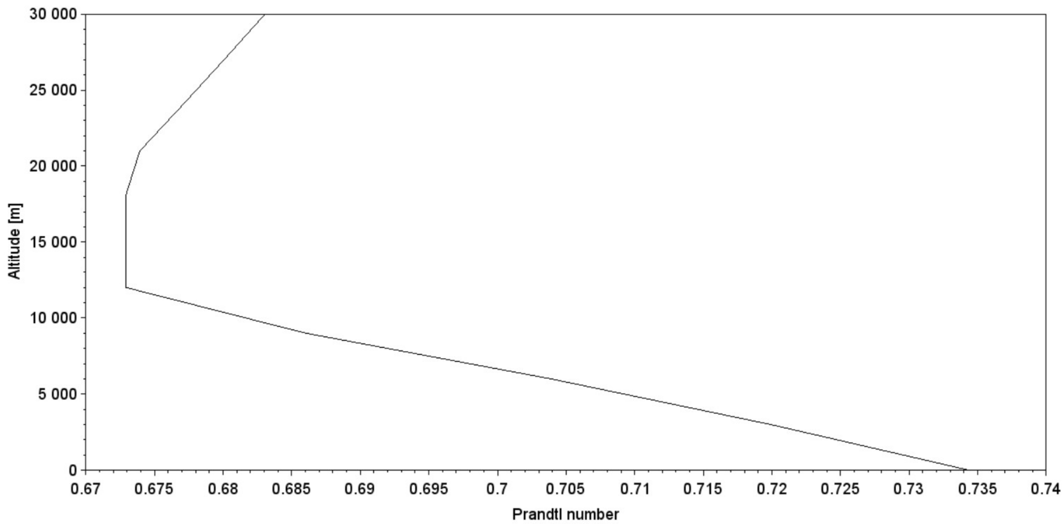

Figure 30: Prandtl number over the solar profile

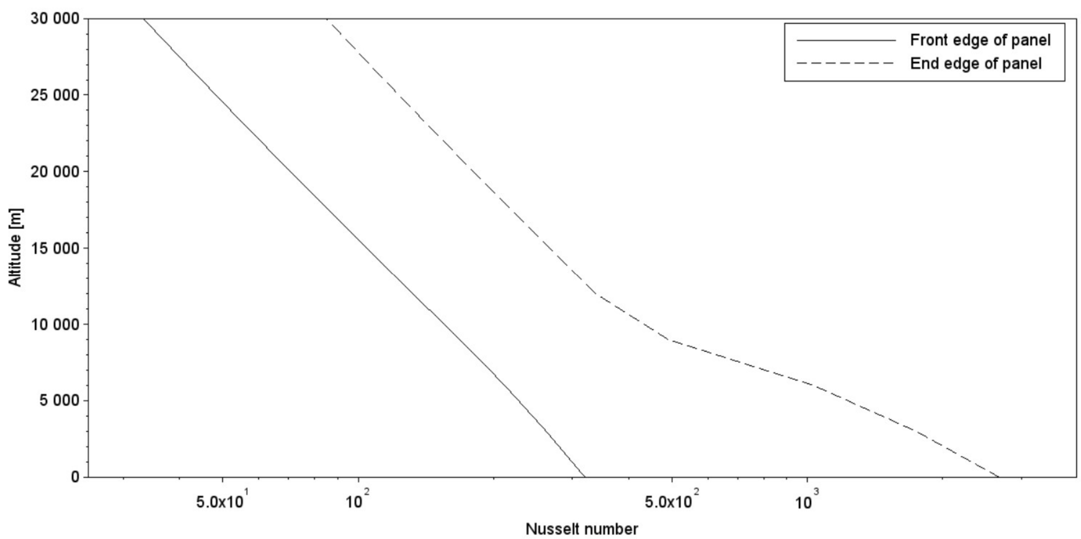

Figure 31: Nusselt number over the solar profile

For a given value of altitude, the Reynolds number and the Nusselt number increase with the coordinate positions along the profile, moving towards the trailing edge. In particular, since on the trailing edge of the profile the Reynolds number is greater than $500{,}000$, the flow is turbulent at altitudes up to $12{,}000\ m$. Above this altitude, the flow is laminar overall the entire airfoil profile. This can be clearly seen in the graph of the Nusselt number, for the curve related to the trailing edge.

7.6 Power densities

Solving system Equations (20) and (27) allows to determine the values of the power densities along the profile as well as for each altitude. Figures 32 and 33 below show the densities of each contributor to the power balance. The plots show the contribution of the useful photovoltaic power versus the other losses generated by radiation, conduction and convection as well as the values in $\left[{}^{W}/_{m^2}\right]$ of the same densities.

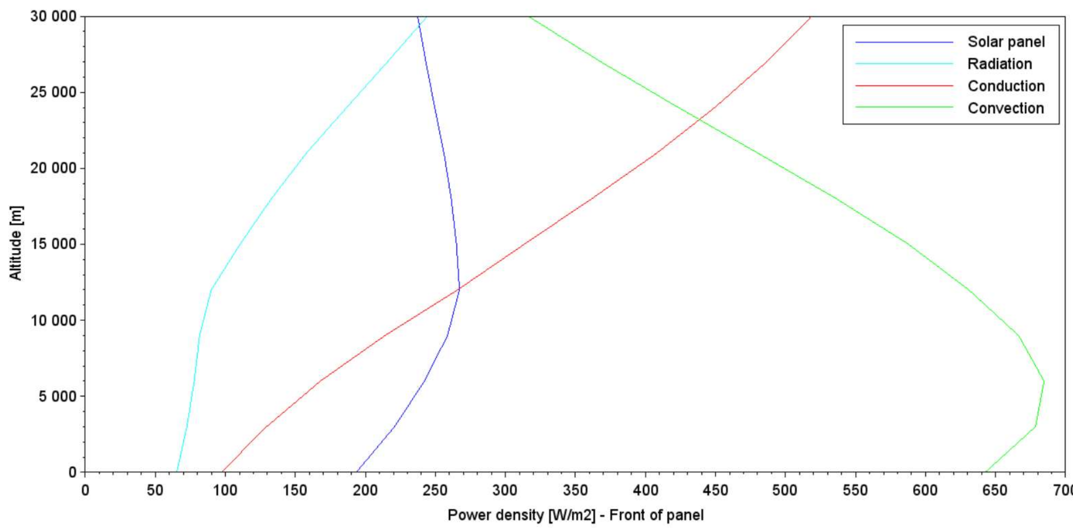

Figure 32: Power densities on the panel as function of altitude (front)

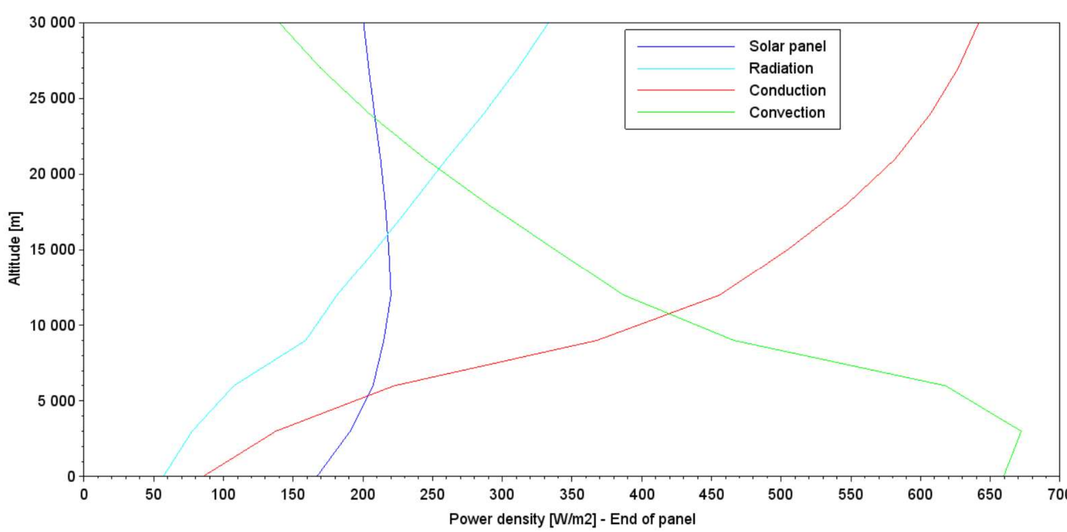

Figure 33: Power densities on the panel as function of altitude (end)

7.7 Calculated temperatures

Solving systems in Equations (23) and (29) leads to the temperature profiles as shown in Figure 34. Temperatures of the panel and the structures are generally higher than the temperatures of the TEG modules; this is also related to the material used in the HeliPlat wing profile. Changing the materials would have an effect on the temperature distribution between the panel and the TEG modules.

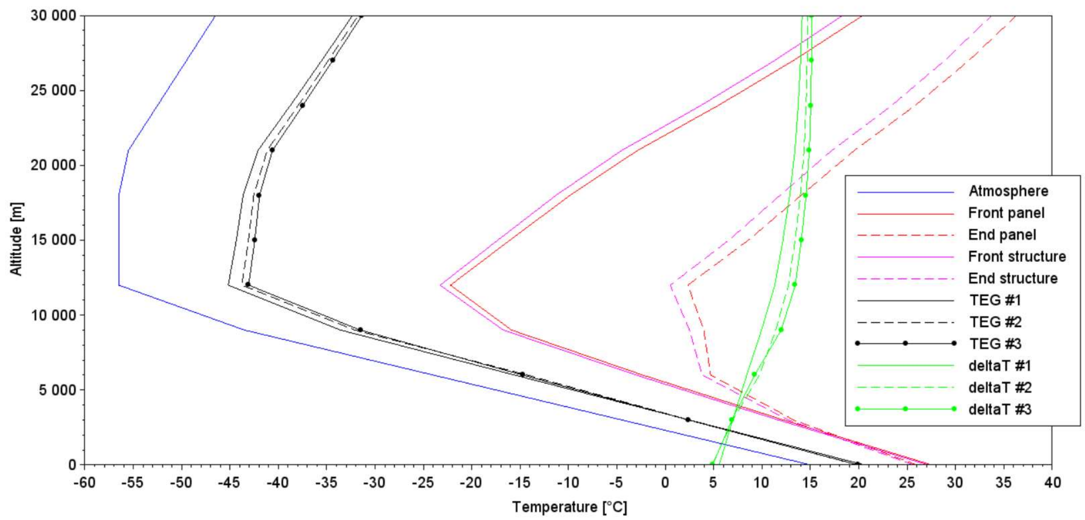

Figure 34: Temperatures on the solar panel

7.8 Power generated by the TEG module

As defined in Chapter 6, the power the TEG module generates is directly proportional to the ΔT value between the hot side of the module and the free air (cold side). The calculated power generated in the modules is shown in Figure 35. In the positions where the TEG module is not present, the power generated is therefore zero.

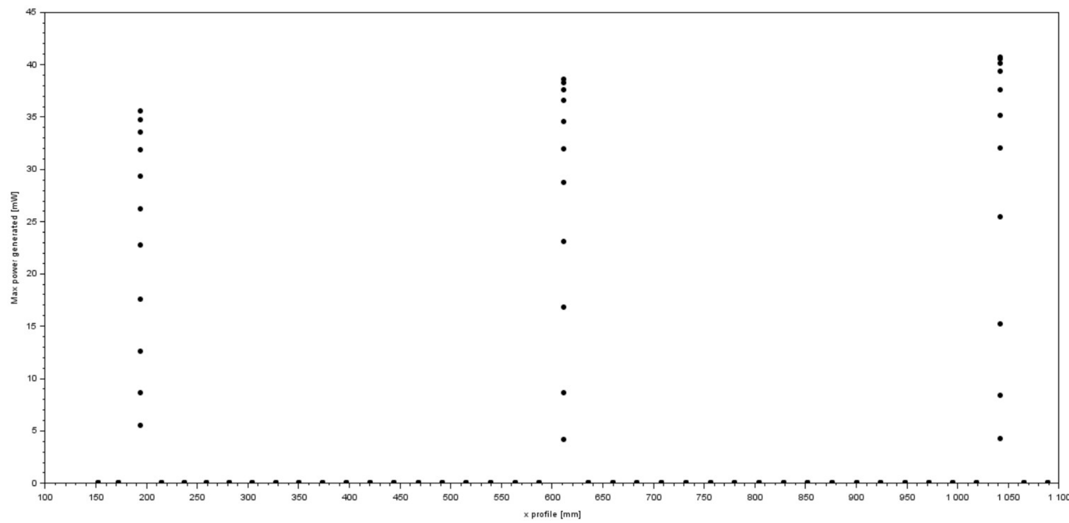

Figure 35: Power generated by the TEG module as function of position on the profile

As it can be seen from this reference case, the position of the TEG module on the profile has an influence: the last module installed at approximately at $1{,}050\ mm$ on the profile produces slightly more power than the one installed close to the leading edge. This can be explained considering the distribution of the power generated by conduction (Figures 33 and 34): the heat generated by conduction increases along the airfoil profile and this happens regardless of the position of the TEG module. Therefore, the more heat produced by conduction, the more power reaches the top hot surface of the TEG module and therefore the value of ΔT increases, leading to a higher power generated in the module. This consideration is valid if the heat is compared across the same altitude h.

Figure 36 shows the curves of the generated power as function of the altitude. The gain in generated power, calculated between TEG module #1 and TEG module #3 is also shown.

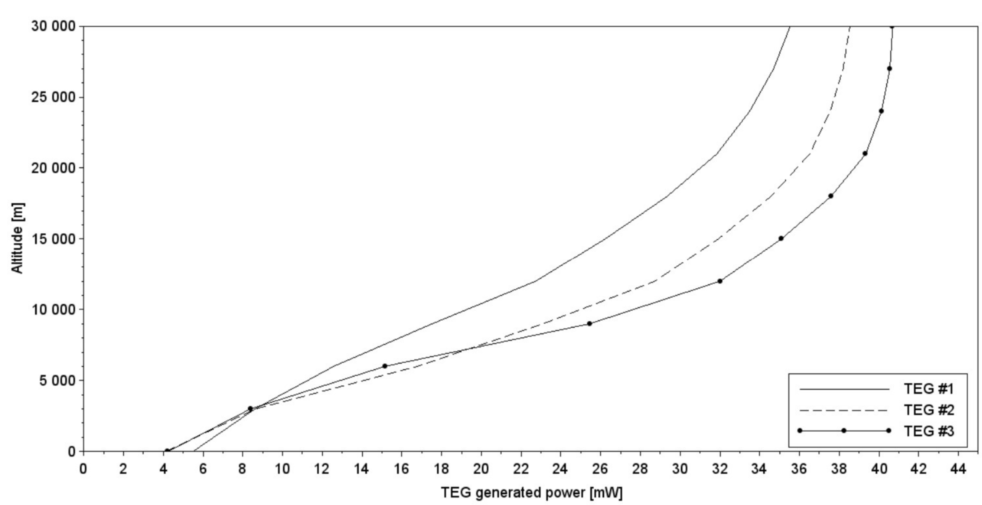

Figure 36: Generated power as function of altitude

When considering the power densities generated by the TEG module, they fall in the range between $2\ {}^{W}/_{m^2}$ and $25\ {}^{W}/_{m^2}$. These values are achieved considering the power generated by the TEG module and dived it by the surface of the module itself.

7.9 Required and available power

The required power necessary to maintain horizontal flight is given by:

$$P_{req} = S_w \cdot \sqrt{\frac{2}{\rho_\infty} \cdot \left(\frac{W_{tot}}{S_w}\right)^{\frac{3}{2}}} \cdot \left(\frac{C_D}{C_L^{\frac{3}{2}}}\right) \cdot \frac{1}{\eta_{prop}}$$

In case of HeliPlat, for an angle of incidence of $\alpha_i = 5°$, the term ${}^{C_D}/_{C_L^{\frac{3}{2}}}$ can be calculated using data from [12] and a value of approximately 45 can be found. In addition to this, considering an altitude of $h = 18{,}000\ m$ and a latitude of $\varphi = 38°$, the required power in case no TEG module is installed is:

$$P_{req} = 7966.43\ W$$

This value represents the minimum power necessary to maintain horizontal flight. Considering the specific days of operation, based on HeliPlat specifications, the averaged power densities provided by the solar panel are shown in Table 10. The average value $\overline{\varepsilon_{PV}}$ is calculate over the profile without considering the presence of the TEG module. In this way, the module will provide additional power to the minimum available generated by the solar panel.

Day of the year	**Average power density** $\left[{}^{W}/_{m^2}\right]$
1st February	158.11
21st June	222.49
30th November	100.38

Table 10: Averaged power densities for the solar panel

The minimum power generated by the panel occurs on 30th November. This value is then considered to calculate the minimum solar panel surface needed to provide the required power (for horizontal flight):

$$\overline{\varepsilon_{PV}} = 100.38\ \frac{W}{m^2}$$

Dividing the required power by the power density, it is possible to find the minimum solar panel surface that would provide such required power:

$$S_{PV} = \frac{P_{req}}{\overline{\varepsilon_{PV}}} = 79.36\ m^2$$

A discretization of the panel can be defined, to create a grid in which each coordinate represents a possible position of a TEG module to be installed under the panel. Considering a surface of the TEG module of $40 \cdot 40\ mm^2$, the maximum number of coordinate points the TEG modules can occupy is:

$$\widetilde{N} = \frac{S_{PV}}{S_{TEG}} = 49{,}602$$

This discretization allows to extend the 2-D data calculated over the profile to the entire surface of the solar panel, using averaged data from the 2-D airfoil profile.

Indicating with N_{TEG} the number of TEG modules installed, the available power can then be calculated as:

$$P_{avail} = \overline{\varepsilon_{PV}} \cdot S_{TEG} \cdot \left(\widetilde{N} - N_{TEG}\right) + \overline{\varepsilon_{PV,TEG}} \cdot S_{TEG} \cdot N_{TEG} + \overline{P_{TEG}} \cdot N_{TEG}$$

Where the symbols $\overline{\varepsilon_{PV}}$ and $\overline{\varepsilon_{PV,TEG}}$ represents the average value across the airfoil profile of the power densities in case the TEG module is not installed or is installed respectively. In a similar way, the symbol $\overline{P_{TEG}}$ represents the average value of the power generated by the TEG modules installed on the airfoil profile.

Considering the parameters defined above, the values of $\overline{\varepsilon_{PV,TEG}}$ and $\overline{P_{TEG}}$ are:

$$\overline{\varepsilon_{PV,TEG}} = 114.72\ \frac{W}{m^2}$$

$$\overline{P_{TEG}} = 0.045\ W$$

It is possible to derive the values of P_{req} and P_{avail} as function of the number of TEG modules N_{TEG} installed. The quantity of TEG modules installed increase the overall weight W_{tot} and consequently it impacts the minimum required surface of solar panel S_{PV}. It is then expected that P_{req} increases with the increase of TEG modules installed; however, the additional power generated by the TEG module should increase with the number of TEG modules installed and consequently provide more power. A summary view of the difference in power generated by the solar panel with TEG modules installed compared to the panel without the TEG modules installed is shown in Figure 37, for 30th November.

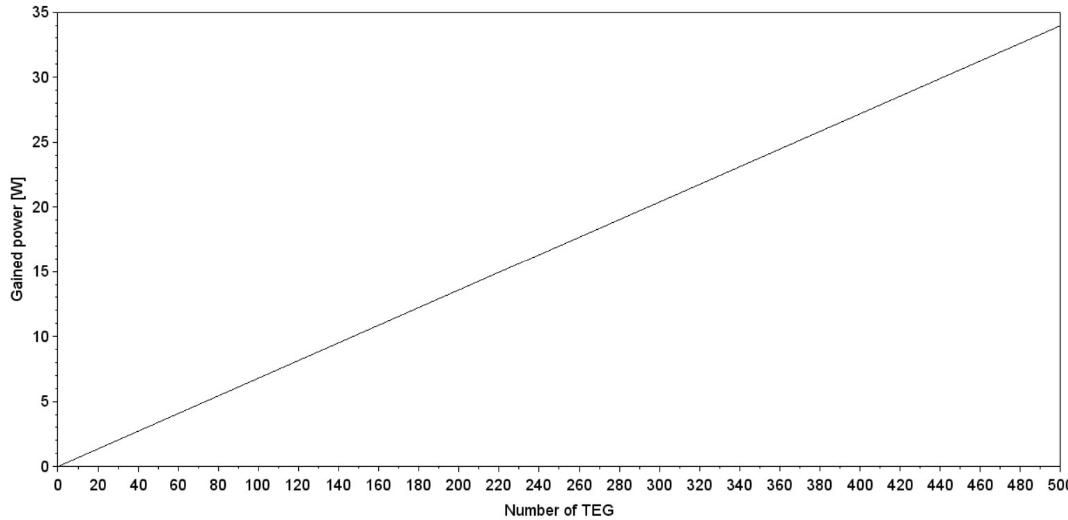

Figure 37: Gained power as function of TEG modules installed; 30th November

As a comparison, the same calculation performed on 21st June leads to the values as shown in Figure 38 below.

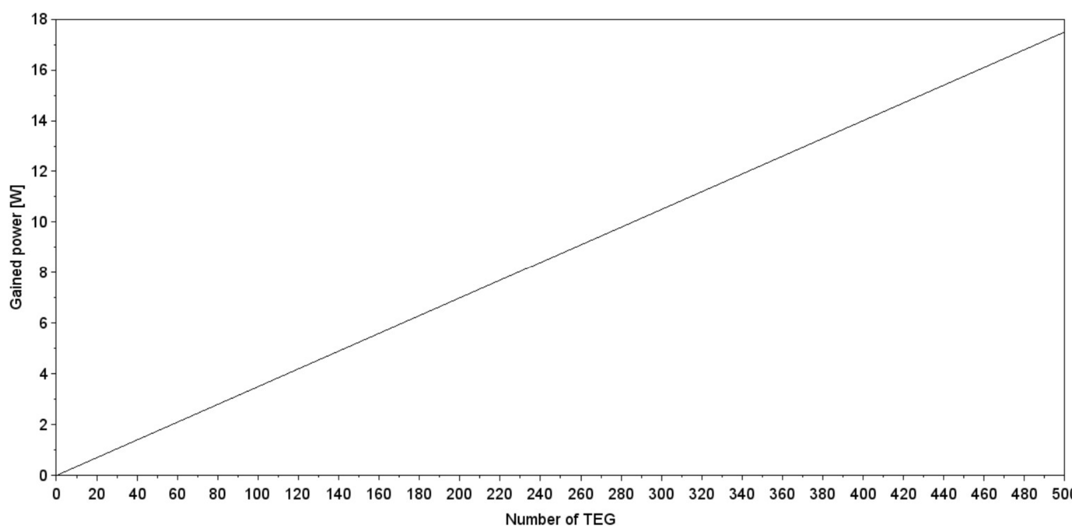

Figure 38: Gained power as function of TEG modules installed; 21st June

Following the calculations and results of Chapters 6 and 7, the contribution of the TEG module is higher when the solar power is reduced (such as during Winter time), therefore Figure 37 shows higher values of power gained through the TEG modules compared to the same configuration in Summer time (Figure 38).

The calculation of the additional weight due to the TEG modules also includes a rough estimation of the wirings necessary to connect the TEG modules to the battery, to store the additional power.

The number of TEG modules considered in Figures 37 and 38 is purely theoretical and has the only scope to show the dependency of the gained power using TEG modules as function of the number of TEG modules itself. As an indication, a simple sensitivity study can be performed on the required power: calculating the derivative of the power required with respect to the weight leads to:

$$\frac{dP_{req}}{dW_{tot}} = S_w^{\frac{1}{3}} \cdot \sqrt{\frac{2}{\rho_\infty} \cdot \frac{3}{2} \cdot W^{\frac{1}{2}} \cdot \left(\frac{C_D}{C_L^{\frac{3}{2}}}\right)} \cdot \frac{1}{\eta_{prop}} = 1.62 \left[\frac{W}{N}\right]$$

One important consideration is that the current (or the voltage) generated by the TEG modules also increases with the number of TEG modules. Whether the system sees a current or a voltage increase depends on the way the connection between the TEG modules is made, parallel or serial. Based on the datasheets of TEG modules and on the results of the calculations, the maximum current that can be generated in a single TEG module is approximately $I_{max} = 0.10\ A$. In a system wired in parallel, multiplying this value by the number of TEG modules installed in the profile can lead to significant value of current generated. Such current must be conducted by wires that must be dimensioned accordingly: this will then add weight to the structure and ultimately to the overall aircraft, impacting the performances and increasing the required power. Alternatively, it is possible to wire the system in series, but the voltage will increase as well as the redundancy of the system will be affected: if a malfunction or damage occur on one of the TEG modules, all the modules will stop working. Another solution can be a combination of parallel and series connection, with a limited increase in current and voltage. Ultimately, a more accurate estimation on the impact of the wiring on the weight of the aircraft requires the knowledge of the detailed structure and geometry of the sub-systems installed in the wings as well as their location with respect to the position of the wings.

7.10 Final considerations

The calculations show that at the coordinates where the TEG modules are installed, the solar panel performances increase, since the temperatures of the panel at those specific coordinates are lower and therefore the efficiency of the panel increases, leading to higher power densities generated. This can be seen in Figure 41, where the temperature profiles are taken at a latitude of 38° at midday. The curves representing the power densities at the coordinates where the TEG modules are installed are shifted to the right side of the plot, indicating higher power densities generated. This can be explained by the use of Rohacell material for the structure where the TEG modules are not installed: its thermal conductivity is higher than Teflon (which is used at the coordinates where the TEG modules are installed). Having such difference in thermal conductivity cause the heat to not pass through the structure from the panel to the internal side of the wing as easy as it is at the coordinates where the modules are present. Therefore, the panel have higher temperatures (Figure 39), causing its efficiency to drop and consequently its generated power density to be lower.

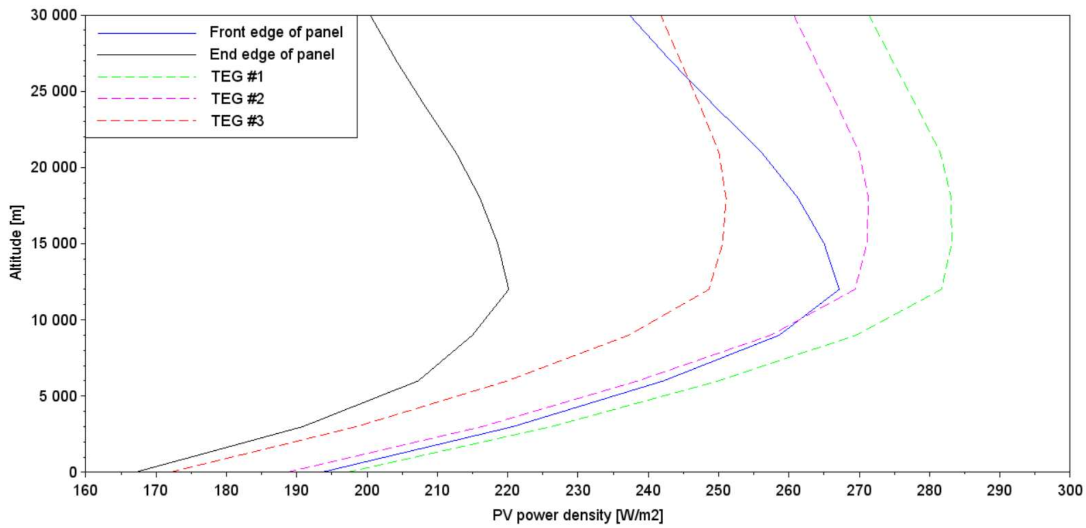

Figure 39: Power densities generated by the solar panel

This also means that for a wing structure with different materials the opposite can also happen, in which the temperatures at the coordinates where the TEG modules are installed can be higher than the ones on the structure, causing the opposite effect on the generated power.

This behaviour is also a consequence of the 2-D simplification of the model, which only considers the discretization of the profile in coordinate points and does not consider the interaction of the surfaces between TEG modules and panel. A more accurate FEM analysis on the portion of panel would show the temperature profile over a surface and consequently mitigate this phenomenon.

For this reason, the increase in performances of the panel at the coordinates where the TEG modules are installed are not considered as a contribution to the gained power given by the TEG modules. The values of additional power are only related to electrical power generated by the TEG modules thanks to the difference in temperatures between the top and bottom side of the TEGs.

8 Effects of variables on the generated power

In the previous chapter all results were presented based on the inputs listed in Table 8. However, in normal conditions these parameters can vary, whether it is for different time and day or for different flight conditions, etc…

In this chapter, some considerations on the effects of these different conditions are analyzed and the results reported:

- Variation of the angle of incidence
- Variation of the latitude
- Variation of the day of the year
- Variation of the efficiency of the panel

8.1 Effect of the angle of incidence

In case the airfoil profile has an angle of incidence with respect the direction of the air speed V_∞, the values of the coefficient of pressure along the profile vary and consequently the air speed over the profile changes as well.

In addition to the case of zero incidence shown in Chapter 7, two additional values of the angle of incidence are considered, $\alpha_i = 5°$ and $\alpha_i = 10°$. The other values are maintained as the same as in Table 8 and Table 9.

The variation of the angle of incidence has a direct impact on the tilting angle. Figure 40 shows the variation in tilting angle for the different angle of incidence.

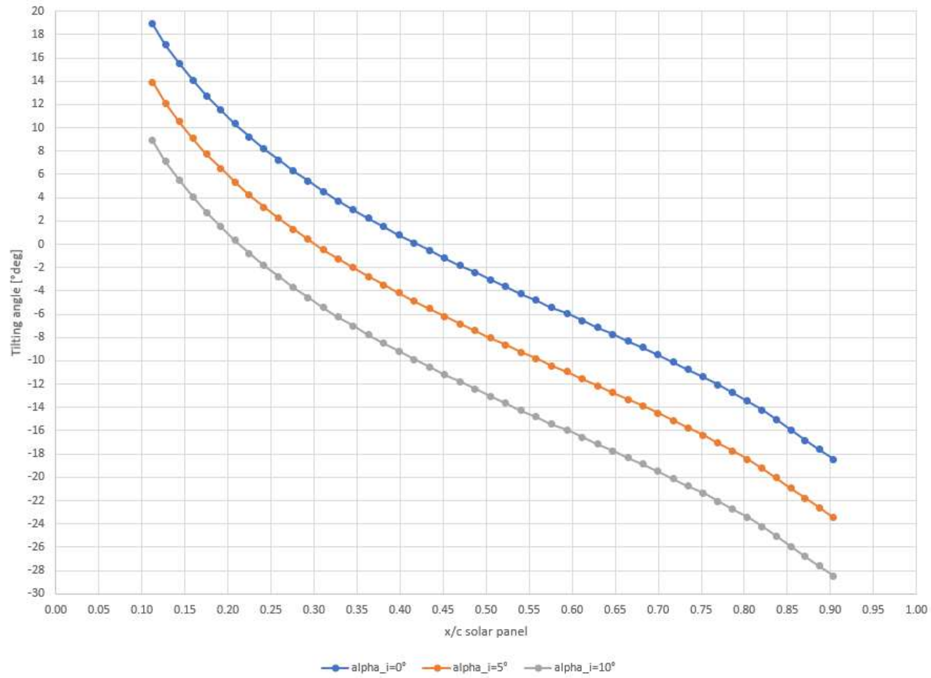

Figure 40: Tilting angles at different angle of incidence

The C_p profile changes as function to the angle of incidence as well, therefore this directly impact the airspeed at which the flow passes over the panel:

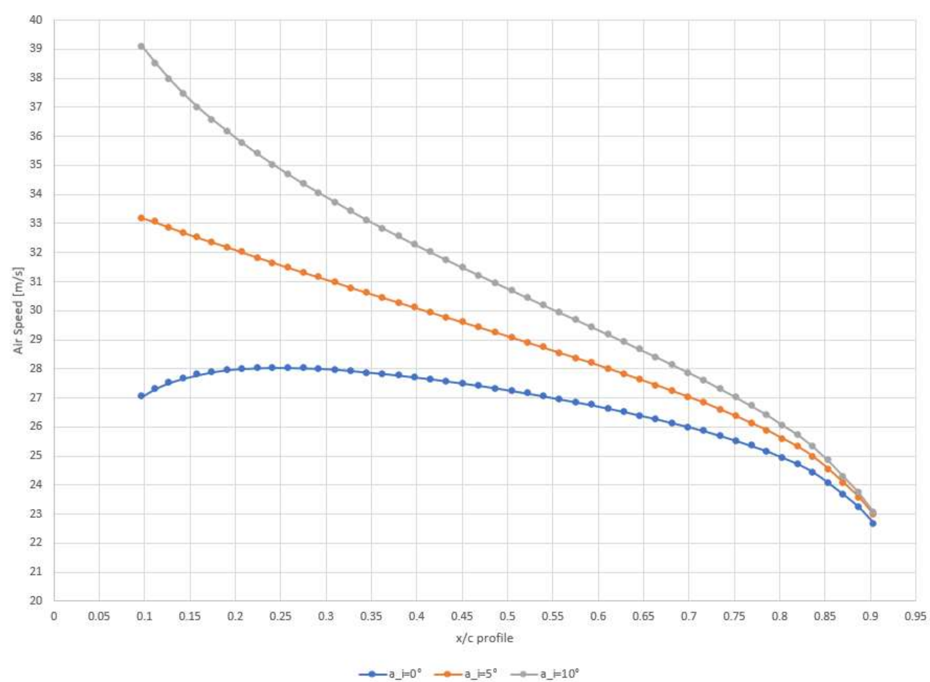

Figure 41: Airspeed over the profile as function of the angle of incidence

Using these different angles of incidence, the calculation leads to the values reported in Figure 42. The range of additional power spans between 1% and 13.5%, depending on the altitude.

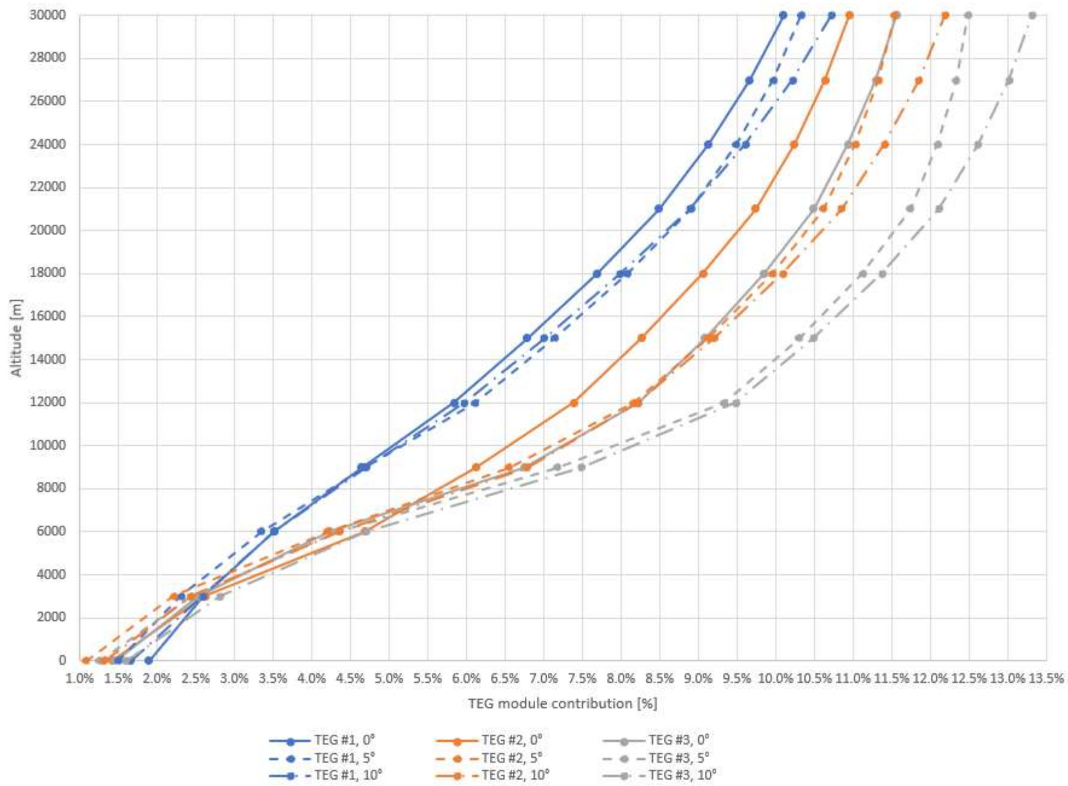

Figure 42: Gained power by the TEG modules as function of the angle of incidence

8.2 Effect of the latitude angle

Based on the definitions in Chapter 2, latitude affects the power flux received by the sun as well as the differences in radiation received across the year. Lower latitudes will provide more power to the panel, while higher latitude will do the opposite.

This impacts the power generated by the TEG modules, although as not as the same rate of the solar panel. The results are shown in Figure 43 below. Reference latitudes are taken from HeliPlat specifications: $\varphi = 36°$, $\varphi = 38°$ and $\varphi = 40°$.

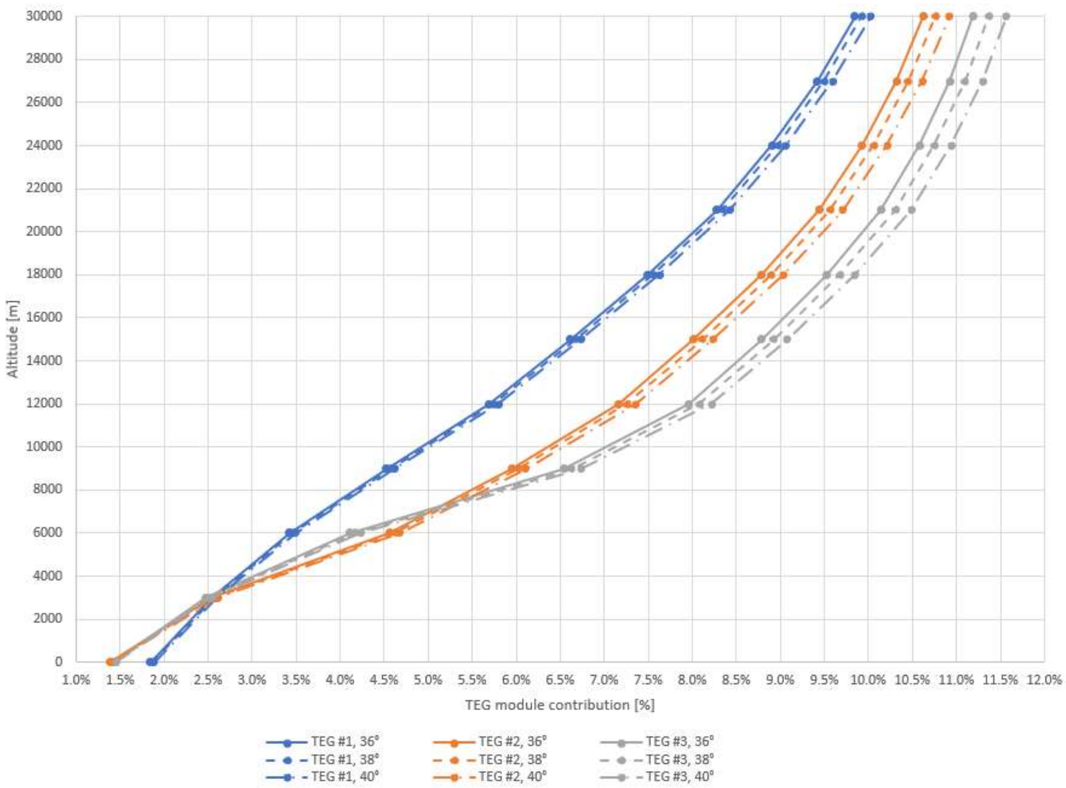

Figure 43: Gained power TEG modules, as function of latitude and altitude, 21st June

These data are calculated considering the other variables according to Table 8 and Table 9.

As it can be seen, the contribution of the TEG modules is between 1.5% and 11.5%, depending on the altitude and the latitude.

8.3 Effect of day of the year

The day of the year has a great influence on the radiation power emitted by the sun which has a direct impact on the power generated by the photovoltaic panel. The calculation shows that the power density generated by the panel is low in Winter time and higher during Summer. On the other hand, the power generated by the TEG module is generally not affected as much by the day of the year, since the power generated by the conduction phenomenon is not as heavily influenced by the day of the year. For this reason, the contribution of the TEG module to the overall power generated by the solar panel is greater. A comparison between Summer time and Winter time is shown in Table 11, and it specifically refers to 21st June and 30th November.

Altitude $h\ [m]$	**Summer – 21st June**			**Winter – 30th November**		
	Gain Power TEG #1	**Gain Power TEG #2**	**Gain Power TEG #3**	**Gain Power TEG #1**	**Gain Power TEG #2**	**Gain Power TEG #3**
0	1.89%	1.41%	1.55%	4.70%	2.89%	1.80%
3,000	2.61%	2.56%	2.67%	6.50%	5.76%	4.17%
6,000	3.51%	4.49%	4.38%	8.79%	10.77%	8.16%
9,000	4.64%	6.27%	6.85%	11.67%	15.76%	14.53%
12,000	5.84%	7.55%	8.53%	14.74%	19.61%	19.87%
15,000	6.79%	8.41%	9.40%	17.11%	22.28%	23.25%
18,000	7.69%	9.20%	10.17%	19.38%	24.70%	26.30%
21,000	8.49%	9.87%	10.80%	21.39%	26.73%	28.84%
24,000	9.13%	10.36%	11.24%	22.99%	28.20%	30.68%
27,000	9.66%	10.75%	11.59%	24.33%	29.37%	32.12%
30,000	10.10%	11.05%	11.85%	25.42%	30.27%	33.20%

Table 11: Gained power densities, solar panel on 21st June and 30th November

The area of the modules considered to calculate the power densities in Table 10 is taken from datasheet [17-20], with a value of $S_{TEG} = 40\ x\ 40\ mm^2$. These data are calculated considering the other variables according to Tables 8 and 9.

As it can be seen, the difference in power gained by using a TEG module is significantly higher considering the day 30th November.

8.4 Effect of the efficiency of the panel

In case new solar panels with higher efficiencies are available in the market, this will directly affect the performances of the panel. The TEG module will be marginally affected by this. Therefore, the contribution of the power from the TEG module is inversely proportional to the efficiency of the panel: if the efficiency increases, the contribution reduces.

Figure 44 compares the power gained for three different values of panel efficiency and at Summer solstice. In general, for an increase in 6% of the panel efficiency, the TEG module contribution is reduced by 50%.

In Winter time the TEG module provides more power when compared to the power generated by the solar panel, therefore the percentage of gained power increases in favour of the TEG module. The day of 21st June is the worst case scenario for the TEG module.

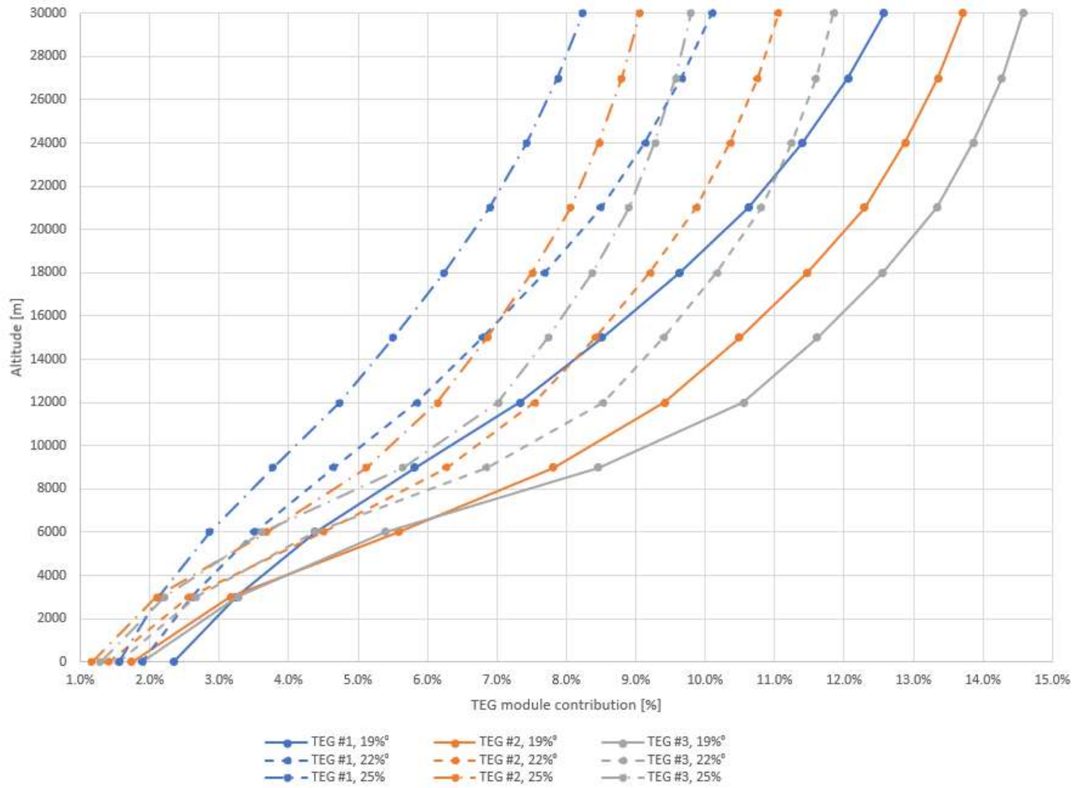

Figure 44: Gained power by TEG module, 21st June

9 Other applications

Solar panels are also widely used in ground applications, to generate power by sunlight and store such power in dedicated batteries. TEG modules can then be applied to these panels in the same way as discussed in Chapter 6 for aerospace applications.

However, there are some significant differences between applications on the ground and on aircrafts:

- Photovoltaic solar cells for traditional commercial and residential applications are different in design and manufacturing compared to solar cells for the aerospace industry
- Temperature ranges depend on locations and seasons rather than altitude
- Altitude has then the only effect on position of the solar panel, since the altitude of ground applications typically varies from sea level to $4{,}000\ m$
- Weight of the solar panels and the additional TEG modules installed has less importance in ground installations, therefore no consideration on the impact of weight over the performances of the panel are taken into account
- Since the panels are installed on the ground, air speed effects are only dependent on the climatic condition, such as no wind or breeze, gust etc.

9.1 Photovoltaic solar panels

In case of a traditional solar panel installation, residential or commercial solar panels can be considered. Table 12 below presents a list of commercially available panels from two different manufacturers. This list of panels is not exhaustive; however, it can be considered as a reference of the technology currently present in the market.

For this case, the model was updated with different values of thermal conductivity, to reflect the different materials used in panels for residential and industrial applications compared to aerospace applications. The materials considered for this case are insulating material for the solar cells (polyester) and Aluminum for the structure.

Manufacturer	Name	Power [W]	Panel efficiency	Power Temperature coefficient	Dimensions [mm by mm]
SunPower	E20-327-COM	327	20.1%	-0.35%/°C	1515 x 982
	E20-435-COM	435	20.1%	-0.35%/°C	2023 x 982
	X22-360-COM	360	22.1%	-0.29%/°C	1515 x 982
	SPR-A400-BLK	400	21.4%	-0.29%/°C	1787 x 952
	SPR-A450-COM	450	22.2%	-0.29%/°C	1955 x 952
	X21-470-COM	470	21.7%	-0.29%/°C	2023 x 982
SolarWatt	Vision 60M Style	320	18.8%	-0.39%/°C	1620 x 930
	EastIn 60M Style	320	19.4%	-0.39%/°C	1642 x 1015
	Vision 60M	320	19.4%	-0.38%/°C	1560 x 930

Table 12: List of solar panels for residential and commercial applications

For the cases below, again a panel thickness of $d = 5\ mm$ is considered, in accordance to the values and the schematics listed in solar panel datasheets.

9.2 No wind condition

It is possible to use the same model as described in Chapter 5, with specific adaptations to Reynolds number, Prandtl number and Nusselt number and by limiting the altitude up to $4{,}000\ m$. Also, the air speed is adjusted to more specific applications on ground installations, therefore values of $V_\infty = 0.1\ {}^{m}/_{s}$ (no wind condition).

Figures 45 and 46 show the power density profile of a panel set at a condition of no wind:

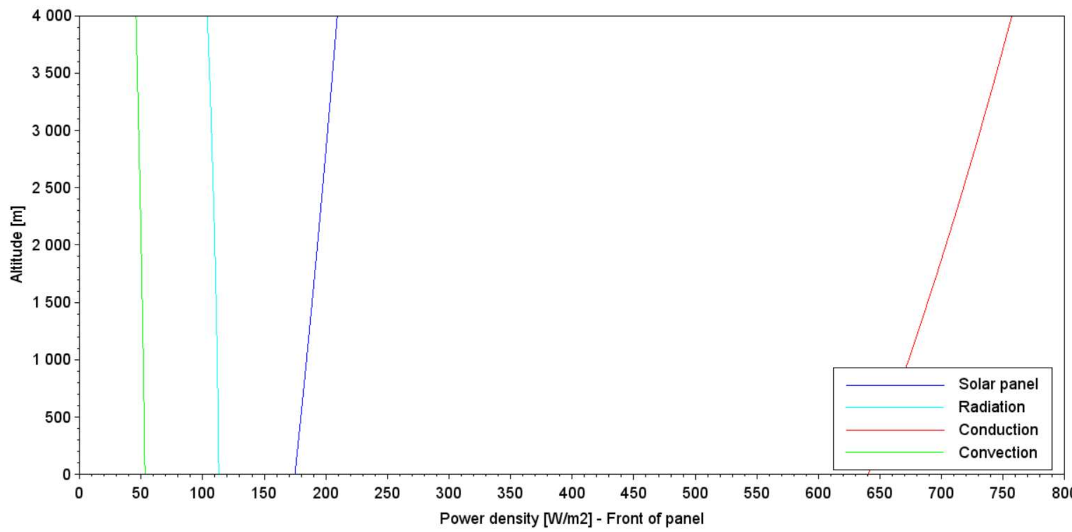

Figure 45: Power densities in no wind condition, front of panel

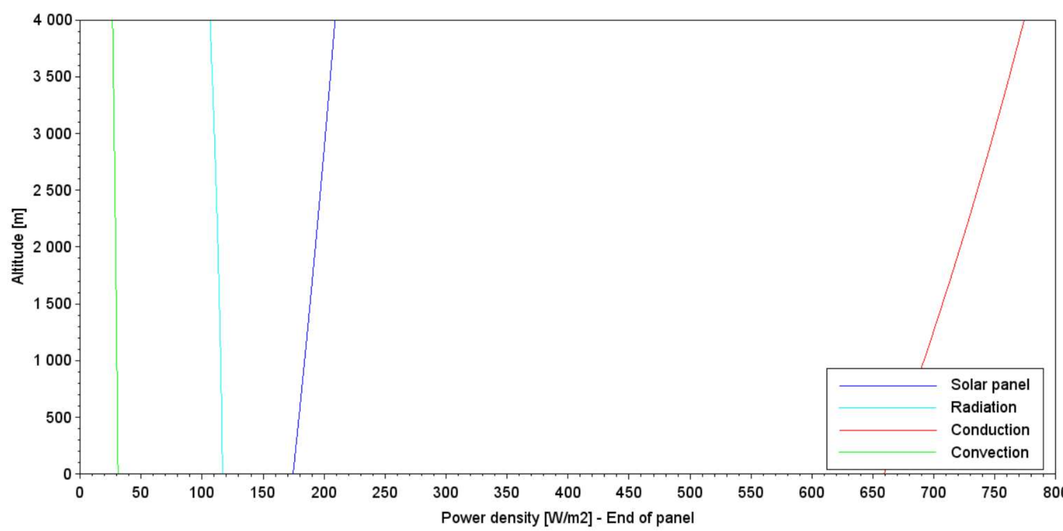

Figure 46: Power densities in no wind condition, end of panel

In case of no wind, the power densities along the panel surface do not vary significantly. This is a direct consequence of the low values of Reynolds and Nusselt numbers. For the same reason as well as the specific flat geometry of a solar panel for ground installations, the power generated by a TEG module placed in different parts of the panel is the same, without a significant difference.

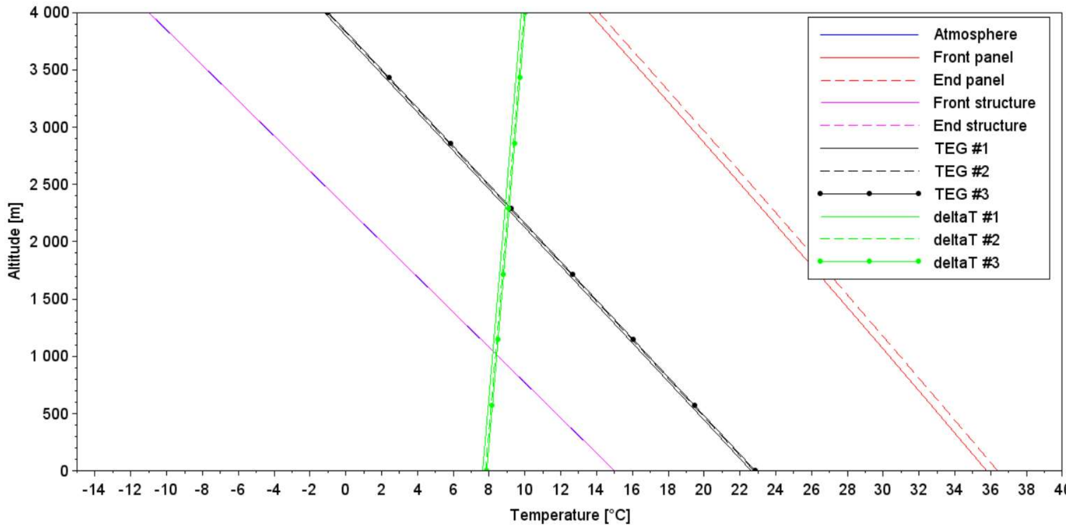

Figure 47: Temperature profile over the panel, 21st June

Temperatures are very similar in each TEG modules as well as the difference in temperatures ΔT. The calculation provides the results as shown in Figure 48 and Table 12, with a gained power between 5.4 $W/_{m^2}$ and 9.1 $W/_{m^2}$ in Winter time, with a contribution between 1% and 1.75% to the total power density. These results are related to the day of 21st June (Summer time).

When a more conductive material is used (Aluminum versus Rohacell), the model shows that the temperatures of the panel at the coordinates where the TEG modules are installed are higher compared to the temperatures at the coordinates where the modules are no installed. This is because the higher conductivity allows the heat to flow better from the top to the bottom of the panel, which leads to have lower temperatures on the areas where no modules are installed and therefore to have better panel efficiencies. For this reason, Figure 48, Table 13 and Table 14 show values listed as gained power: this is the additional power produced by the TEG module after recovering from the loss of performances on the panel at those specific coordinates.

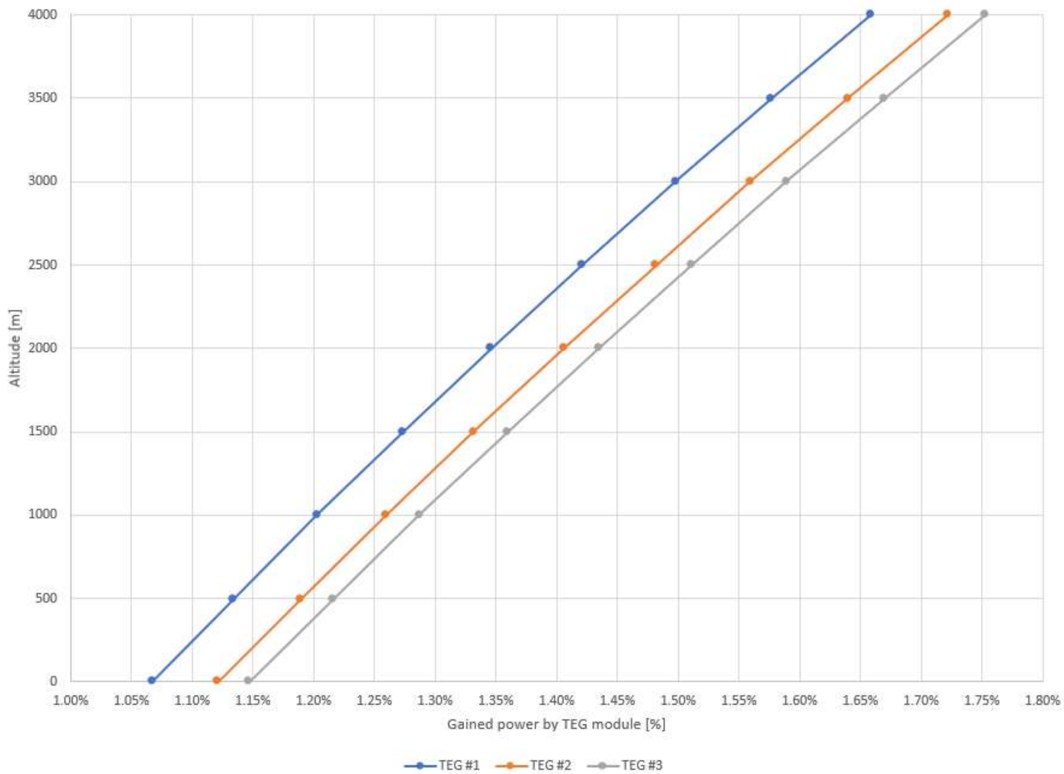

Figure 48: Power generated by the TEG module

Following the same process as the application for HeliPlat, in case Winter time is considered, the contribution of the TEG module becomes more significant. Table 17 summarizes the changes in gained power between Summer and Winter's solstices.

Altitude $h\ [m]$	Summer – 21st June			Winter – 21st December		
	Gained Power TEG #1	Gained Power TEG #2	Gained Power TEG #3	Gained Power TEG #1	Gained Power TEG #2	Gained Power TEG #3
0	1.07%	1.12%	1.15%	5.39%	5.62%	5.73%
500	1.13%	1.19%	1.22%	5.80%	6.05%	6.16%
1000	1.20%	1.26%	1.29%	6.19%	6.44%	6.57%
1500	1.27%	1.33%	1.36%	6.59%	6.85%	6.97%
2000	1.35%	1.41%	1.43%	6.99%	7.26%	7.39%
2500	1.42%	1.48%	1.51%	7.40%	7.68%	7.81%
3000	1.50%	1.56%	1.59%	7.82%	8.10%	8.24%
3500	1.58%	1.64%	1.67%	8.25%	8.54%	8.67%
4000	1.66%	1.72%	1.75%	8.69%	8.98%	9.12%

Table 13: Comparison in gained power, 21st June and 21st December

9.3 Panel surface perpendicular to sunlight

Considering Summer's solstice, a latitude of 45°, at 12 pm, it is possible to calculate the angle at which sunlight reaches the panel, with the panel surface facing the light perpendicularly. This provides the optimal case for the solar cells to generate power, therefore it can be interesting to verify hoe the TEG module performs. Results are shown in Table 14 and no appreciable difference can be seen compared to a panel with a tilting angle of zero degrees.

Altitude $h\ [m]$	**Summer – 21st June**		
	Gained Power TEG #1	**Gained Power TEG #2**	**Gained Power TEG #3**
0	1.06%	1.12%	1.14%
500	1.13%	1.18%	1.21%
1000	1.20%	1.25%	1.28%
1500	1.27%	1.33%	1.35%
2000	1.34%	1.40%	1.43%
2500	1.41%	1.47%	1.51%
3000	1.49%	1.55%	1.58%
3500	1.57%	1.63%	1.66%
4000	1.65%	1.71%	1.75%

Table 14: Gained power for solar panels perpendicular to sunlight

This type of result is expected considering that, in this condition, the panel works at optimal conditions, therefore its efficiency is better. However, the contribution of the TEG module does not suffer from it and the tilting angle appear to have a low effect on the TEG module performance. For this reason, the module is still applicable when the panel works in optimal conditions.

10 Conclusions

The application of TEG modules to airfoil profile of aircrafts has been evaluated at a theoretical level by considering information available in the market and using them into a model code, written with the limitations mentioned at the beginning in the Introduction. Although the results are proposed with a reference case of the HeliPlat project, the model works with any profile, should the geometrical coordinates of the airfoil be provided. Based on the proposed model, the addition of TEG modules provides benefits to the solar panel, in terms of power output generated. Many variables affect the results; however, a visible trend is that the contribution is higher when the panel produces less power. The variation of power generated by the TEG module appears to be less affected by the changes in variables compared to the variation of the power generated by the solar panel. This is a beneficial point in favour of TEG modules, since they can support the solar panel in some specific circumstances.

Variables such as altitude, latitude and day of the year have a significant impact on the balance of power around the panel. Other variables, such as the angle of incidence have less impact on the changes in power.

Each TEG module can contribute with few tenths of milli-Watt of power in the system, given the small surfaces of TEG modules considered.

The results are of course directly dependent to the energy balance in a specific configuration or application. Aircrafts flying at higher altitudes appear to receive more benefits from the application of TEG modules. On the other hand, too many TEG modules increase the weight of the wing and could impair the function and the performance of the entire aircraft. For this reason, the application of TEG modules in aeronautical application must come with a verification of positive versus negative factors.

A possible mission profile or aircraft configuration would be a stratospheric flight at high latitudes, during the months when less sunlight is expected. In this way it is possible to maximize the effect of the installation of TEG modules. Flights at low speed benefit the most from the module as well.

Solar panels are also widely used in ground applications; therefore, the model was also applied to such applications. The results show a positive balance of power gained when using TEG modules, although the gain is lower in percentage compared to the one for aeronautical applications. This is because ground applications limit the altitude to around $4{,}000\ m$. However, the data still show that the contribution given by the TEG module is more effective in applications on higher ground level, such as mountain regions, for example.

Another point to consider is the connection between the TEG modules installed under the panels: they can be connected in series or in parallel. This mainly depends on the system and how the battery work, since it is possible to increase the current output or the voltage output to feed the battery. In any case, the power out from the TEG module increases when the number of TEG modules increases.

The limitation in the number of TEG modules that can be used is also given by the additional weight and complexity of the circuit. This is more significant in aeronautical application, where weight is an important factor to measure the performances.

These results are obviously affected by the limitations and assumptions mentioned in the Introduction, therefore further effort on this subject could improve the current model by:

- Consider a 3-D environment, where tridimensional aerodynamic effects could impact the energy balance and therefore the calculated results (temperatures and power densities)
- Consider the flow as viscous around the profile, changing the dynamic of heat transfer between conduction and convection and impacting the transition between laminar and turbulent flow
- Adding atmospheric effects such as wind/gust or statical data related to seasons; this will impact the Standard Atmospheric data considered in this work and adapt the atmosphere to a more realistic behaviour
- Evaluation of FEM analysis in the area where TEG modules and panels interact, to have a temperature and heat exchange in these areas that is affected by the other adjacent coordinates

References

[1] Bernhard Keidel, *Auslegung und Simulation von hochfliegenden, dauerhaft stationierbaren Solardrohnen*, Technische Universitat Munchen

[2] Theodore L. Bergman, Adreinne S. Lavine, Frank P. Incropera, David P. Dewitt, *Fundamentals of heat and mass transfer*, 7th edition, John Wiley and Sons

[3] Nabil Karami, Nazih Moubayed, *New modeling approach and validation of a thermoelectric generator*, IEEE 2014

[4] David H. Walls, Charles D. Fortenbach, Emaunal V. Dimiceli and Robert W> Perks, *A preliminary study of solar powered aircraft and associated power trains,* Nasa contractor report 3699, 1983

[5] M. D. Bailey, M. V. Bower, *High altitude solar power platform*, NASA TM-103578, 1992

[6] Anthony J. Colozza, *Effect of power system technology and mission requirements on high altitude long endurance aircraft*, NASA contractor report 194455

[7] Anthony Colozza, *Initial feasibility assessment of a high altitude long endurance airship*, NASA/CR-2003-212724, 2003

[8] Lanchuan Zhang, Mingyun Lv, Junuhui Meng, Haufei Du, *Optimisation of solar-powered hybrid airship conceptual design*, Aerospace science and technology, 2017

[9] Ahmet Senpinar, *Optimisation of slope angles of photovoltaic arrays for different seasons*, ScienceDirect, 2018

[10] Review of photovoltaic cells for solar-powered aircraft applications, Safyanu Bashir Danjuma, Zamri Omar, Mohld Noor Abdullah, 2018

[11] Andre' Noth, *Design of solar powered airplanes for continuous flight*, Ecole Polytechnique Federale de Lausanne, 2008

[12] Giulio Romeo, Giacomo Frulla, Enrico Cestino, Guido Corsino, *HELIPLAT: design, aerodynamic, structural analysis of long-endurance solar-powered stratospheric platform*, Politecnico di Torino, 2004

[13] Hsu-Yung Chen, Chih-Chang Yu, Kuo-Chang Hsu, Chi-Chang Chan, Mei-Hui Tseng and Chih-Lung Lin, *Estimating solar irradiance on tilted surface with arbitrary orientations and tilt angles*, Energies, 2019

[14] www.sunpower.com

[15] www.solarwatt.com

[16] www.TEGpro.com

[17] www.customthermoelectric.com

[18] www.rmtltd.ru

[19] www.tecteg.com

[20] www.teconversion.com

[21] www.rohacell.com

[22] www.wikipedia.org

Appendix I

Overview of HeliPlat concept:

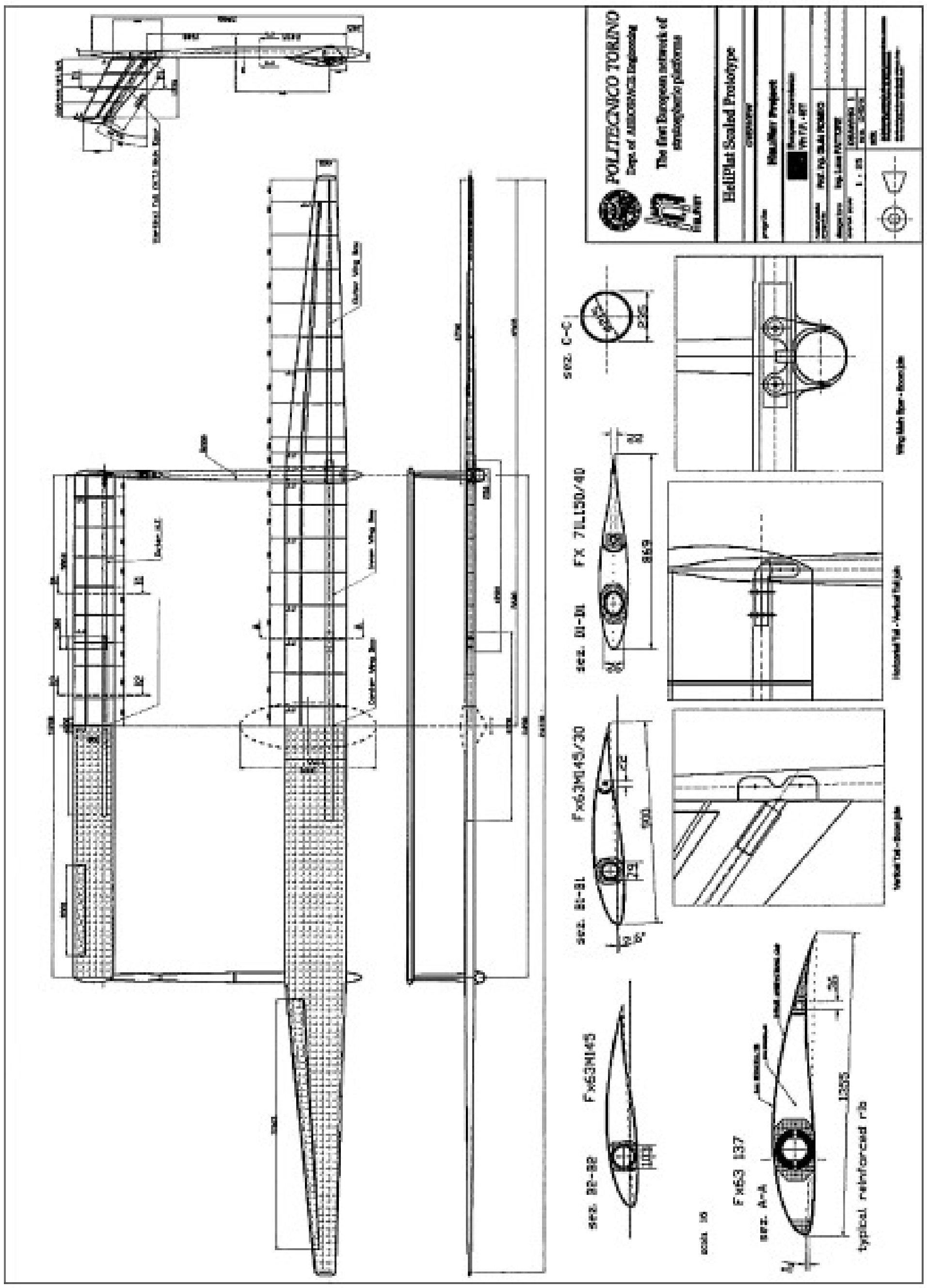

Appendix II

II.1 RMT 1MD02-035-xxTEG

RMT Thermoelectric Power Generating Solutions

Performance Parameters — 1MD02-035-xxTEG

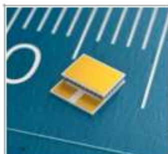

	TEG PERFORMANCE AT SPECIFIED HOT SIDE TEMPERATURE												H mm
	Optimum Power Output Pout, W			Optimum Voltage Uout, V			Open Circuit Voltage Uoc, V			Resistance ACR, Ohm			
	85ºC	55ºC	35ºC	85ºC	55ºC	35ºC	85ºC	55ºC	35ºC	85ºC	55ºC	35ºC	
1MD02-035-03TEG	0.03	0.01	0.001	0.51	0.24	0.07	0.88	0.42	0.12	6.06	5.63	5.34	0.8

Performance values are specified for TEG cold side at +27ºC, Dry Air. Optimum Power and Voltage are given at Optimum Load Resistance

Dimensions

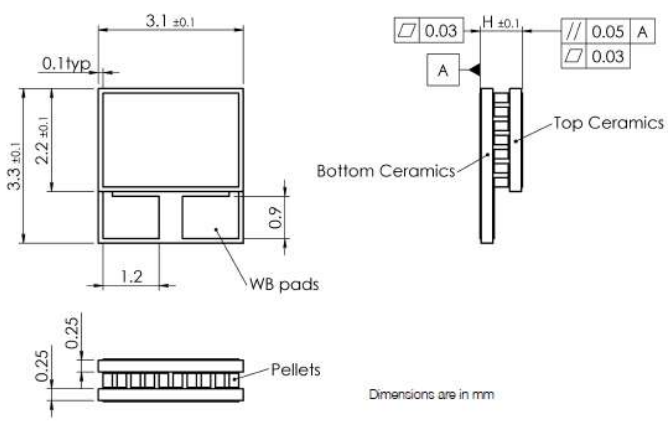

Dimensions are in mm

Manufacturing options

A. TEG Assembly:
1. Solder Sn-Sb, T_{melt}=230°C (default assembly solder)
2. Solder Au-Sn, T_{melt}=280°C (optional solution, by request)

B. TEG Ceramics:
1. Al_2O_3(100%) - default
2. AlN - by request

C. Ceramics Surface Options:
1. Blank ceramics - default
2. Metallized (Au plating)
3. Metallized and pre-tinned with:
   - 3.1. In-Sn, T_{melt} =117°C
   - 3.2. Sn-Bi, T_{melt} = 138°C
   - 3.3. In-Ag, T_{melt} = 143°C
   - 3.4. In, T_{melt} = 157°C
   - 3.5. Pb-Sn, T_{melt} =183°C
   - 3.6. Optional type (can be specified by Customer)

D. Thermistors (optional)
Can be mounted to ceramics edge. Calibration is available by request.

E. Terminal contacts
1. Blank, tinned Copper Wires
2. Insulated Wires
3. Insulated, color coded
4. WB pads or Posts (default)
5. Flip-Chip (optional)

RMT Thermoelectric Power Generating Solutions

Performance Data — 1MD02-035-03TEG

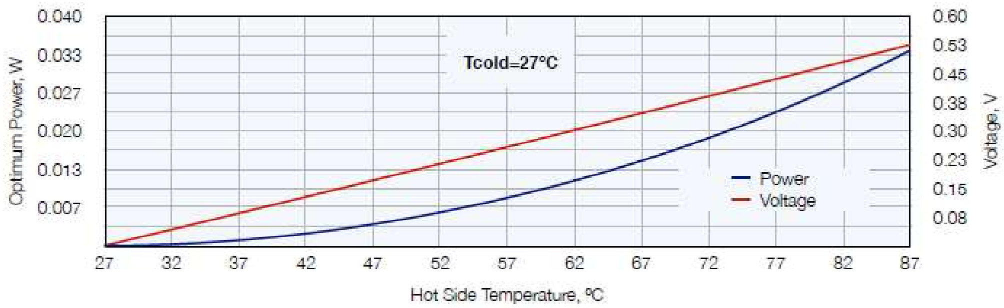

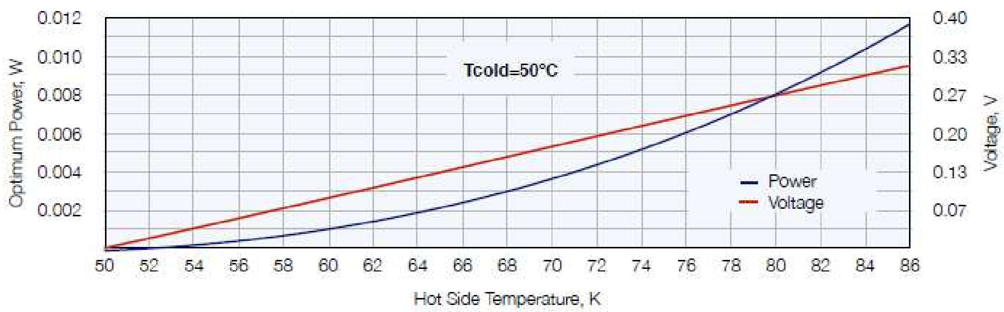

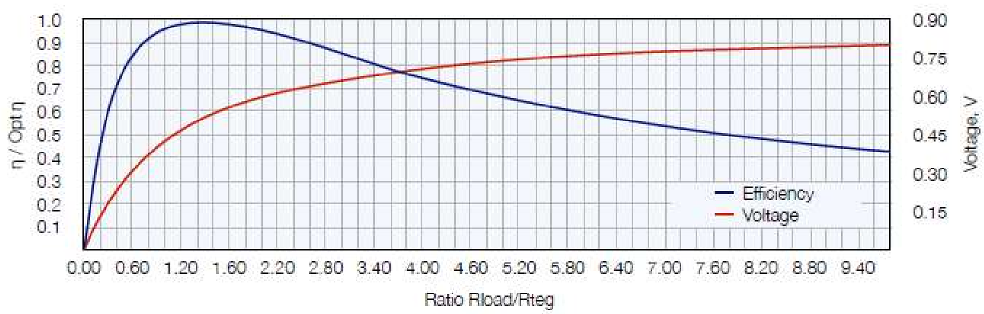

Performance data at Optimum Load Resistance (Rload)

Parameter	Units	Values at Hot Side Temperature		
		85°C	55°C	35°C
Cold Side Temperature, Tcold	°C	27	27	27
Optimum Efficiency, Opt η	%	2.67	1.34	0.39
Optimum Power, Popt	W	0.031	0.008	0.001
Optimum Voltage, Uopt	V	0.507	0.241	0.068
AC Resistance, Rteg	Ohm	6.06	5.63	5.34
Optimum Load Resistance, Rload	Ohm	8.18	7.60	7.16
Open Circuit Voltage,Uoc	V	0.88	0.42	0.12
Short Circuit Current, Isc	A	0.15	0.07	0.02
Thermal Resistance, Rt	°C/W	49.21	49.16	49.06

Note: Power Generation performance charts are specified in Optimum conditions, dry air, with cold side temperature set at +27°C and 50°C. Heatsink thermal resistance is not included into estimations.

II.2 Custom Thermoelectric 1261G-7L31-04CQ

TEG Specification Sheet

CUSTOM THERMOELECTRIC
Your Thermoelectric Partner

Seebeck Thermoelectric Generator

Part #	T_{max} (°C)
1261G-7L31-04CQ	320°C

Note:
Hot side is rated to a maximum of 320°C continuous
Cold side is rated to a maximum of 180°C continuous.

Both sides of the TEG have a graphite foil pre-applied as a thermal interface material (TIM). There is no need to add any additional thermal grease or compounds.

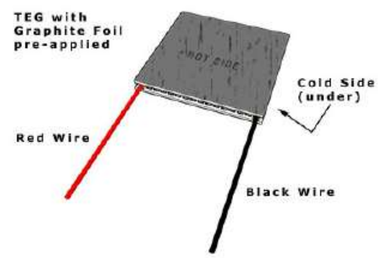

Top Plate				Bottom Plate				Height w/ Foil		Lapped Height	
A		B		C		D		H		H	
mm	in	mm	in	mm	in	mm	in	mm	in	mm	in
40.0	1.57	40.0	1.57	40.0	1.57	40.0	1.57	3.75	0.148	3.5	0.138

Weight (w/o leads)
25 grams

AC Resistance
1.7 ohms @ 27°C

Thermal Conductivity
1.2 watts/m K @ T_h=300°C

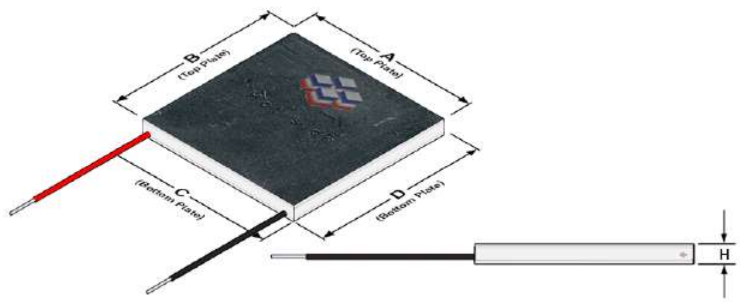

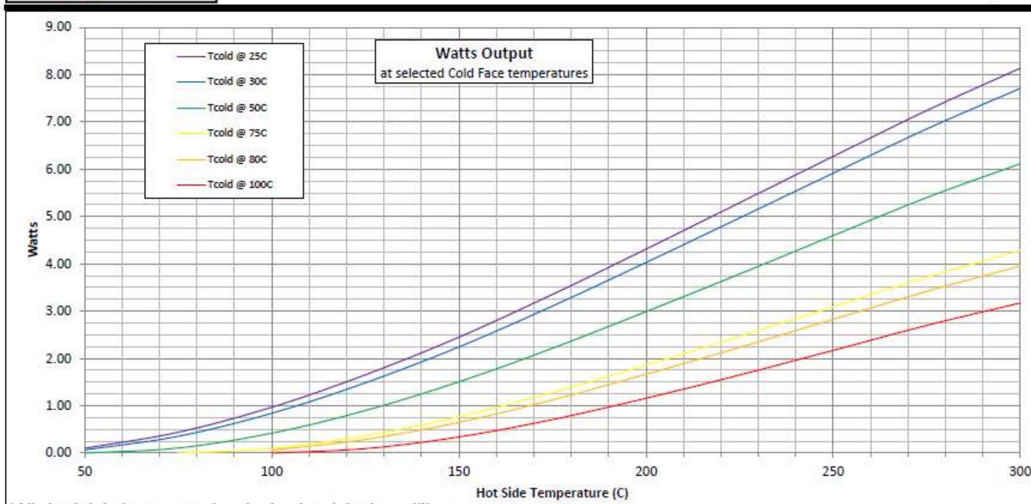

*All chart data is measured under load matched conditions.

TEG Specification Sheet

CUSTOM THERMOELECTRIC
Your Thermoelectric Partner

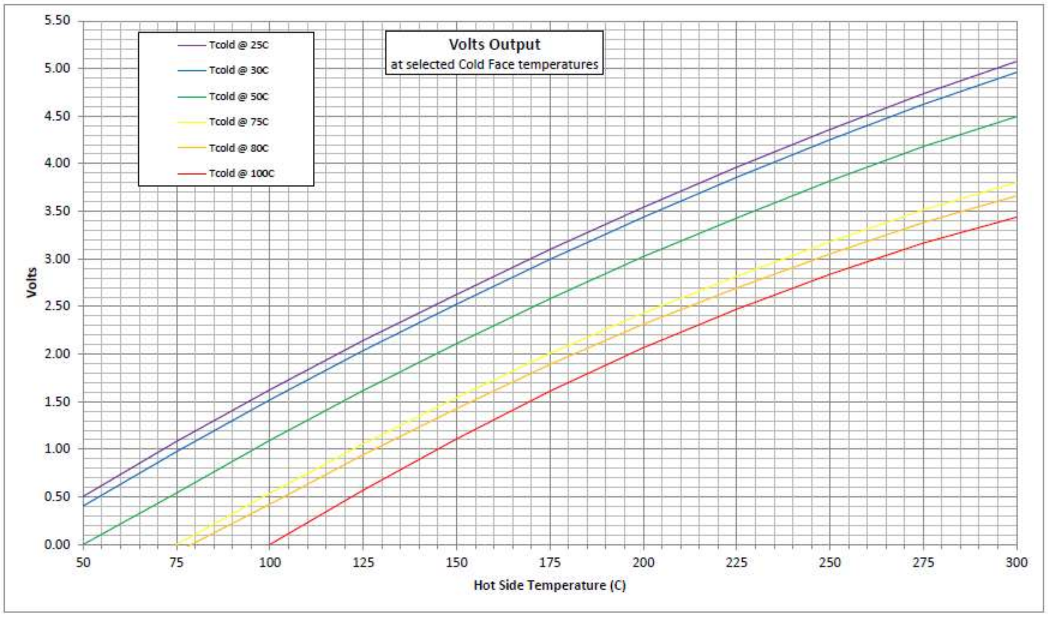

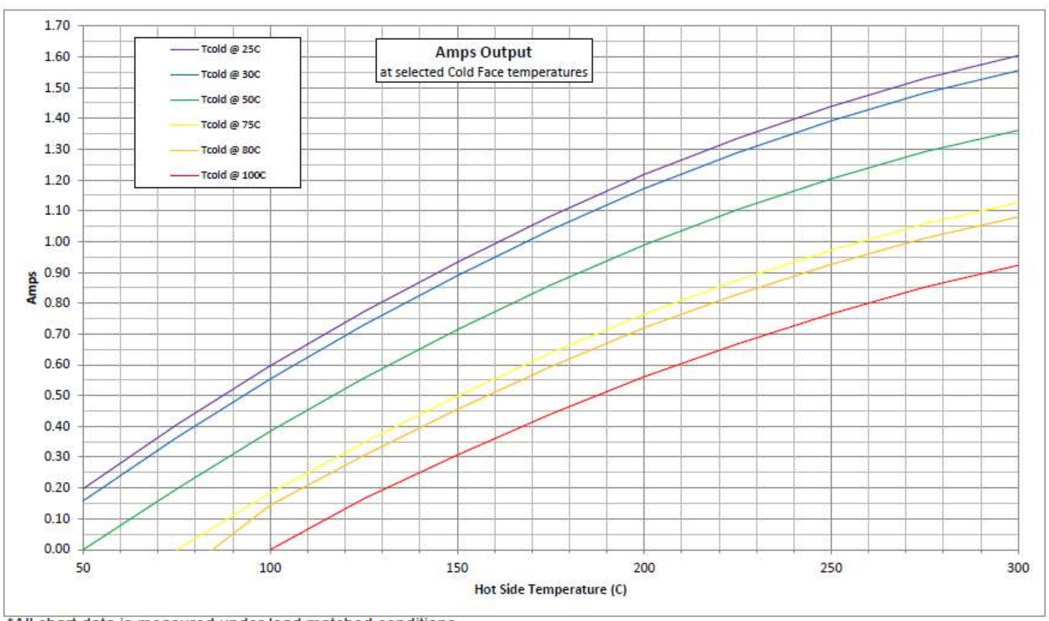

*All chart data is measured under load matched conditions.

II.3 Open circuit voltage to temperature difference

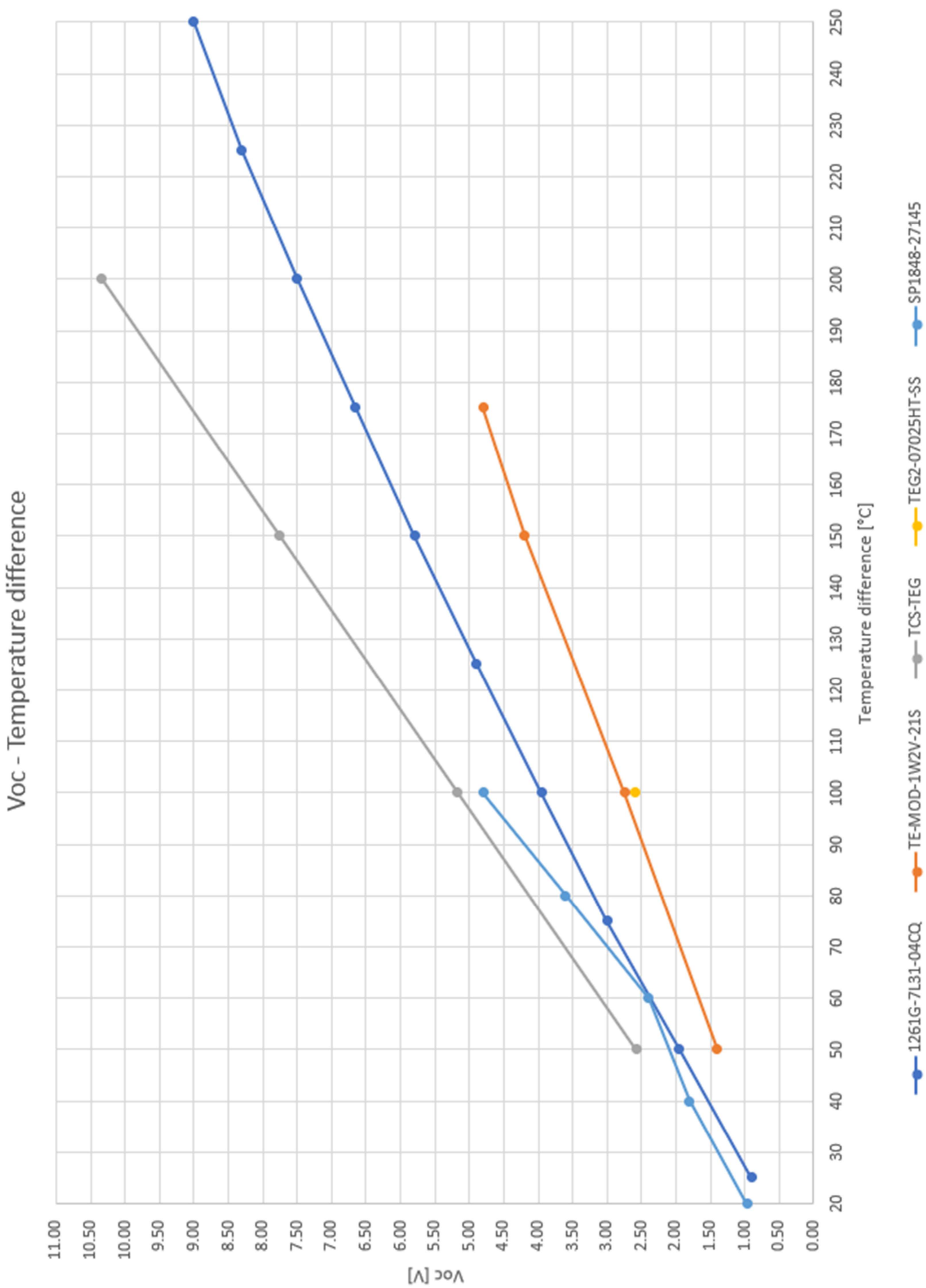

II.4 Voltage to temperature difference

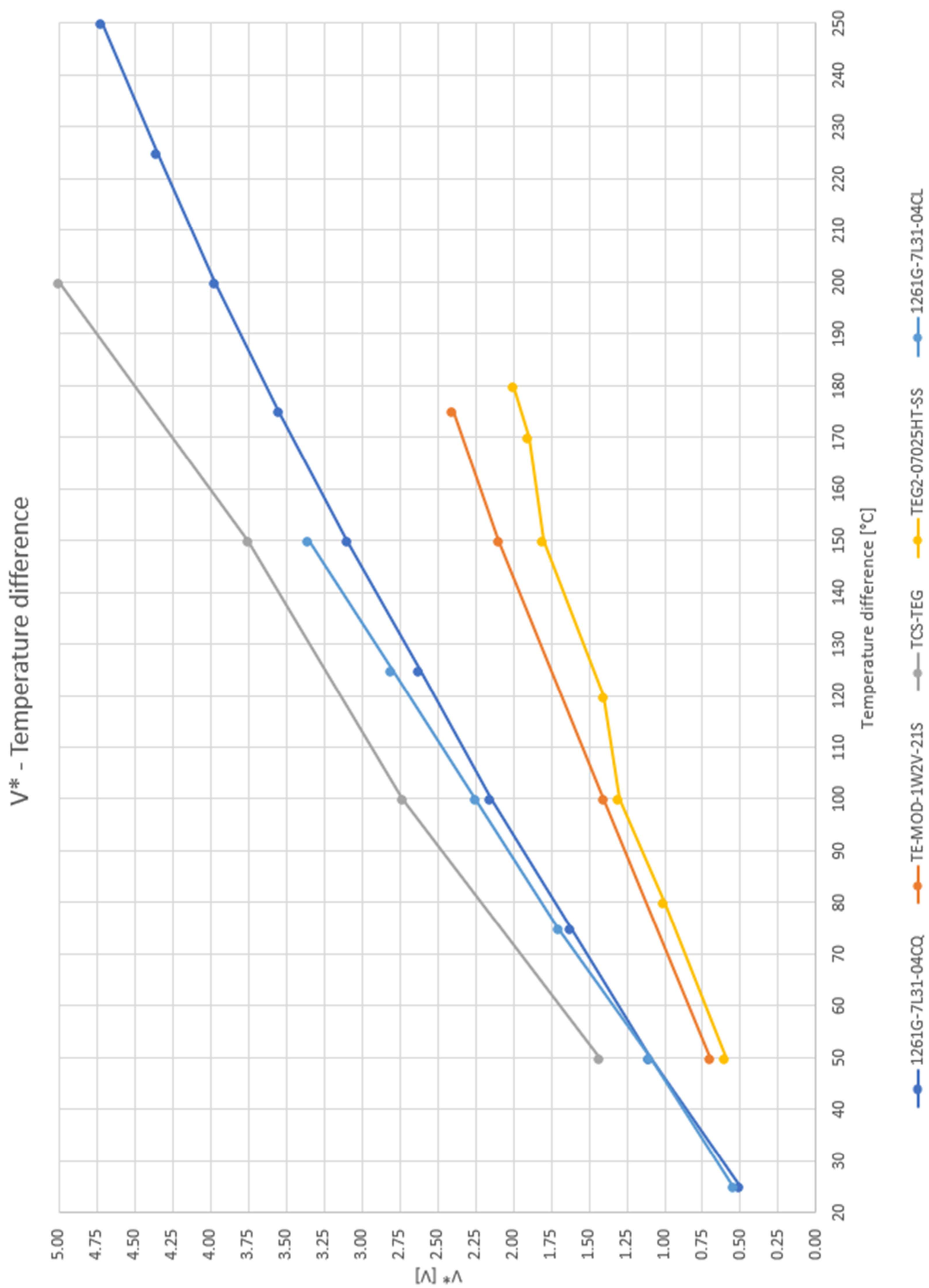

II.5 Current to temperature difference

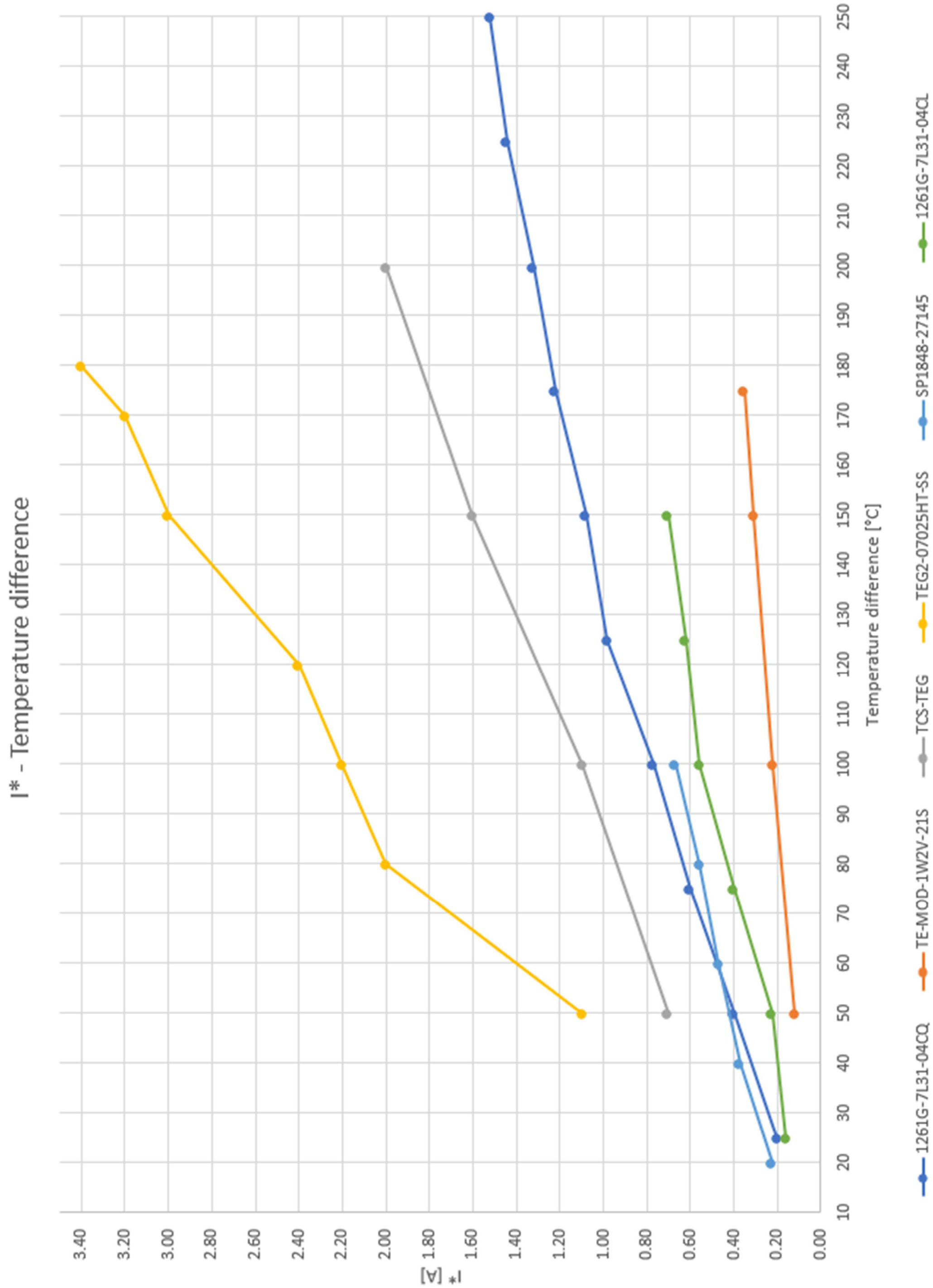

II.6 Resistance to temperature difference